DEPARTMENT OF COMMERCE
LUTHER H. HODGES, Secretary

WEATHER BUREAU
F. W. REICHELDERFER, Chief

MONTHLY WEATHER REVIEW

JAMES E. CASKEY, JR., Editor

Volume 89
Number 3

MARCH 1961

Closed February 15, 1961
Issued March 15, 1961

A PROPOSED STAGGERED-GRID SYSTEM FOR NUMERICAL INTEGRATION OF DYNAMIC EQUATIONS

D. K. LILLY

U.S. Weather Bureau, Washington, D.C.
[Manuscript received September 15, 1960; revised January 3, 1961]

ABSTRACT

A system is proposed for grid allocation and differencing of apparently general applicability to purely marching-type systems of equations of fluid dynamics. The method is based on casting of the equations into the conservation form, which then permits use of a staggered space-time grid system with interpolations required only in certain linear terms. The method is illustrated by application to two systems of equations, on one of which numerical experiments have been successfully performed. Advantages and drawbacks of the method are described in comparison to other currently used grid systems, and the possibility and desirability of parametric simulation of turbulent eddy exchange processes are discussed.

1. INTRODUCTION

The recent development of methods of numerical integration of the equations of fluid dynamics in a more-or-less primitive form, i.e., of first order, except for diffusion terms, is focusing attention upon new aspects of numerical analysis. During the early development of geostrophic or balanced models which involved a vorticity equation, perhaps the most pressing practical problems were to solve rapidly and accurately certain rather complex elliptic second order partial differential equations. In dealing with undifferentiated systems one finds that the basic equations are much simpler to apply but must, for the sake of computational stability, be applied at very short time intervals compared to the time scales of the significant meteorological phenomena. This is because the normal Courant-Friedrichs-Lewy stability criterion requires essentially that motions or waves allowed in the system not be able to travel from one grid point to the next in one time step, and the undifferentiated systems usually allow faster-moving waves than those of meteorological interest. It is also noted that the boundary conditions and various consistency requirements, if not more complex, are more critical when a single computation run may include several thousand time steps. Under these circumstances it is desirable to examine the time-space grid data allocation and differencing scheme with a view toward eliminating, if feasible, some of the redundant time resolution and thus save time and computation expense. It also appears that when integrating a set of non-linear equations over a moderate number of time steps, say several hundred, a certain form of instability arises, which is related to spatial truncation error in the non-linear terms. This non-linear instability, discussed by Phillips [7], seems to occur much more rapidly in primitive equations models than in those using a vorticity equation, though it is uncertain whether this is due to differences in the physical or mathematical behavior of the systems. At any rate there appear to be several possible devices for elimination of this instability, which will be mentioned later.

As a method of eliminating some of the computational redundancy, Eliassen [3] proposed a method of handling a two-level primitive equations model, in which variables are staggered in space and time in a somewhat complex manner. The principle on which the system was based was that the linear terms of the equations would be available at the correct grid points with minimal trunca-

tion error, but that certain non-linear terms would be formed from products of interpolated values. The reason for doing this, presumably, was that the linear terms of the motion equations, the pressure gradient and Coriolis terms, are generally an order of magnitude larger than the others and errors in these terms might be thought to be most damaging. On the other hand the advective terms may contribute as much, and in many cases much more, toward significant rates of change of quantities than the combination of the nearly balanced linear terms. As long as truncation error does not disturb the existing quasi-balance between the linear terms which is most pronounced for the larger scales of motion, there seems no reason to require interpolation to be done only on the advective terms. It will be shown that the truncation error of interpolation in the proposed system is, at most, of the same order as that arising from the finite difference pressure gradient term, but that the latter is evaluated with less truncation error in the Eliassen grid than in that proposed.

Hinkelmann [4] and Smagorinsky [13] have successfully applied hydrostatically filtered equations of two-dimensional flow without the use of time or space staggering of the variables. In both of these models the external gravitational motions were filtered out by the vanishing boundary conditions on dp/dt, and it was therefore necessary to solve a Poisson equation at each time step. Both used the marching equations in the conservation form, and it was found that non-linear computational instability ensued, in the absence of specific damping terms, within two or three days of commencement of integration. Phillips [8] has recently developed a barotropic divergent (free surface) primitive equations model, in which the Eliassen grid system has been applied, with central time and space differencing, and also with a one-sided space difference scheme [9] oriented according to the wind direction and related to that originally proposed by Courant, Isaacson, and Rees [1]. The latter method introduces some computational damping and seems effectively to prevent development of non-linear instability.

2. PRINCIPLES OF PROPOSED SYSTEM AND APPLICATION

A method will now be presented for stepwise integration of initial-value boundary-value problems using non-linear hydrodynamic equations. The method appears to be generally applicable to meteorological problems when the system of equations is of an explicit marching type, that is when there are no physical approximations or constraints which involve the solution of an elliptic equation at each time step. It is evidently not particularly suitable for application to, for example, the barotropic vorticity equation, or to primitive equations models such as those of Smagorinsky and Hinkelmann in which external gravity waves are filtered out, because in these systems further interpolations would be necessary. A principal feature of the method is the casting of the equations into the conservation form, the form in which all advective terms appear as flux divergences. When this is done it becomes very natural to set up a central time and space differencing system on a space-time staggered grid, in which interpolations may be required only in certain linear terms. The method of interpolation is largely optional, but time interpolation is generally most accurate. If frictional terms are present (and it is believed that they generally should be) these are most naturally computed by forward differencing, which then simultaneously preserves linear computational stability in these terms. The method will be illustrated by application to a free surface model similar to that of Phillips.

If the atmosphere is considered as a homogeneous incompressible fluid with a free upper surface, whose height is ϕ/g, the two-dimensional, hydrostatically filtered equations of motion may be written, in Cartesian coordinates, as

$$\frac{\partial u_i}{\partial t}+u_j\frac{\partial u_i}{\partial x_j}-f\epsilon_{ij3}u_j+\frac{\partial \phi}{\partial x_i}=\frac{1}{\phi}\frac{\partial \tau_{ij}}{\partial x_j} \tag{1}$$

where ϵ_{ijk} is the permutation tensor, equal to plus or minus unity for $i, j, k=1, 2, 3$ or $2, 1, 3$ respectively.

Upon application of the viscosity hypothesis, but without assuming constant viscosity, the frictional stress may be written as

$$\tau_{ij}=\phi K\left(\frac{\partial u_i}{\partial x_j}+\frac{\partial u_j}{\partial x_i}-\frac{2\delta_{ij}}{\delta_{ii}}\frac{\partial u_k}{\partial x_k}\right). \tag{2}$$

The repeated index implies summation, so that δ_{ii} equals two in this case. If we were considering a physical system whose characteristic Reynolds number was small, for example a "dishpan" experiment, we could reasonably assume ϕK constant and the stress terms would reduce to the common Laplacian form. For the atmospheric system we want the stress tensor to describe the transfers of energy, momentum, etc., performed by turbulent eddy motions, the scales of which range between that of the smallest explicitly described motions and that of molecular dissipation. Smagorinsky [14] proposes that for fully turbulent flow K be made proportional to the deformation, i.e.

$$K=(kl)^2\left|\frac{\tau_{ij}}{\phi K}\right| \tag{3}$$

where l is the scale of the smallest resolvable motions (the grid scale in a finite difference formulation) and k is a universal constant of order unity. From consideration of the similarity of the above expression to that frequently applied in turbulent boundary layer theory we consider k to be analogous to the Kármán constant. The appearance of a particular length scale in the definition is a reflection of the essential correspondence of the frictional stress to the Reynolds stress, also defined in terms of the same length scale.

The form proposed by Smagorinsky is similar to one

applied by von Neumann and Richtmyer [10] in their "pseudo-viscosity" method for representing shock waves. It has been introduced here because of its seeming importance in elimination of the non-linear computational instability which is otherwise permitted by the proposed grid differencing scheme (and many others in current use). The physical significance and justification of these terms will be shown by Smagorinsky and are not discussed further here.

The continuity equation is a prediction equation for the height of the free surface, written as:

$$\frac{\partial \phi}{\partial t}+\frac{\partial(\phi u_j)}{\partial x_j}=0. \tag{4}$$

If (4) is multiplied by u_i and combined with (1), a momentum equation is obtained, that is

$$\frac{\partial(\phi u_i)}{\partial t}+\frac{\partial}{\partial x_j}(\phi u_i u_j)-f\epsilon_{ij3}\phi u_j+\frac{\partial(\phi^2/2)}{\partial x_i}=\frac{\partial \tau_{ij}}{\partial x_j}. \tag{5}$$

We now assume that motions within a rectangular area of dimensions L_i are cyclically symmetric in all directions, so that the boundary conditions may be written, in terms of an arbitrary dependent variable χ, as

$$\chi(x_1, x_2, t)=\chi(x_1\pm L_1, x_2, t)=\chi(x_1, x_2\pm L_2, t). \tag{6}$$

Equations (4), (5), and (6) are a complete set of prediction equations for the dependent variables, ϕu_i, ϕ, written in the conservation form.

We divide the $L_1\times L_2$ area into pq grid squares, each of area Δ^2, where p and q are both even numbers. Letting l and m represent the index numbers of grid intersections, and n a time index, we define

$$\chi_{l,m}^{(n)}=\chi(l\Delta, m\Delta, n\Delta t)=\chi_{l\pm p,m}^{(n)}=\chi_{l,m\pm q}^{(n)} \tag{7}$$

the latter two equalities proceeding directly from (6).

Let us now specify all the dependent variables at the even intersections ($l+m$ even) for even n and also all of them at the odd intersections for odd n. We then may approximate (4) and (5) by finite difference equations as follows:

$$\phi_{l,m}^{(n+1)}=\phi_{l,m}^{(n-1)}-\frac{\Delta t}{\Delta}[(\phi u_1)_{l+1,m}-(\phi u_1)_{l-1,m}+(\phi u_2)_{l,m+1}-(\phi u_2)_{l,m-1}]^{(n)} \tag{8}$$

$$(\phi u_1)_{l,m}^{(n+1)}=(\phi u_1)_{l,m}^{(n-1)}-\frac{\Delta t}{\Delta}[(\phi u_1^2+\phi^2/2-\tau_{11})_{l+1,m}-(\phi u_1^2+\phi^2/2-\tau_{11})_{l-1,m}+(\phi u_1 u_2-\tau_{12})_{l,m+1}-(\phi u_1 u_2-\tau_{12})_{l,m-1}]^{(n)}+2f\Delta t\overline{(\phi u_2)}_{l,m}^{(n)} \tag{9}$$

$$(\phi u_2)_{l,m}^{(n+1)}=(\phi u_2)_{l,m}^{(n-1)}-\frac{\Delta t}{\Delta}[(\phi u_1 u_2-\tau_{21})_{l+1,m}-(\phi u_1 u_2-\tau_{21})_{l-1,m}+(\phi u_2^2+\phi^2/2-\tau_{22})_{l,m+1}-(\phi u_2^2+\phi^2/2-\tau_{22})_{l,m-1}]^{(n)}-2f\Delta t\overline{(\phi u_1)}_{l,m}^{(n)}. \tag{10}$$

The stresses and the viscosity coefficient K may also be approximated, from (2) and (3) as:

$$(\tau_{11})_{l,m}^{(n)}=-(\tau_{22})_{l,m}^{(n)}=(\phi_{l,m}^{(n)}K_{l,m}^{(n-1)}/\Delta)[(u_1)_{l+1,m}-(u_1)_{l-1,m}-(u_2)_{l,m+1}+(u_2)_{l,m-1}]^{(n-1)} \tag{11}$$

$$(\tau_{12})_{l,m}^{(n)}=(\tau_{21})_{l,m}^{(n)}=(\phi_{l,m}^{(n)}K_{l,m}^{(n-1)}/\Delta)[(u_1)_{l,m+1}-(u_1)_{l,m-1}+(u_2)_{l+1,m}-(u_2)_{l-1,m}]^{(n-1)} \tag{12}$$

$$K_{l,m}=k^2\Delta\{[(u_1)_{l+1,m}-(u_1)_{l-1,m}-(u_2)_{l,m+1}+(u_2)_{l,m-1}]^2+[(u_1)_{l,m+1}-(u_1)_{l,m-1}+(u_2)_{l+1,m}-(u_2)_{l-1,m}]^2\}^{1/2}. \tag{13}$$

The bar over the Coriolis terms in (9) and (10) indicates that some form of interpolation or replacement must be done, since the quantities involved are not defined at the proper time-space grid points.

Four possible methods of interpolation are suggested. Spatial interpolation would involve replacement of the barred quantities in (9) and (10) as follows, according to either a 2-point or 4-point formula.

$$\left.\begin{aligned}&\overline{(\phi u_1)}_{l,m}^{(n)}\text{ is replaced by }1/2\,[(\phi u_1)_{l,m+1}+(\phi u_1)_{l,m-1}]^{(n)}\\&\text{and}\\&\overline{(\phi u_2)}_{l,m}^{(n)}\text{ is replaced by }1/2\,[(\phi u_2)_{l+1,m}+(\phi u_2)_{l-1,m}]^{(n)}\end{aligned}\right\} \tag{14}$$

or

$$\overline{(\phi u_i)}_{l,m}^{(n)}\text{ is replaced by }1/4\,[(\phi u_i)_{l+1,m}+(\phi u_i)_{l-1,m}+(\phi u_i)_{l,m+1}+(\phi u_i)_{l,m-1}]^{(n)}. \tag{15}$$

Other methods of spatial interpolation would involve somewhat larger truncation errors. For time interpolation one would use similar replacements as follows:

$$\overline{(\phi u_i)}_{l,m}^{(n)}\text{ is replaced by }1/2\,[(\phi u_i)_{l,m}^{(n+1)}+(\phi u_i)_{l,m}^{(n-1)}] \tag{16}$$

where (9) and (10) would then have to be linearly combined to eliminate the implicit terms. The resulting system will be shown to have negligible truncation error in the Coriolis terms, as well as a slightly less restrictive computational stability criterion. A simpler method involving somewhat larger but still acceptable truncation errors is a forward-backward scheme similar to that introduced by Courant, Friedrichs, and Lewy [2] for a linear wave problem. In this case the barred quantities in (9) and (10) are replaced as follows:

$$\left.\begin{aligned}&\overline{(\phi u_1)}_{l,m}^{(n)}\text{ is replaced by }(\phi u_1)_{l,m}^{(n-1)}\\&\overline{(\phi u_2)}_{l,m}^{(n)}\text{ is replaced by }(\phi u_2)_{l,m}^{(n+1)}.\end{aligned}\right\} \tag{17}$$

It may be noted that the frictional terms in (11), (12), and (13) involve velocity derivatives at time index $(n-1)$ weighted by ϕ values at time index (n). This inconsistency (if such it is) seems from experience to be totally

unimportant. It has, in fact, been convenient to compute similar frictional terms over considerably longer time steps than the remainder of the calculations, and little error is so introduced. It is well known, however, that straightforward central differencing for the diffusion equations may lead to linear computational instability (see, e.g., Richtmyer [10]).

With regard to initial conditions, it may be desired to begin computations with values of variables all pertaining to the same time, rather than in the staggered grid. In this case it is satisfactory to make an initial half-time step, and similarly to interpolate between time steps in order to obtain a simultaneous display at a later time.

3. TRUNCATION ERROR AND COMPUTATIONAL STABILITY

We shall not attempt to give a complete discussion of the computational stability and truncation error of finite difference formulations of (1)–(4). We have, however, determined the stability properties of linearized versions of several finite difference equivalents of the frictionless system and first approximations to the truncation errors of various terms in the motion equations. This material is assembled in tables 1 and 2. The expressions given for truncation error are the lowest order terms of the Taylor series, and are presented in this form for comparative purposes rather than for any attempt at numerical evaluation. The grid formulations used include (a) the normal advective form, based on equation (1) with central differencing and no interpolations; (b) the proposed staggered grid system with 2-point and 4-point space interpolations, time interpolation, and forward-backward treatment of the Coriolis terms; and (c) the Eliassen grid as used by Phillips [8]. Figures 1 and 2 illustrate the essential difference between these grid systems. In the normal advective scheme all variables are defined at all intersections of figure 1, while in the proposed staggered system all quantities are defined for even time-steps at grid points marked "E" and for odd time at points "O". In the Eliassen scheme the geopotential, ϕ, is defined on grid "A" of figure 2 for even time and grid "D" for odd time, u_1 is defined on grid "B" for odd time and grid "C" for even, and u_2 on grid "C" for odd time and grid "B" for even. The grid interval shown on figure 2 was altered to $(1/\sqrt{2})$ of that defined by Phillips in order that the truncation errors for the various systems be comparable. Thus in all cases the total number of points describing a given field, combining odd and even time steps, is given by the ratio of the total area to Δ^2.

Table 1 shows that the non-viscous linear computational stability characteristics are similar for all the grid-differencing systems considered. The differences lie in the Coriolis term, which is ordinarily two to three orders of magnitude smaller than that arising from the external gravity wave propagation. It may be easily demonstrated that the friction terms, computed in the form described, exert an effect on the stability criterion of at most the same order of magnitude as the advection.

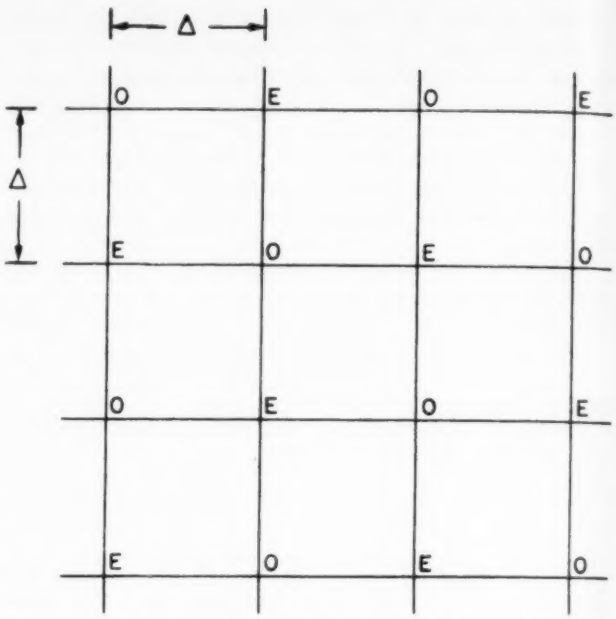

FIGURE 1.—Grid system for normal advective scheme, in which all variables are defined at all intersections; and for proposed staggered system, in which all quantities are defined for even time-steps at points E and for odd time at points O.

Upon careful examination of table 2 we find that truncation errors also do not present any clear superiority of one system over another. Truncation errors in the geostrophic terms are certainly minimized in the Eliassen scheme, because of the smaller differencing interval in the pressure term. Nevertheless the unavoidable error of first-order differencing of the pressure term is of the same order as that of spatial interpolation of the balancing Coriolis term, so that introduction of the latter breeds no

Table 1.—*Linear computational stability criteria*

Normal advective	$\frac{\Delta}{\Delta t} > \lvert u_i \rvert + \sqrt{2\phi + (f\Delta)^2}$
Space-interpolated staggered	$\frac{\Delta}{\Delta t} > \lvert u_i \rvert + \sqrt{2\phi + (f\Delta)^2}$
Time-interpolated staggered	$\frac{\Delta}{\Delta t} > \lvert u_i \rvert + \sqrt{2\phi}$
Forward-backward staggered	$\frac{\Delta}{\Delta t} > \lvert u_i \rvert + \sqrt{2\phi + (f\Delta)^2}$
Eliassen	$\frac{\Delta}{\Delta t} > \lvert u_i \rvert + \sqrt{2\phi + (f\Delta)^2/2}$

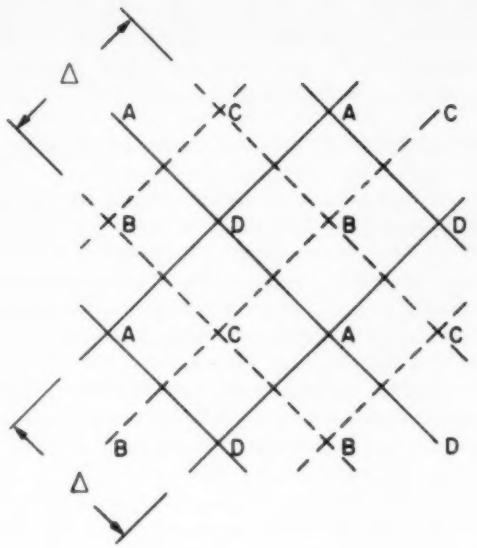

FIGURE 2.—The Eliassen scheme in which the geopotential ϕ is defined on grid A for even time and on grid D for odd time, u_1 is defined on grid B for odd time and on grid C for even time, and u_2 is defined on grid C for odd time and on grid B for even time.

new sources of error. Proper comparison of the various methods of interpolating the Coriolis term is dependent upon specification of characteristic time and space scales of motion. For typical meteorological motions (small gravity-wave amplitude) the time interpolation has the smallest error, only a little larger than that of the time derivative term. The error of the forward-backward scheme is considerably larger and may be nearly as large as that of the space-interpolation method, depending on the spatial smoothness of the fields. Comparison of the truncation errors associated with the non-linear terms is more difficult. It appears, however, that terms of all systems are of roughly the same size except the Eliassen component along the wind, which is about four times larger.

All results available to the author indicate that all the systems considered above exhibit non-linear computational instability unless their short-wave components are effectively damped. Our understanding of this phenomenon is, however, severely restricted by the present lack of general methods of its analysis. Phillips' [7] method may be used to prove instability, in some cases, but it can never prove stability. Trial-and-error methods are rather inefficient, with the large number of possible methods to choose among. Shuman [11] has, however, recently performed one-dimensional numerical experiments, the results of which raise the possibility that certain reasonable

TABLE 2.—*Truncation errors of terms in equations of motion*

1. Pressure derivative term; e.g. $\frac{\partial \phi}{\partial x_1}$	
Normal advective	$\frac{\Delta^2}{6}\frac{\partial^3 \phi}{\partial x_1^3}$
Staggered	$\frac{1}{\phi}\frac{\Delta^2}{12}\frac{\partial^3 \phi^2}{\partial x_1^3}$
Eliassen	$\frac{\Delta^2}{12}\frac{\partial^3 \phi}{\partial x_1^3}$
2. Coriolis term; e.g. fu_2	
Normal advective	None
2-point space-interpolated staggered	$\frac{f}{\phi}\frac{\Delta^2}{8}\frac{\partial^2(\phi u_2)}{\partial x_1^2}$
4-point space-interpolated staggered	$\frac{f}{\phi}\frac{\Delta^2}{16}\nabla^2(\phi u_2)$
Time-interpolated staggered	$\frac{f}{\phi}\frac{(\Delta t)^2}{2}\frac{\partial^2(\phi u_2)}{\partial t^2}$
Forward-backward staggered	$\frac{f}{\phi}(\Delta t)\frac{\partial(\phi u_2)}{\partial t}$
Eliassen	None
3. Time derivative, e.g. $\frac{\partial u_1}{\partial t}$	
Normal advective	$\frac{(\Delta t)^2}{6}\frac{\partial^3 u_1}{\partial t^3}$
Staggered	$\frac{1}{\phi}\frac{(\Delta t)^2}{6}\frac{\partial^3(\phi u_1)}{\partial t^3}$
Eliassen	$\frac{(\Delta t)^2}{6}\frac{\partial^3 u_1}{\partial t^3}$
4. Advection term along wind component; e.g. $u_1\frac{\partial u_1}{\partial x_1}$	
Normal advective	$\frac{\Delta^2}{6}u_1\frac{\partial^3 u_1}{\partial x_1^3}$
Staggered	$\frac{1}{\phi}\frac{\Delta^2}{6}\frac{\partial^3(\phi u_1^2)}{\partial x_1^3}$
Eliassen	$\frac{\Delta^2}{6}\left(\frac{\partial^2}{\partial x_1^2}+3\frac{\partial^2}{\partial x_2^2}\right)\frac{\partial u_1^2}{\partial x_1}$
5. Advective term across wind component; e.g. $u_2\frac{\partial u_1}{\partial x_2}$	
Normal advective	$\frac{\Delta^2}{6}u_2\frac{\partial^3 u_1}{\partial x_2^3}$
Staggered	$\frac{1}{\phi}\frac{\Delta^2}{6}\frac{\partial^3(\phi u_1 u_2)}{\partial x_2^3}$
Eliassen	$\frac{\Delta^2}{12}u_2\left(3\frac{\partial^2}{\partial x_1^2}+\frac{\partial^2}{\partial x_2^2}\right)\frac{\partial u_1}{\partial x_2}$

difference schemes may be stable without damping. If these results can be shown to apply to a more general model we may have a close counterpart to the spectral method which in some cases may conserve energy identically.

The eddy-viscosity term proposed by Smagorinsky obviously exerts a damping which is highly selective in scale. For a given amplitude of disturbance kinetic energy and a given grid interval the value of K is proportional to the finite difference approximation of the deformation amplitude. When central differencing is used each contribution to this amplitude will be proportional to sin $(2\pi\Delta/\lambda)$, where λ is the wavelength of a motion component. Thus damping is maximized for wavelengths at and near 4Δ and actually vanishes at $\lambda=2\Delta$. Since components with wavelengths between 2Δ and 4Δ are most directly involved in non-linear instability it is therefore suggested that the viscosity term prevents the instability indirectly. That is, it reduces the amplitudes of the intermediate scale (stable) components which would otherwise generate small-scale (unstable) components. If this is the case we may have reasonable confidence that the important effects of the analytic viscosity terms (2), (3) are fairly well approximated by their finite difference formulation.

Other methods that have been used to prevent nonlinear instability do more or less violence to the physics. Probably the worst method is to use a constant viscosity, or its equivalent in a difference system or smoothing filter. Experiments have shown that in order to be effective the viscosity must be large enough so that the *greatest* characteristic grid Reynolds number of the field is of order unity, where by contrast we note that Smagorinsky's eddy viscosity is of such a form that the grid Reynolds number is *everywhere* of order unity. In order to simulate motions of a turbulent fluid one would then have to carry millions of grid points, otherwise the system would be essentially laminar and the large-scale components severely oversmoothed. Lax [6] suggested a space-time staggered grid for integration of equations in the conservation form. Forward-time differencing was used and variables at the previous time were space-averaged before differencing. This process effectively introduces a very large constant computational viscosity, essentially equal to $\Delta^2/4\ \Delta t$, and the grid Reynolds number is of order $u/\sqrt{\phi}\ll 1$. On somewhat the opposite extreme of selectivity is the method used by Phillips [7] in his general circulation calculations, which consisted of Fourier-analyzing the motion field and removing all components with wavelengths less than 4Δ. Somewhere between these extremes lies the one-sided difference scheme first suggested by Courant, Isaacson, and Rees [1], in which the advective form of the vector equation of motion is used and spatial derivatives are taken along the characteristics (streamlines) upward of the central point. Variants of this method have been used by Kasahara [5] and Phillips [9]. Motions are damped, but rather selectively, and the general results appear to be very similar to those obtained using Smagorinsky's eddy friction form, although the physical significance is unclear.

4. OTHER COMPUTATIONAL FEATURES

An advantage of the proposed system, in comparison with, for example, the Eliassen grid, is the vanishing truncation error of volume integrals (numerical sums) of the prediction variables. Smagorinsky [12] has shown that this is assured by application of certain auxiliary boundary conditions (mainly symmetry conditions) and these in turn prevent development of another type of computational instability. The importance of this feature probably depends somewhat on the use to which the particular prediction system is put. For general circulation studies, where integrated momentum budgets, heat budgets, etc. are of fundamental interest, it seems very desirable to know that, for example, the mean geopotential is only a function of the boundary conditions. For operational forecasting this may be of less direct interest, though perhaps comforting knowledge. In any case it has proven to be valuable for "debugging" machine program logic, for determination of machine errors, and for evaluation of round-off errors.

The proposed system has certain other practical advantages for application to a high-speed electronic computer, not all of which are shared by other systems. First, only one set of variables need be stored for each point, in distinction to the two or three required for a non-staggered grid using forward-differenced viscous terms. Second, there are just two kinds of points, rather than four as in the Eliassen system, which makes the logic somewhat simpler. On the other hand, application of any staggered grid system adds definite logical complications to a machine program, thus increasing the programming and check-out time and, to a small extent, the time spent by the machine in logical testing.

5. APPLICATION TO OTHER MODELS

The proposed method was originally developed for, and applied to, integration of a set of two-dimensional (x_1, x_3) equations used for the simulation of dry convective motions. The system used was the following:

$$\frac{\partial(\rho u_i)}{\partial t}+\frac{\partial}{\partial x_j}(\rho u_i u_j)+\frac{\partial p}{\partial x_i}+g\rho\delta_{i3}=\frac{\partial \tau_{ij}}{\partial x_j}$$

$$\frac{\partial \rho}{\partial t}+\frac{\partial}{\partial x_j}(\rho u_j)=0$$

$$\frac{\partial(\rho\theta)}{\partial t}+\frac{\partial}{\partial x_j}(\rho u_j\theta)=\frac{\partial H_j}{\partial x_j}$$

where pressure is obtained from the equation of state in the form

$$\frac{p}{p_0}=\left(\frac{R\rho\theta}{p_0}\right)^{\kappa}$$

and the friction-diffusion terms were of a similar form, though more complex, than those described above.

The grid scheme outlined above is clearly applicable to this set, where the linear density term in the vertical momentum equation must be interpolated. In this case it is possible to interpolate density either spatially or timewise. Integrations have been successfully performed using two-point (vertical) and four-point spatial interpolation and linear time interpolation, the results of which will be reported elsewhere.

If the above set of equations were modified to exclude sound wave propagation, by elimination of the time derivative of density and formation of a vorticity equation, it would then not be practical to apply the proposed system. On the other hand, it can evidently be applied to a multi-level hydrostatically filtered baroclinic model, provided that the vertically integrated divergence is not constrained. The applicability of the system depends not on the scale or complexity of the model but only on the absence of a constraining elliptic differential equation.

6. SUMMARY

It has been demonstrated theoretically and, in one particular case, practically, that the staggered grid system here proposed can be advantageously applied in the integration of purely marching type hydrodynamic-thermodynamic models. The method is of a similar type to Eliassen's but essentially opposite in its basic principles, in that here the linear terms may be interpolated, spatially or perhaps preferably in time, while the advective terms are applied with centered differencing in the conservation form. Physical considerations suggest the abstraction of energy from grid-scale motions by parametric simulation of eddy exchange processes, and Smagorinsky's suggested method for doing this seems to be sufficient for maintenance of computational stability. The essential features of the system have been described within the framework of a rotating incompressible barotropic fluid model with a free surface, while its practical application has been to a somewhat more complex model of a compressible fluid with thermal convection.

REFERENCES

1. R. Courant, E. Isaacson, and M. Rees, "On the Solution of Non-Linear Hyperbolic Differential Equations by Finite Differences," *Communications Pure and Applied Mathematics*, vol. 5, 1952, p. 243.
2. R. Courant, K. O. Friedrichs, and H. Lewy, "Über die partiellen Differenzengleichungen der Mathematischen Physik," *Mathematische Annalen*, vol. 100, 1928, p. 32.
3. A. Eliassen, "A Procedure for Numerical Integration of the Primitive Equations of the Two-Parameter Model of the Atmosphere," *Scientific Report* No. 4 on Contract AF19(604)–1286, Dept. of Meteorology, University of California at Los Angeles, 1956, 53 pp.
4. K. Hinkelmann, "Ein Numerisches Experiment mit den primitiven Gleichungen," pp. 486–500 of *The Atmosphere and the Sea in Motion* (Rossby Memorial Volume), Rockefeller Institute Press, in association with Oxford University Press, New York, 1959, 509 pp.
5. A. Kasahara, "A Numerical Experiment on the Development of a Tropical Cyclone," *Technical Report* No. 12 on U.S. Weather Bureau Contract No Cwb–9718, The University of Chicago, 1960.
6. P. D. Lax, "Weak Solutions of Non-Linear Hyperbolic Equations and their Numerical Computation," *Communications Pure and Applied Mathematics*, vol. 7, 1954, p. 159.
7. N. A. Phillips, "An Example of Non-Linear Computational Instability," pp. 501–504 of *The Atmosphere and the Sea in Motion* (The Rossby Memorial Volume), Rockefeller Institute Press in association with Oxford University Press, New York, 1959, 509 pp.
8. N. A. Phillips, "Numerical Integration of the Primitive Equations on the Hemisphere," *Technical Report*, Numerical Weather Prediction Project, Department of Meteorology, Massachusetts Institute of Technology, Cambridge, Mass., 1959.
9. N. A. Phillips, "Calculations for the Hemisphere with the Barotropic Primitive Equations," Paper presented at the International Symposium on Numerical Weather Prediction, Tokyo, Japan, November 7–13, 1960.
10. R. D. Richtmyer, *Difference Methods for Initial-Value Problems*, Interscience Publishers, Inc., New York, 1957, 238 pp.
11. F. G. Shuman, "A Numerical Study of Non-Linear Computational Instability," Paper presented at the Third Numerical Weather Prediction Conference, June 27–30, 1960, Chicago, Ill.
12. J. Smagorinsky, "On the Numerical Integration of the Primitive Equations of Motion for Baroclinic Flow in a Closed Region," *Monthly Weather Review*, vol. 86, No. 12, Dec. 1958, pp. 457–466.
13. J. Smagorinsky, "General Circulation Experiments with the Primitive Equations: I. The Basic Experiment," 1961. (To be published.)
14. J. Smagorinsky, 1961. (To be published.)

Publications by Weather Bureau Authors

H. L. Crutcher, "Upper Wind Statistics of the Northern Hemisphere," vol. I (850, 700, and 500-mb. levels), and vol. II (300, 200, and 100-mb. levels), *NAVAER* 50-1C-535, Office of the Chief of Naval Operations, August 1959.

G. C. Holzworth (with J. A. Maga), "A Method for Analyzing the Trend in Visibility," *Journal of the Air Pollution Control Association*, vol. 10, No. 6, Dec. 1960, pp. 430–435.

C. D. Hopkins, Jr., "A Method of Estimating Basin Temperatures in New England and New York," *Journal of Geophysical Research*, vol. 65, No. 11, Nov. 1960, pp. 3767–3771.

L. F. Hubert, S. Fritz, and H. Wexler, "Pictures of the Earth from High Altitudes and Their Meteorological Significance," pp. 3–7 of *Space Research, Proceedings of the First International Space Science Symposium, Nice, January 11–16, 1960*, H. K. Bijl, ed., North-Holland Publishing Co., Amsterdam, 1960.

J. D. Kangos, "A Preliminary Investigation of the Heat Flux from the Ocean to the Atmosphere in the Antarctic Region," *Journal of Geophysical Research*, vol. 65, No. 12, Dec. 1960, pp. 4007–4012.

A. L. King, "Drainage, A Vital Need in Irrigated Humid Areas," *Journal of the Irrigation and Drainage Division, Proceedings of the American Society of Civil Engineers*, vol. 86, No. IR4, Dec. 1960, pp. 81–100.

P. M. Kuhn (with C. B. Tanner and J. A. Businger), "The Economical Net Radiometer," *Journal of Geophysical Research*, vol. 65, No. 11, Nov. 1960, pp. 3657–3667.

P. M. Kuhn (with V. E. Suomi), "Infrared Radiometer Soundings on a Synoptic Scale," *Journal of Geophysical Research*, vol. 65, No. 11, Nov. 1960, pp. 3669–3677.

J. K. McGuire (with L. A. Kapp), "The Influence of Climate on Patients with Cardiovascular Disease," *CP* (The General Practitioner), vol. XXII, No. 6, Dec. 1960, pp. 89–99.

J. Namias, "Snowfall over Eastern United States: Factors Leading to Its Monthly and Seasonal Variations," *Weatherwise*, vol. 13, No. 6, Dec. 1960, pp. 238–247.

M. J. Rubin, "Review of 'Notes on Weather Analysis in the Falkland Islands Dependencies, Antarctica,' by A. W. Mansfield and S. D. Glassy, *Scientific Report* No. 16, Falkland Islands Dependencies Survey, Colonial Office, London, 1957," *Bulletin of the American Meteorological Society*, vol. 41, No. 12, Dec. 1960, p. 703.

J. Smagorinsky (with A. Eliassen and J. S. Sawyer), "Upper Air Network Requirements for Numerical Weather Prediction," *Technical Note* No. 29, World Meteorological Organization, Geneva, 1960.

D. Q. Wark, "On Indirect Temperature Soundings of the Stratosphere from Satellites," *Journal of Geophysical Research*, vol. 66, No. 1, Jan. 1961, pp. 77–82.

H. Wexler, "Meteorology," in Chapter III "The Earth," pp. 14–22 of *Science in Space*, Space Science Board, NAS–NRS, 1960.

H. Wexler, "Review of *Atlantic Hurricanes* by G. E. Dunn and B. I Miller, Louisiana State University Press, 1960 326 pp.," *Science*, vol. 132, No. 3437, Nov. 11, 1960, p. 1392.

C. L. Woffinden, "Blocking Action," Letter to Editor, *The Meteorological Magazine*, vol. 89, No. 1058, Sept. 1960, pp. 236–240.

New Weather Bureau Publication

Research Paper No. 42, "A Detailed Analysis of the Fargo Tornadoes of June 20, 1957," by T. Fujita, U.S. Weather Bureau, Washington, D.C., 1960, 67 pp. For sale by Superintendent of Documents, U.S. Government Printing Office, Washington 25, D.C. Price: 45 cents.

The research reported in this paper was conducted by the University of Chicago for the U.S. Weather Bureau. Using the abundant photographs of the five individual tornadoes of this family, the author successfully triangulated the dimensions of the system from the tornado funnel to the entire rotating cloud. Important results in regard to the intense vertical motion inside the wall cloud and the possibility of liquid water storage inside the rotating cloud will lead to future theoretical studies of tornadoes and their related systems. Numerous photographs show the tornadoes in action.

DIAGNOSIS OF DIVERGENCE IN A THREE-PARAMETER NUMERICAL PREDICTION MODEL

A. WIIN-NIELSEN

Joint Numerical Weather Prediction Unit, Air Weather Service, Suitland, Md.
[Manuscript received November 9, 1960; revised January 11, 1961]

ABSTRACT

The equation for the vertical velocity in a quasi-non-divergent, three-parameter model has been solved for a certain simple flow pattern. The importance of vertical variation of static stability and of the horizontal wind is discussed from the solutions. Examples showing the distribution of divergence relative to the synoptic systems are computed and compared with those obtained by other investigators. A general discussion of the factors influencing the mid-tropospheric divergence follows in section 4, and section 5 contains finally some remarks on the divergence in very long waves.

1. INTRODUCTION

The distribution of convergence and divergence and of vertical velocity relative to the atmospheric flow pattern has been a very important and most intriguing problem in synoptic and dynamic meteorology for many years. Due to the fact that these quantities have to be obtained by indirect methods numerous rules relating the distribution of divergence to the synoptic flow pattern have been formulated. Intensive synoptic studies (Fleagle, [2]) have resulted in characteristic distributions of divergence relative to the troughs and ridges. Theoretical studies by Charney [1] and others using a very general continuous model gave as a by-product the divergence fields in baroclinic waves. General agreement between the results of the synoptic and theoretical studies was apparent.

The different dynamical models applied in numerical weather prediction and in studies of the general circulation, except the non-divergent model, contain implicitly distributions of divergence and vertical velocity, but because most of the time integrations have been made with one- or two-parameter models it has not been too interesting to study the predicted distributions since the vertical variations are constrained to very simple patterns like parabolic distributions of vertical velocity with pressure and linear variations of divergence.

The experiments with quasi-non-divergent two-parameter models have shown that these models are not sufficiently accurate to predict the developments of strong baroclinic nature. Several reasons may be mentioned for these somewhat discouraging results, but it is evident that the two-parameter model which assumes a constant direction of the thermal wind is not able to describe the vertical variation of the temperature advection pattern. Quite frequently we find regions of cold air advection superimposed on warm air advection in the same vertical column and vice versa. The only way to incorporate such features is to introduce more information levels to get a better vertical resolution of the model.

From the operational point of view it is obvious that as few levels as possible are desirable. Not only does this decrease the time required to compute the forecasts, but the analysis problem becomes also less time consuming. One may therefore ask whether the addition of one extra information level will change the behavior of the model to such an extent that we can expect substantial differences between the three- and the two-parameter models.

It is the purpose of this study to show that the distributions of divergence and vertical velocity which are inherent in the three-parameter model show a great similarity to the distributions obtained by Charney [1], Fleagle [2] and more recently Hinkelmann [3]. A treatment of the three-parameter model as compared to the continuous case has the advantage that the solutions for divergence and vertical velocity considering relatively simple flow patterns can be expressed in such a form that the importance of the different factors contained in the solution can be easily investigated. We shall thus be able to consider the importance of the vertical variation of stability and the variation of wind speed with height, especially a crude measure of the curvature of the wind profile. Another advantage in this case is that we shall be able to study the solution for different horizontal scales.

The vertical variation of static stability will in this study be prescribed as a function of pressure in such a way that we obtain the major part of its systematic climatological variation. It should be stressed that this variation does not necessarily correspond to the synoptic variability.

It is necessary to restrict the investigation in this paper to flow patterns where the zonal wind is constant in each

581868—61——2

isobaric surface, but of course can vary with pressure, and to waves of the simple sinusoidal type. The results which can be obtained in this way are of course not directly applicable to the real atmosphere with its much more complicated flow pattern. Solutions for observed atmospheric flow patterns can be obtained by numerical methods. The diagnosis of the real atmosphere using equations very similar to those in this paper is presented by Cressman in another paper in this issue.

2. THE COMPUTATION OF VERTICAL VELOCITY IN THE THREE-PARAMETER CASE

The three-parameter representation of the atmosphere allows a solution for the vertical velocity at two internal levels in each vertical column in addition to the two values obtained from the boundary conditions at the top of the atmosphere and at the ground. Using a finite difference form of the continuity equation we can consequently obtain three values of the divergence at the intermediate levels. In this paper we shall for simplicity divide the atmosphere into six layers, each corresponding to $p_g/6$ cb., where p_g is the pressure at the ground (fig. 1). We shall assume that $p_g=100$ cb. and thus neglect the effect of topography. The boundary conditions for the vertical velocity, $\omega=dp/dt$, will be $\omega=0$ for $p=0$ and $p\equiv p_g$. It is quite likely that it will be an advantage to assume $\omega=0$ at some level in the stratosphere in the practical application and also to include the effects of the topography and friction at the lower boundary.

The equation for the vertical velocity is obtained from the vorticity equation in the form:

$$\frac{\partial\zeta}{\partial t}+\mathbf{V}\cdot\nabla(\zeta+f)=f_0\frac{\partial\omega}{\partial p} \tag{2.1}$$

and the adiabatic equation

$$\frac{\partial}{\partial t}\left(\frac{\partial\psi}{\partial p}\right)+\mathbf{V}\cdot\nabla\left(\frac{\partial\psi}{\partial p}\right)+\frac{\sigma}{f_0}\omega=0. \tag{2.2}$$

In (2.1) and (2.2) $\mathbf{V}=\mathbf{k}\times\nabla\psi$ is the horizontal wind assumed to be nondivergent, $\mathbf{k}$ a vertical unit vector, ψ the streamfunction, $\zeta=\nabla^2\psi$ the vertical component of the relative vorticity, f the Coriolis parameter, $\omega=dp/dt$ the vertical velocity, and $\sigma=-\alpha\partial\ln\theta/\partial p$ a measure of static stability; α is specific volume and θ potential temperature. The vertical derivative of the geopotential has been replaced by the vertical derivative of the streamfunction in the adiabatic equation (2.2) using the approximate relation (Phillips [5])

$$\partial\psi/\partial p=1/f_0\cdot\partial\phi/\partial p \tag{2.3}$$

where $\phi=gz$ is the geopotential, g the acceleration of gravity, and z the height of the isobaric surface.

From (2.1) and (2.2) we obtain the ω-equation

$$\sigma\nabla^2\omega+f_0^2\frac{\partial^2\omega}{\partial p^2}=f_0\left[\frac{\partial}{\partial p}\left(\mathbf{V}\cdot\nabla\left(\zeta+f\right)\right)-\nabla^2\left(\mathbf{V}\cdot\nabla\frac{\partial\psi}{\partial p}\right)\right]. \tag{2.4}$$

In the derivation of (2.4) it has further been assumed that the horizontal variation of the static stability can be neglected, while a vertical variation is still possible.

The procedure to be followed is now to apply (2.4) at the levels 2 and 4 (see fig. 1), to approximate vertical derivatives by finite differences in a straightforward way, and in this way obtain two equations both containing ω_2 and ω_4 as unknowns. The streamfunction, ψ, has then to be known at the levels 1, 3, and 5. It is, however, convenient to introduce the new quantities

$$\left.\begin{aligned}\psi'&=\psi_1-\psi_3\\ \psi''&=\psi_3-\psi_5\end{aligned}\right\} \tag{2.5}$$

ψ' and ψ'' are the streamfunctions for the thermal flow in the layers between levels 1 and 3 and levels 3 and 5, respectively, and are of course measures of the mean temperatures in these layers.

Applying finite differences and using the boundary conditions for ω, we arrive after certain simple manipulations at the following set of equations for ω_2 and ω_4:

$$\left.\begin{aligned}\sigma_2\nabla^2\omega_2-\frac{2f_0^2}{P^2}\omega_2+\frac{f_0^2}{P^2}\omega_4&=\frac{f_0}{P}\left[\nabla^2(\mathbf{V}_3\cdot\nabla\psi')\right.\\ &\qquad\left.-\mathbf{V}_3\cdot\nabla\zeta'-\mathbf{V}'\cdot\nabla\eta_3-\mathbf{V}'\cdot\nabla\zeta'\right]\\ \sigma_4\nabla^2\omega_4-\frac{2f_0^2}{P^2}\omega_4+\frac{f_0^2}{P^2}\omega_2&=\frac{f_0}{P}\left[\nabla^2(\mathbf{V}_3\cdot\nabla\psi'')\right.\\ &\qquad\left.-\mathbf{V}_3\cdot\nabla\zeta''-\mathbf{V}''\cdot\nabla\eta_3+\mathbf{V}''\cdot\nabla\zeta''\right].\end{aligned}\right\} \tag{2.6}$$

P is a constant pressure interval equal to $33\frac{1}{3}$ cb. Equations (2.6) is the system which has to be solved for ω_2 and ω_4 given the three streamfunctions ψ_3, ψ', and ψ''.

The three streamfunctions will be prescribed by the expressions:

$$\left.\begin{aligned}\psi_3&=-U_3y+A_3\sin kx\\ \psi'&=-U'y+A'\sin(kx+\alpha')\\ \psi''&=-U''y+A''\sin(kx+\alpha'').\end{aligned}\right\} \tag{2.7}$$

U_3, U', and U'' are the zonal wind at level 3 and the thermal winds in the layers above and below this level. All three will be assumed to be constant. A_3, A', and A'' are the amplitudes of the streamfunctions. It is seen that kA_3, kA' and kA'' are the maximum meridional wind components in the three fields. α' and α'' measure the phase lag of the two thermal fields relative to the streamfunction at level 3. Positive values of the α's mean that the thermal field is lagging behind the stream field at level 3.

It is pertinent to mention that the values of α' and α'' determine the mean slope of the trough and ridge lines in the layers between the levels 1 and 3 and the levels 3 and 5, respectively. α' and α'' determine together a measure of the change in slope with height of the pressure systems.

The flow pattern at level 1 is obtained by adding the expressions for ψ_3 and ψ'. Applying simple trigonometric formulas we may write the streamfunction at level 1 in the form:

$$\psi_1=-(U_3+U')y+A_1\sin(kx+\gamma_1) \tag{2.8}$$

where

$$A_1=(A_3^2+A'^2+2A_3A'\cos\alpha')^{1/2} \tag{2.9}$$

and

$$\tan\gamma_1=\frac{A'\sin\alpha'}{A_3+A'\cos\alpha'}. \tag{2.10}$$

It is thus seen that γ_1 will be positive if $\alpha'>0$ provided α' is not so large that $A_3+A'\cos\alpha'<0$. In a similar way the flow pattern at level 5 can be written:

$$\psi_5=-(U_3-U'')y+A_5\sin(kx-\gamma_5) \tag{2.11}$$

where

$$A_5=(A_3^2+A''^2-2A_3A''\cos\alpha'')^{1/2} \tag{2.12}$$

and

$$\tan\gamma_5=\frac{A''\sin\alpha''}{A_3-A''\cos\alpha''}. \tag{2.13}$$

Again we find that γ_5 and α'' in general have the same sign for atmospheric flow patterns. We have thus seen that positive values of α' and α'' mean that the flow at level 1 is lagging behind the flow pattern at level 3, while the flow pattern at level 5 precedes that at level 3. Positive values of α' and α'' indicate therefore the usual westward tilt of the pressure systems, but the slope of a system is not necessarily linear in pressure.

When the expressions (2.7) are substituted in the right hand sides of equations (2.6) we get the following set of equations:

$$\left.\begin{aligned}\sigma_2\nabla^2\omega_2-\frac{2f_0^2}{P^2}\omega_2+\frac{f_0^2}{P^2}\omega_4&=\frac{f_0}{P}\,[2U'k^3A_3\cos kx\\&\quad -kA'(\beta-U'k^2)\cos(kx+\alpha')]\\ \sigma_4\nabla^2\omega_4-\frac{2f_0^2}{P^2}\omega_4+\frac{f_0^2}{P^2}\omega_2&=\frac{f_0}{P}\,[2U'''k^3A_3\cos kx\\&\quad -kA''(\beta+U'''k^2)\cos(kx+\alpha'')].\end{aligned}\right\} \tag{2.14}$$

The solutions to the system (2.14) will be of the form:

$$\left.\begin{aligned}\omega_2&=B_1\cos kx+B_2\cos(kx+\alpha')+B_3\cos(kx+\alpha'')\\ \omega_4&=C_1\cos kx+C_2\cos(kx+\alpha')+C_3\cos(kx+\alpha'').\end{aligned}\right\} \tag{2.15}$$

The amplitudes $B_{1,2,3}$ and $C_{1,2,3}$ can be determined by substitution of (2.15) into (2.14) and equating the coefficients of $\cos kx$, $\cos(kx+\alpha')$, and $\cos(kx+\alpha'')$. When this procedure is carried through we find the following expressions for the two vertical velocities:

$$\omega_2=\frac{1}{\Delta}\frac{f_0}{P}\left[-\left\{U'\left(\sigma_4k^2+\frac{2f_0^2}{P^2}\right)+U'''\frac{f_0^2}{P^2}\right\}k^2c_3+\left(\sigma_4k^2+\frac{2f_0^2}{P^2}\right)(\beta-U'k^2)v'+\frac{f_0^2}{P^2}(\beta+U'''k^2)v''\right] \tag{2.16}$$

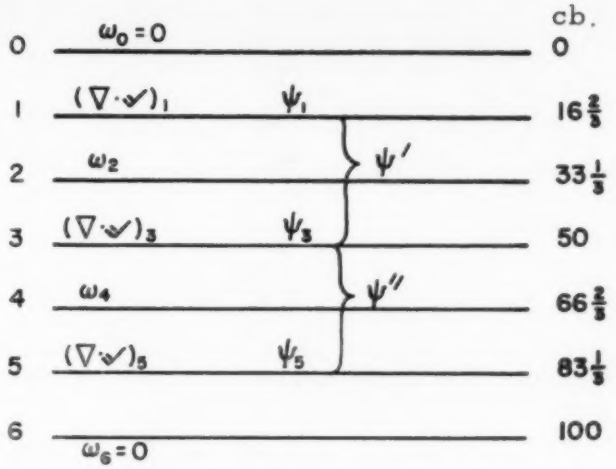

FIGURE 1.—Division of the atmosphere into six layers.

$$\omega_4=\frac{1}{\Delta}\frac{f_0}{P}\left[-\left\{U'\frac{f_0^2}{P^2}+U'''\left(\sigma_2k^2+\frac{2f_0^2}{P^2}\right)\right\}k^2c_3+\frac{f_0^2}{P^2}(\beta-U'k^2)v'+\left(\sigma_2k^2+\frac{2f_0^2}{P^2}\right)(\beta+U'''k^2)v''\right]. \tag{2.17}$$

The quantity, Δ, appearing in (2.16) and (2.17) is a notation for the following expression

$$\Delta=\left(\sigma_2k^2+\frac{2f_0^2}{P^2}\right)\left(\sigma_4k^2+\frac{2f_0^2}{P^2}\right)-\left(\frac{f_0}{P}\right)^4. \tag{2.18}$$

The meridional components $c_3=kA_3\cos kx$, $v'=kA'\cos(kx+\alpha')$, and $v''=kA''\cos(kx+\alpha'')$ have also been introduced in the solutions (2.16) and (2.17).

From the knowledge of ω_2 and ω_4 obtained from (2.16) and (2.17) we can evaluate the divergence at the levels 1, 3, and 5, if we at the same time use the boundary conditions for ω; i.e., $\omega=0$ for $p=0$ and $p=p_g$.

The divergences are evaluated from the continuity equation in finite difference form. We get

$$(\nabla\cdot\mathbf{V})_1=-\frac{\omega_2}{P},\quad(\nabla\cdot\mathbf{V})_3=-\frac{\omega_4-\omega_2}{P},\quad(\nabla\cdot\mathbf{V})_5=\frac{\omega_4}{P} \tag{2.19}$$

3. DISCUSSION OF THE SOLUTION AND SOME EXAMPLES

To best illustrate the distribution of divergence and vertical motion zonal cross-sections are appropriate. To produce such cross-sections it is necessary to obtain values for the parameters, which are parts of the coefficients.

In the first example we have chosen a wavelength of 4000 km. The stability parameters, σ_2 and σ_4, were determined in such a way that they correspond to the usual increase of this parameter with height. It has been shown (Wiin-Nielsen [6]) that the variation of σ with pressure is described with good accuracy using the expression

TABLE 1.—*Values of U' and U''.*

Date, GMT	U', m.sec.$^{-1}$	U'', m.sec.$^{-1}$
Feb. 8, 1959, 1200	22.0	14.0
Feb. 10, 1959, 1200	21.4	12.6
Feb. 12, 1959, 1200	21.2	10.8
Feb. 16, 1959, 1200	17.2	9.8
Feb. 20, 1959, 1200	8.8	13.2
Mean	18.1	12.1

$$\sigma(p)=\sigma_3\left(\frac{50}{p}\right)^2 \tag{3.1}$$

where σ_3 is the value of the stability at 50 cb. The present operational model applies a value of σ_3 equal to approximately 3 MTS-units. Using (3.1), we get

$$\sigma_2\simeq 9 \text{ MTS-units}, \quad \sigma_4\simeq 2.25 \text{ MTS-units}. \tag{3.2}$$

The values of the thermal winds, U' and U'', were determined from actual wind data for a number of individual days. The mean zonal winds were available at the levels 85, 50, and 30 cb. U' and U'' were then obtained by linear extrapolation and interpolation. The values are given in table 1.

The mean values, $U'=18$ m.sec.$^{-1}$, $U''=12$ m.sec.$^{-1}$ were used in the examples. The striking feature for the five days in February 1959 is that the average shear is 50 percent larger in the upper layer than in the lower layer. It is interesting to see whether this result holds in general for the middle latitude in winter. From wind statistics for the period February 10, 1959 to April 10, 1959 it was found that the mean value of U' was 16 m.sec.$^{-1}$ and of U'' 9.5 m.sec.$^{-1}$ Data presented by Petterssen ([4], p. 98) for Larkhill covering a 2-year period gave the values $U'=14$ m.sec.$^{-1}$, $U''=7$ m.sec.$^{-1}$ It may therefore be safely concluded that the vertical shear of the horizontal wind is somewhat larger above than below 50 cb. in middle latitudes in winter. The maximum values of the meridional wind components were chosen to be: $v'=12$ m.sec.$^{-1}$, $v''=8$ m.sec.$^{-1}$, and $v_3=16$ m.sec.$^{-1}$

The last two parameters for which numerical values have to be chosen are α' and α''. In the first computation the values $\alpha'=10°$ and $\alpha''=20°$ were selected. These values correspond to $\gamma_1=4°$ and $\gamma_5=14°$ as computed from (2.10) and (2.13). As 360° corresponds to 4000 km. we find that the trough line at level 1 is only about 44 km. behind the trough line at level 3, while the trough line at the lower level (level 5) precedes the trough at level 3 by about 156 km. This first case has therefore a very small slope but a somewhat larger slope in the lower layer than in the upper. This difference in slope is characteristic for many atmospheric systems.

Figure 2 shows the distribution of the divergence in a zonal cross-section through a half wavelength. The heavy dashed line in the central part of the figure is the position of the trough line. The heavy solid line is the isoline for zero-divergence. We find in this case that the nondivergent level outside the trough region is situated a little above the 500-mb. surface. However, as we approach the trough line from the west the line for zero-divergence goes down to lower levels and intersects level 5 to the west of the trough position. Approaching the trough line from the east the zero-divergence line goes up and intersects with level 1 to the east of the trough at this level. We find therefore convergence at all levels in the trough. At the lower level we find convergence to the east of the trough and divergence to the west, while the opposite is the case at the higher level.

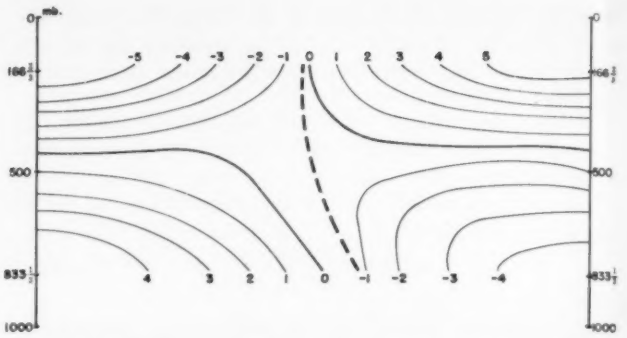

FIGURE 2.—Distribution of divergence in a zonal cross-section through a half wavelength. In this case the wavelength is 4000 km. and the stability parameters correspond to the usual increase of stability with height. West is to the left, east to the right. The heavy dashed line is the position of the trough line.

The distribution of divergence shown in figure 2 agrees to a very large extent with the distributions computed by Charney [1], Fleagle [2], and Hinkelmann [3]. It seems therefore that the major features of the distribution of divergence in a continuous model can be reproduced by a three-parameter model.

It was found of interest to investigate the distribution of divergence in the same zonal cross-section, if the vertical variation of the stability parameter was disregarded. In this computation it was assumed that $\sigma_2=\sigma_4=\sigma_3$ where σ_3 was set equal to a standard value. The resulting distribution of divergence is reproduced in figure 3. Comparing figure 2 with figure 3 one sees that the distributions are similar in a qualitative sense. The divergence pattern at level 3 has, however, an amplitude about 6 times larger in figure 3 than in figure 2, while the divergence is increased by a factor of 2 at level 1. It seems therefore important at least to incorporate an increase of the stability parameter σ with height in an operational model because the divergence and the vertical velocity are quite sensitive to this variation.

This fact is also illustrated in figure 4 which shows the distribution of the vertical velocity through a half wavelength at level 2. The solid line corresponds to the case where the vertical variation of stability is incorporated, while the dashed line is the distribution of the vertical

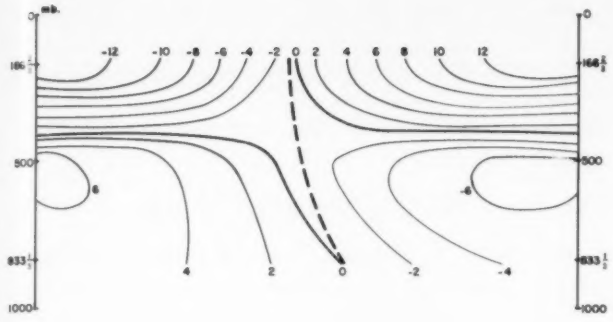

FIGURE 3.—Distribution of divergence in the same zonal cross-section as in figure 2. In this case the stability parameter is set to a standard value and does not vary in the vertical.

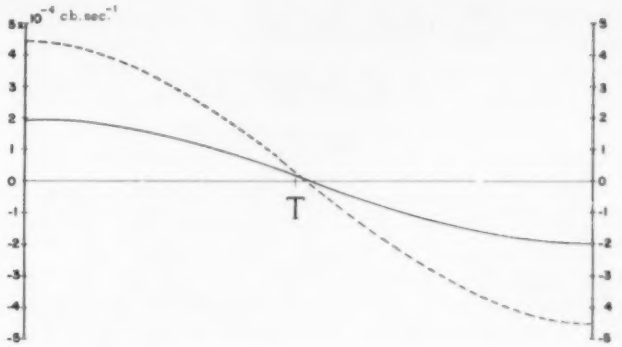

FIGURE 4.—Distribution of vertical velocity through a half wavelength at level 2 (33⅓ cb.). The solid line corresponds to the case with vertical variation of stability, the dashed line to the case of no vertical variation of stability. "T" designates position of the trough line.

velocity in the case where $\sigma_2=\sigma_4=\sigma_3$. The damping influence of the increase of the stability parameter, σ, is clearly seen in the figure. A similar figure (not reproduced) at the lower level (level 4) shows a very small difference between the corresponding curves. This is explained by the very small vertical variation of σ in the lowest layer of the troposphere.

4. ON SOME FACTORS INFLUENCING THE MID-TROPOSPHERIC DIVERGENCE

The divergence at level 3 estimated from the values of ω_2 and ω_4, which in turn are found by solving the two coupled ω-equations, will be used in a numerical prediction in the divergence term in the vorticity equation. It is therefore of importance to investigate the different factors which influence the distribution and magnitude of this divergence. In the present model with three information levels we have at least a first approximation to the curvature of the vertical profile of the zonal wind. We have further found in the preceding section that the vertical variation of the stability parameter is of importance for the magnitude of the mid-tropospheric divergence, but not so much for the distribution.

In order to simplify the first part of the discussion we shall for a moment neglect the vertical variation of the stability σ. With this simplification we obtain from (2.16) and (2.17)

$$(\nabla\cdot\mathbf{V})_3=\frac{f_0}{\sigma P^2+3f_0^2/k^2}\cdot[-2(U'-U'')r_3 -(U'-\beta/k^2)v'-(U''+\beta/k^2)v'']. \quad (4.1)$$

The first term in the bracket of (4.1) represents the influence on the divergence patterns at level 3 caused by the crude measure of the curvature of the vertical profile of the horizontal wind. It is seen that $(U'-U'')$ is proportional to the second derivative of U with respect to pressure:

$$\frac{d^2U}{dp^2}\simeq\frac{1}{P^2}(U'-U''). \quad (4.2)$$

If $U'>U''$ as in the example represented in figures 2 and 3 the first term will result in convergence where $r_3>0$, i.e. between the trough and the next ridge downstream, and divergence between the ridge and the following trough. The opposite distribution will result if $U'<U''$. The influence of the first term is therefore to increase the instantaneous speed of propagation of the wave if $U'>U''$, and to decrease the speed if $U'<U''$, but the term has no influence on the instantaneous deepening or filling.

In barotropic forecasts for 500 mb. it is often found that a trough is forecast to move too slowly in the southern portion, essentially in the region of the subtropical jet stream. According to synoptic investigations of the vertical wind profile in this wind system we find $U'>U''$. It is therefore possible that the contribution from the first term in (4.1) will help to remove this error.

Let us next turn our attention to the last two terms in (4.1). If the wavelength is so short that $(U'-\beta/k^2)$ is positive we find that both terms produce convergence where v' and v'' are positive and divergence where they are negative. If therefore the temperature patterns, ψ' and ψ'', are lagging behind the flow ψ_3, both of these terms contribute to produce convergence in the trough and thus give a tendency for deepening. However, for waves which are so long that $(U'-\beta/k^2)$ is negative, the second term changes sign and the two last terms counteract each other. In a qualitative way this argument shows that the shorter waves develop faster than the longer.

Equation (4.1) is somewhat simplified because we have assumed that $\sigma_2=\sigma_4$. If this assumption is removed we get a more complicated expression for the mid-tropospheric divergence. Subtracting (2.16) and (2.17) we obtain:

$$(\nabla \cdot \mathbf{V})_3 = \frac{f_0 k^2}{P^2 \Delta} [-\{U'(\sigma_4 k^2 + f_0^2/P^2) - U''(\sigma_2 k^2 + f_0^2/P^2)\} v_3$$

$$-(\sigma_4 k^2 + f_0^2/P^2)(U' - \beta/k^2) v'$$

$$-(\sigma_2 k^2 + f_0^2/P^2)(U'' + \beta/k^2) v'']. \quad (4.3)$$

The more general expression (4.3) shows that it is not only the difference in the vertical shear which counts in the first term in the bracket. The thermal wind U' in the upper layer is now multiplied by a factor depending on the stability in the lower layer, while U'' is multiplied by a factor containing the stability in the upper layer. Using standard values of σ_2 and σ_4 we can find the ratio $(U'/U'')_c$ which would give no contribution from the first term in the bracket of (4.3). The ratio $(U'/U'')_c$ is given as a function of wavelength in table 2 computed from the formula:

$$\left(\frac{U'}{U''}\right)_c = \frac{\sigma_2 k^2 + f_0^2/P^2}{\sigma_4 k^2 + f_0^2/P^2}. \quad (4.4)$$

From the table it is seen that the vertical variation of stability has the greatest influence on the divergence for the shorter waves. With no variation of the stability we get convergence ahead of the trough if only $(U' - U'')$ is positive. The values in table 2 show that U' would have to be at least two times larger than U'' to get the same sign of the divergence for a wave with a wavelength of 4000 km. The table shows also that only a minor modification is introduced for the very long waves as compared to the results derived from the simplified formula (4.1). For a given value of (U'/U'') characteristic of atmospheric conditions, say 1.5, the first term in (4.3) would result in divergence ahead of the trough in short waves, but convergence in the same region for long waves.

With respect to the last two terms in (4.3) we find some modification of the magnitude, but no change of the sign. The contributions from the terms are, however, large enough to give convergence to the east of the trough line in figure 2 as well as in figure 3.

Figure 5 shows the distribution of convergence and divergence in a zonal cross-section in a more extreme case. The distribution shown in figure 5 was computed using the same parameters as in figure 2 except that the phase differences between the temperature fields and the stream function at 500 mb. were larger in the case illustrated by figure 5. In the construction of figure 5 it was assumed that $\alpha' = 45°$ and $\alpha'' = 90°$, which means that the temperature field in the upper layer lags ⅛ of a wavelength behind the streamfunction at 500 mb., while the lag in the lower layer is ¼ of a wavelength. The result of the assumption is a larger slope of the trough line. From the formulas (2.10) and (2.13) it follows that the trough at level 5 precedes the 500-mb. trough by about 300 km., while the trough at level 1 lags about 210 km. behind the 500-mb. trough.

TABLE 2.—*Values of* $(U'/U'')_c$ *as a function of wavelength.*

$L \times 10^{-3}$ km.	1	2	3	4	5	6	7	8	10	12	14	28
$(U'/U'')_c$	3.6	3.0	2.4	2.0	1.7	1.5	1.4	1.3	1.2	1.2	1.1	1.0

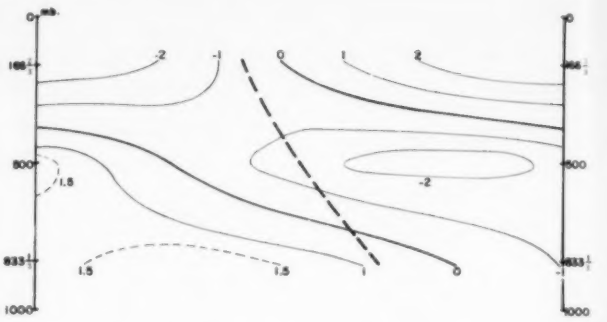

FIGURE 5.—Distribution of divergence in the same zonal cross-section as in figure 2. In this case the phase differences between the temperature fields and streamfunction at 500 mb. were larger than in case shown in figure 2.

The main effect of the greater vertical tilt of the system is, as seen from figure 5, to produce a larger slope of the convergence pattern. The convergence in and ahead of the trough line has now a maximum in the midtroposphere amounting to about 2×10^{-6} sec.$^{-1}$ with divergence above and below.

5. REMARKS ON THE DIVERGENCE IN VERY LONG WAVES

Due to the special difficulties encountered in forecasting the very long waves in the atmosphere it is of interest to investigate the distribution of divergence in such waves in the present model. It is apparent from (4.3) that the terms containing the vertical stability become of minor importance when the wave number is small. In the same case it is seen that the two β-terms become dominating in the last two terms of the bracket in (4.3). These two β-terms appear, however, with opposite sign and therefore tend to compensate if v' and v'' are of the same order of magnitude and in phase. The importance of the first term for the determination of the divergence distribution in this model is the difference, $(U' - U'')$. As we find that $(U' - U'')$ is positive in the jet stream regions where the waves have the greatest amplitude, the contribution is to produce convergence to the east of the trough and divergence to the west in the very long waves and thus obtain a decrease of the retrogression. Forecast experiments with the model will show whether the magnitude of the divergence is large enough to control the very long waves.

We may estimate the divergence from (4.3). Assuming the same values of the stability as in figure 3 ($\sigma_2=9$ and $\sigma_4=2.25$ MTS-units) and further $U'=18$ m.sec.$^{-1}$, $U''=12$ m.sec.$^{-1}$ we find in middle latitudes ($f_0=10^{-4}$ sec.$^{-1}$) for $k^2=0.2\times10^{-12}$m.$^{-2}$, corresponding to two waves around the hemisphere:

$$(\nabla\cdot\mathbf{V})_3=-[0.29\ v_3-3.78\ v'+6.29\ v'']\times10^{-8}\ \text{sec.}^{-1} \quad (5.1)$$

Assuming further that the waves v_3, v', and v'' are in phase and adopting the values $v_{3,\max}=16$ m.sec.$^{-1}$, $v'_{\max}=12$ m.sec.$^{-1}$, and $v''_{\max}=8$ m.sec.$^{-1}$ we find that

$$(\nabla\cdot\mathbf{V})_3\cong-10^{-7}\cos kx \quad (5.2)$$

if the streamfunction at level 3 is

$$\psi_3=-U_3\ y+A_3\sin kx. \quad (5.3)$$

We find therefore in this case a distribution of divergence which would counteract the retrogression of the very long waves.

6. SUMMARY AND CONCLUSIONS

The distribution of vertical velocity and divergence in a three-parameter model of the atmosphere has been investigated. Section 2 contains the formulation of the problem and the formal solution of the equation for the vertical velocity in the model for simple sinusoidal waves. The solution obtained in section 2 is discussed in the next section, where the importance of the vertical variation of static stability and the vertical profile of the horizontal wind is pointed out. Examples showing the distribution of divergence in zonal cross-sections are shown. It is found that the distribution of divergence in the three-level model to a large extent resembles distributions by others with more complicated models.

The different factors influencing the mid-tropospheric divergence are investigated in section 4. It is found that the vertical profile of the wind is most important for the speed of propagation of the waves, while the vertical slope of the waves contributes to the development.

The last section contains a discussion of the distribution of divergence in very long waves and an example is computed.

REFERENCES

1. J. G. Charney, "The Dynamics of Long Waves in a Baroclinic Westerly Current," *Journal of Meteorology*, vol. 4, No. 5, Oct. 1947, pp. 135–162.
2. R. G. Fleagle, "Quantitative Analysis of Factors Influencing Pressure Change," *Journal of Meteorology*, vol. 5, No. 6, Dec. 1948, pp. 281–292.
3. K. Hinkelmann, "Ein Numerisches Experiment mit den primitiven Gleichungen," pp. 486–500 of *The Atmosphere and the Sea in Motion* (Rossby Memorial Volume), Rockefeller Institute Press, in association with Oxford University Press, New York, 1959, 509 pp.
4. S. Petterssen, *Weather Analysis and Forecasting*, vol. 1 "Motion and Motion Systems," McGraw-Hill Book Co. Inc., New York, 1956.
5. N. A. Phillips, "Geostrophic Errors in Predicting the Appalachian Storm of November 1950," *Geophysica*, vol. 6, No. 3–4, 1958, pp. 389–405.
6. A. Wiin-Nielsen, "On Barotropic and Baroclinic Models, with Special Emphasis on Ultra-Long Waves," *Monthly Weather Review*, vol. 87, No. 5, May 1959, pp. 171–183.

A DIAGNOSTIC STUDY OF MID-TROPOSPHERIC DEVELOPMENT

GEORGE P. CRESSMAN

Joint Numerical Weather Prediction Unit, U.S. Weather Bureau, Suitland, Md.

[Manuscript received November 9, 1960; revised January 11, 1961]

ABSTRACT

An equation for vertical velocity is applied to data from 850, 500, and 200 mb. for calculations of vertical velocity and divergence in special cases characterized by pronounced failures of barotropic forecasts. The results of the calculations show that a non-development situation was adequately described by the equivalent-barotropic picture of a single quasi-horizontal surface of non-divergence. The onset of mid-tropospheric development, as shown by the appearance of large errors of the barotropic forecast, was characterized by the appearance of a double surface of non-divergence, with a deep mid-tropospheric convergence layer in the vicinity of the trough line. This picture of development is confirmed by a second case study.

The appearance of the mid-tropospheric convergence layer is related to the low-level cold push, the tilt of the flow patterns with height, and the high-level jet stream, confirming synoptic studies by J. J. George, H. Riehl, and others.

1. INTRODUCTION

In considering the problem of baroclinic development, usually associated with cyclogenesis, one is often led to consider the various theoretical studies of baroclinic instability. Such studies for two-parameter prediction models yield quantitative instability criteria. However, when applied to atmospheric data, two-parameter prediction models produce forecast failures strikingly similar to those of barotropic forecasts, especially in cases of pronounced baroclinic development.

In considering the capabilities of a two-parameter model which contains representations of vertical shear and vertical velocity, from which vertical momentum advection can be computed, it is difficult to imagine one which does not contain, by implication at least, a quasi-horizontal surface of non-divergence. It therefore seems likely that a feature of the atmospheric circulations not found in two-parameter models, geostrophic, balanced, or primitive equation models, might be of considerable importance in the development process. One such feature which should be considered is the mid-tropospheric divergence, which can be computed from an atmospheric model having three or more parameters in the vertical.

This study will attempt to throw some light on the development process by means of computing vertical velocities and various derived fields by means of a three-level model of the atmosphere. For the purpose of this study, development can be considered as the processes which lead to error in the barotropic forecast (over areas of good data). We shall also exclude special mountain and friction effects from this study. In order to bring out more clearly the development processes, the actual events will be described in terms of the errors of the barotropic forecasts. Vertical motion, divergence, and vertical momentum advection can then be discussed in terms of these errors.

2. THE VERTICAL VELOCITY EQUATION

The vertical velocity equation is obtained in the usual method from the vorticity equation and the adiabatic equation written in the following form:

$$\frac{\partial \zeta}{\partial t}+\mathbf{V}\cdot\nabla\eta-\eta_0\frac{\partial \omega}{\partial p}=0 \tag{1}$$

$$\frac{\partial}{\partial t}\left(\frac{\partial \phi}{\partial p}\right)+\mathbf{V}\cdot\nabla\frac{\partial \phi}{\partial p}+\omega\sigma=0. \tag{2}$$

In (1) and (2) $\mathbf{V}$ is the horizontal wind; ζ is the relative vorticity; η is the absolute vorticity; η_0 is the absolute vorticity at 500 mb. which can also be used to represent a vertical average of η; $\omega=dp/dt$, the vertical velocity; ϕ is the geopotential; and σ is a measure of the static stability given by $\sigma=-\alpha\partial\ln\theta/\partial p$, where α is specific volume and θ is potential temperature.

We now assume that for the purposes of calculating horizontal advection the horizontal wind is non-divergent, and can be represented by a streamfunction, i. e., $\mathbf{V}=\mathbf{k}\times\nabla\psi$. In place of the usual formulation of the geostrophic approximation necessary to obtain an equation for ω, we shall make an approximation to the temperature field that $\partial\phi/\partial p=f\partial\psi/\partial p$. Introduction of these approximations into (1) and (2) leads to the ω-equation:

$$\nabla^2\omega+\frac{f\eta_0}{\sigma}\frac{\partial^2\omega}{\partial p^2}=\frac{f}{\sigma}\left[\frac{\partial}{\partial p}(\mathbf{V}\cdot\nabla\eta)-\nabla^2\left(\mathbf{V}\cdot\nabla\frac{\partial\psi}{\partial p}\right)\right]. \tag{3}$$

This involves the assumption that horizontal variations

of static stability can be neglected, although σ is permitted to vary in the vertical. The appearance of $f\eta_0$ as a coefficient of the second term in equation (3) was required for special reasons not relevant to this study. However, different versions of equation (3) were used in calculations in which (a) static stability varied freely, involving extra terms in σ, and (b) f_0^2 (at 45° N.) replaced $f\eta_0$. The results which applied to this study were not significantly affected by these changes.

The finite difference system in the vertical consisted of using data from 850, 500, and 200 mb. An interpolation was made enabling the use of 800, 500, and 200 mb. in the calculations. In computing finite differences at the low levels, the variable height of the ground was taken into consideration. The upper and lower boundary conditions consisted of $\omega=0$ at $p=0$ and $\omega=\mathbf{V}_g\cdot\nabla p_g$ at the lower boundary p_g, the standard atmosphere pressure at the variable height of the ground.

For finite differences in the horizontal the Joint Numerical Weather Prediction Unit's (JNWP) grid on a polar stereographic map having a mesh length of 381 km. at 60° N. was used. In the computation of Laplacians and Jacobians, a consistent system was used in which the components u and v of the wind were taken over a double mesh length. The calculations were made on the IBM 704 computer.

Before proceeding to the case studies, let us consider certain implications of the vertical velocity equation. For this purpose we can simplify equation (3) to the form:

$$\frac{\partial^2\omega}{\partial p^2}-A\omega=F, \tag{4}$$

where $A=k^2\sigma/f\eta_0$, k being a horizontal wave number. The right-hand side of the equation is represented as the forcing function, F, determined by the vertical variation of vorticity advection and the Laplacian of the temperature advection. In a quasi-geostrophic model, n-1 values of F can be obtained from n parameters in the vertical. The usual two-parameter prediction model therefore contains sufficient information for only one value of F in the vertical. If we then take F as independent of pressure, and apply as boundary conditions $\omega=0$ at 1000 mb. and at 0 mb., the ω-profile is symmetric about 500 mb., where a surface of non-divergence is found. This is represented by figure 1a. Of course it would be possible, in the absence of other than climatological information, to make an assertion regarding the variation of F with pressure in such a model. The only effect of this would be to change the pressure of the non-divergent surface. However, a continuous non-divergent surface corresponding with an isobaric surface would still exist.

Suppose instead that we consider a model with sufficient parameters in the vertical (minimum of three) to provide information on the slope of the vertical F-profile. Figures 1b and 1c represent the shapes of the ω-profile associated with two simple distributions of F. It is clear that if the slope of the F-profile changes sign from one place to another significant areas of mid-tropospheric convergence or divergence may occur. An atmospheric model with three or more levels is thus suitable for calculation of mid-tropospheric divergence. Although detailed numerical calculations will be necessary before the question of the number of levels required for adequate vertical resolution can be settled, it is clear that three levels represents the minimum number required if mid-tropospheric divergence is an important baroclinic phenomenon.

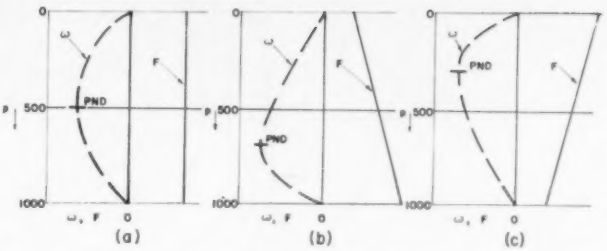

FIGURE 1.—Three vertical profiles, (a), (b), and (c), of forcing function, F, and vertical velocity, ω, as a function of pressure p. PND refers to the pressure at which no horizontal divergence exists.

3. CASE STUDIES

(I). JANUARY 21–22, 1959

On January 22, 1959, a notable cyclogenesis was observed over North America. A sea level cyclone passed across the Great Lakes and travelled into Labrador, deepening rapidly. Of special interest was the fact that large errors rather suddenly appeared in even short-range barotropic forecasts.

The development was preceded by the motion of a 500-mb. trough through the central United States. Figure 2a shows that 24 hours in advance of the development the atmosphere was behaving barotropically, as shown by the small errors of the barotropic forecasts. The cross-section of horizontal divergence for the same time (fig. 2b) shows the familiar equivalent barotropic pattern of a quasi-horizontal surface of non-divergence near 500 mb. with compensating convergence and divergence patterns above and below the surface. Some distortion of the pattern is found over the mountains as a consequence of the ascent of the air to the west and the descent to the east of the highest terrain.

Figure 3 shows a more complicated situation by 1200 GMT of January 21. This could be regarded as a period of transition from an equivalent barotropic situation to a baroclinic situation. The errors of the barotropic forecast for the subsequent 12 hours increased to amounts which were not negligible. The cross-section (fig. 3b) shows a split of the surface of non-divergence in the vicinity of the trough line. The signs of the convergence and divergence patterns in mid-troposphere are consistent with the errors observed in the barotropic forecast.

581868—61——3

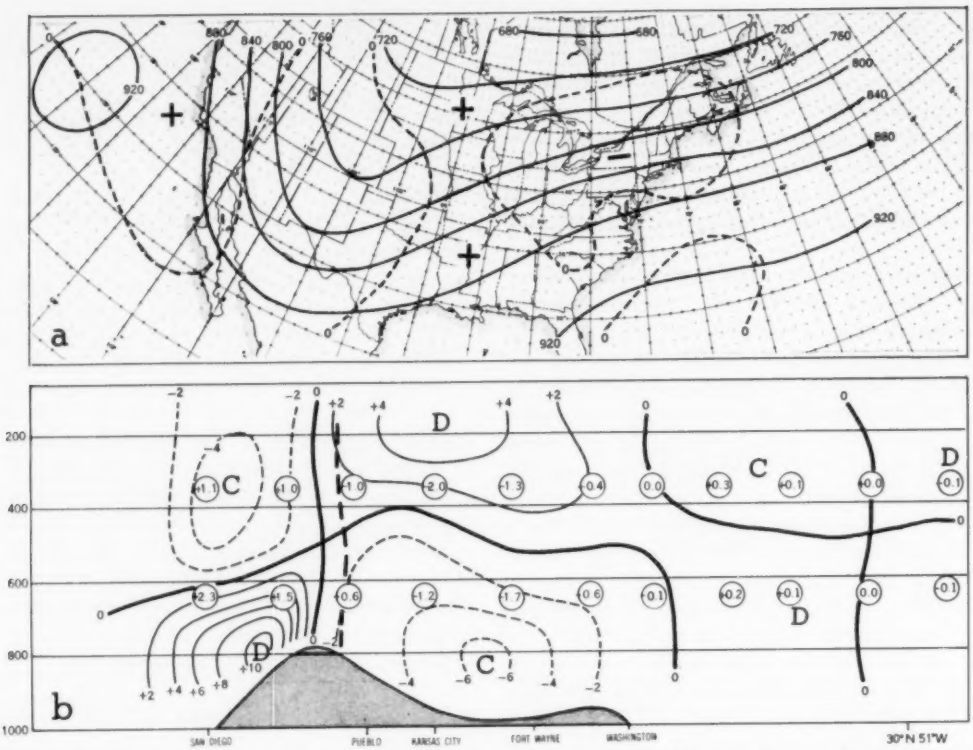

FIGURE 2.—(a) Error in decafeet (dashed lines) of the 12-hr. barotropic forecast from 0000 GMT, January 21, 1959, superimposed on the 500-mb. contours (solid lines) for that time. (b) Cross-section of horizontal divergence in units of 10^{-6} sec.$^{-1}$. The numbers in circles are ω in units of 10^{-2} mb. sec.$^{-1}$. Heavy dashed line is the trough line.

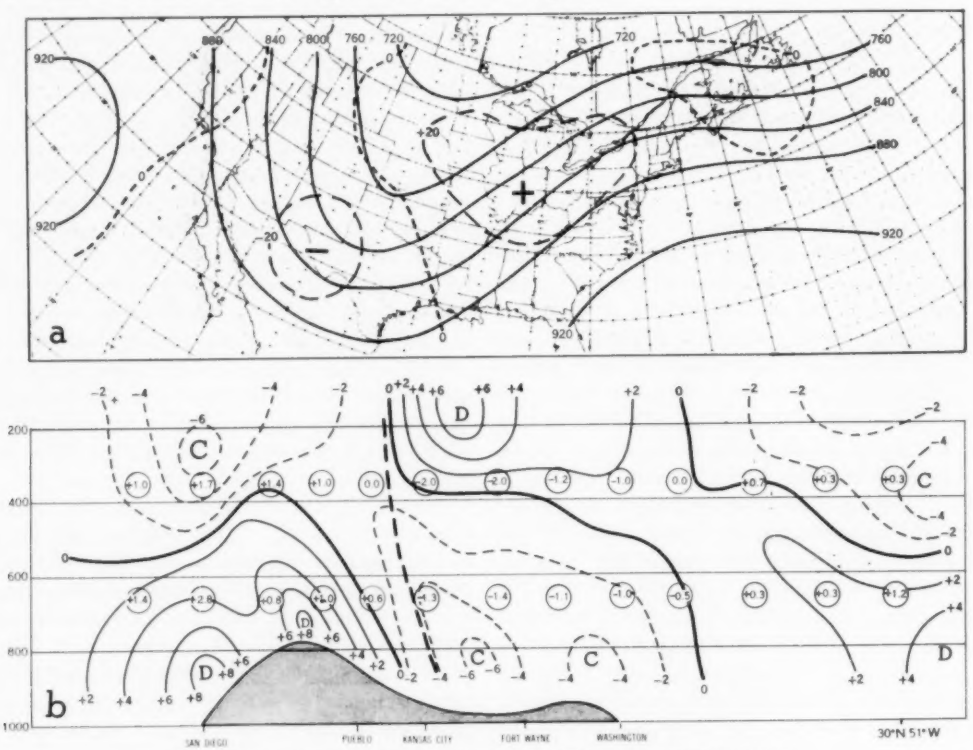

FIGURE 3.—Same as figure 2 except for 1200 GMT, January 21, 1959.

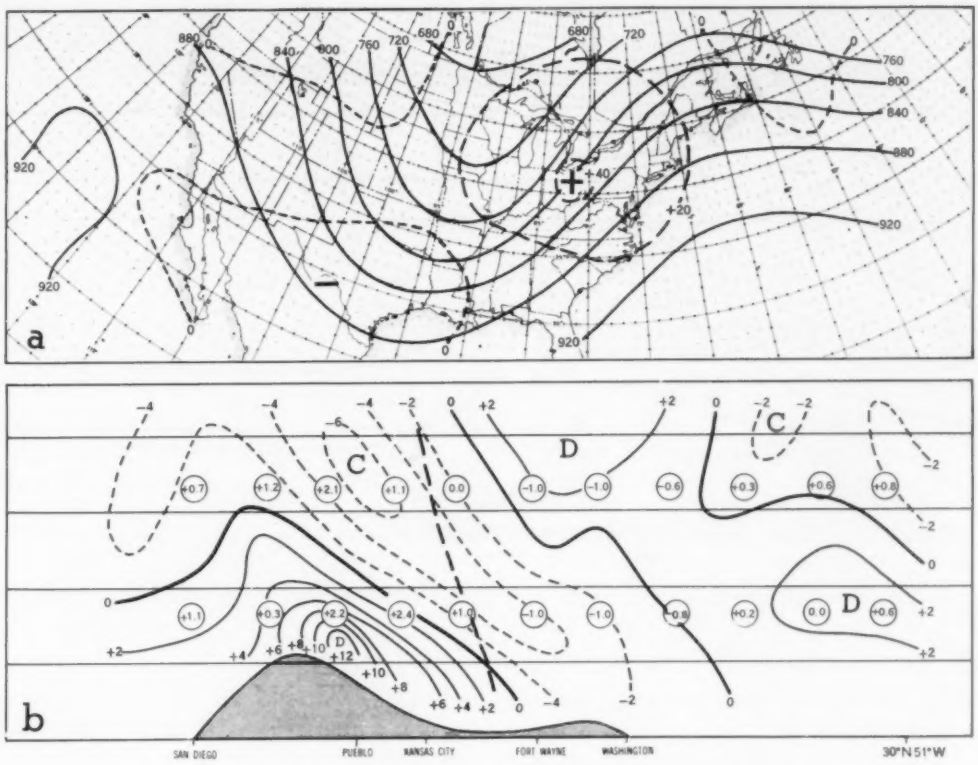

FIGURE 4.—Same as figure 2 except for 0000 GMT, January 22, 1959.

In figure 4 the development is shown proceeding in strength. The error of the barotropic forecast over the eastern United States was extreme. The cross-section (fig. 4b) shows a most significant change from conditions 24 hours earlier. In the vicinity of the trough line there was a double surface of non-divergence, one at high levels and one at low levels, with a deep layer of convergence in mid-troposphere. This cross-section of a developing trough resembles similar cross-sections obtained by Charney [3] and by Hinkelmann [6] from idealized data, as well as those computed from real data by Bundgaard [2] and by Fleagle [4].

Having the vertical velocities, one can compute the effects at 500 mb. of the vertical advection of momentum. The tendency of the 500-mb. height arising from the vertical momentum advection is shown in figure 5. It can be seen that in this situation this effect is generally of a sign to reduce 500-mb. error, but can account at the most for about 20 percent of the error.

In considering that vertical velocities of 10^{-3} mb./sec, or more over large areas are relatively common in winter, one sees that vertical displacements of 100 mb./day should result. If the vertical velocity is downward in a trough line, this could result in a strengthening of the flow

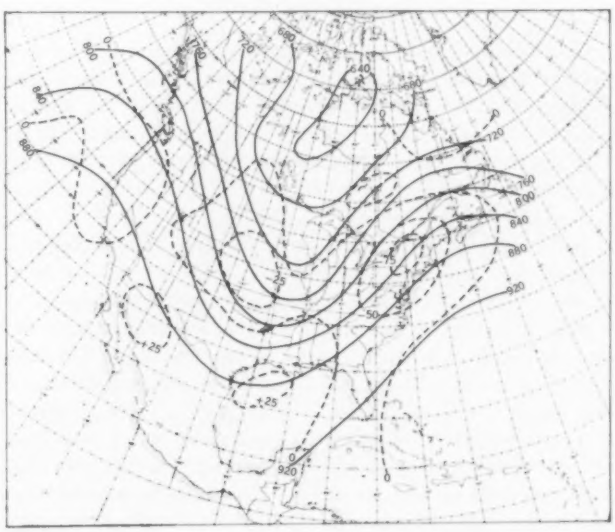

FIGURE 5.—Contribution of the vertical advection of momentum to the 500-mb. height tendency (dashed lines; units of ft. per 12 hr.) for 0000 GMT January 22, 1959, superimposed on the 500-mb. contours (solid lines) for that time.

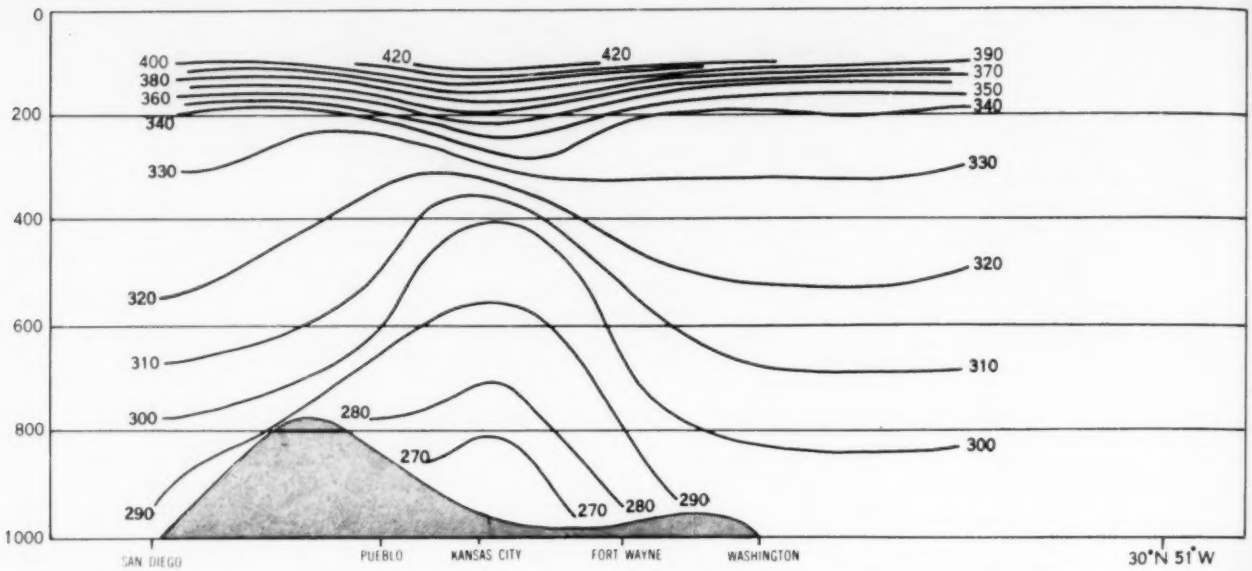

FIGURE 6.—Cross-section for 0000 GMT, January 22, 1959, showing potential temperature in the same vertical plane as in figure 4b.

through a deep layer by 20 percent in 24 hours, an amount which is by no means negligible.

In figure 6, the intersections of the isentropic surfaces with the cross-section are shown. These show the pronounced cold dome, and cold push, to be a feature of the lower two-thirds of the atmosphere. Above this we find a warm push, associated with the low warm stratosphere.

(II). DECEMBER 6, 1959

On December 6, 1959, a cyclogenesis occurred along the eastern United States coast. Figures 7 and 8 show the extreme error of the barotropic forecast over the southeastern States as the low-level cyclogenesis took place. The computed vertical velocities at 650 and 350 mb., together with the computed 500-mb. divergence, are shown in figures 9, 10, and 11. Examining the areas of the southeastern States, we can see that a large area of 500-mb. convergence was associated with two separate features. Ahead of the trough the ascending motion was stronger at high levels than at low levels, and in the trough line the descending motion was stronger at low levels. A 500-mb. divergence area is found just behind the trough line, where the descent was strongest at high levels. The 500-mb. divergence pattern of figure 10 can be compared with that of figure 6b in the paper by Brown and Neilon [1], who obtained their map by assuming that the entire error of the barotropic forecast was a result of the 500-mb. divergence pattern. Although there are considerable differences in details, there is a good resemblance of the major features.

Another view of this can be obtained from cross-sections running just north of the main centers of activity. The orientation of the cross-section (fig. 12) was chosen to coincide with that presented in the following paper by Brown and Neilon. This gives the reader an opportunity to check two completely independent determinations of vertical velocity and divergence. The cross-section of divergence (fig. 12b) shows a pattern in the developing trough similar to that of figure 4. The vertical velocity cross-section (fig. 12a) shows that in this case the convergence associated with the trough was associated mainly with a strong ascending motion at high levels. This relatively strong high-level ascent, as well as the strong descent behind the trough, was a consequence of a strong 200-mb. jet stream in strongly curved flow through the trough. If there had been no phase shifts in the vertical, this would merely have resulted in a faster eastward displacement of the 500-mb. trough than given by the barotropic forecast, since at 500 mb. there would have been convergence ahead of and divergence behind the trough. However, the phase shift in the vertical resulted in an extension of the 500-mb. convergence area into the trough line as well as an enlargement of the convergence area. This conclusion is in agreement with the results of Wiin-Nielsen [9] who showed that the lagging of the temperature field behind the flow leads to a mid-tropospheric tendency for deepening in the trough line.

4. GENERAL REMARKS

A feature of both cases was the tendency for the sinking of cold air to be at a maximum in the lower levels. A well-known characteristic of strong cold-air outbreaks is the tendency for the maximum cold-air advection to occur in the lowest half of the atmosphere, with a low, warm stratosphere prominent in the higher levels.

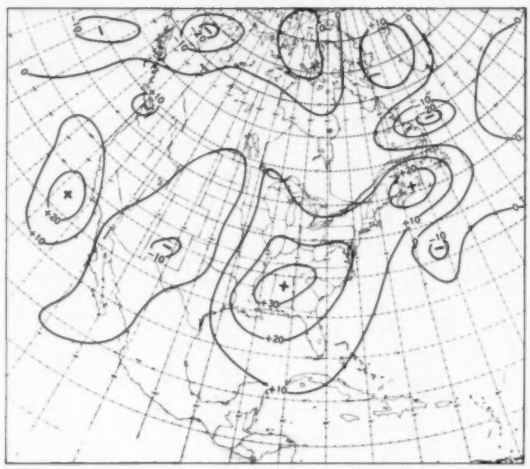

FIGURE 7.—Error in decafeet of 12-hr. barotropic forecast from 0000 GMT December 6, 1959.

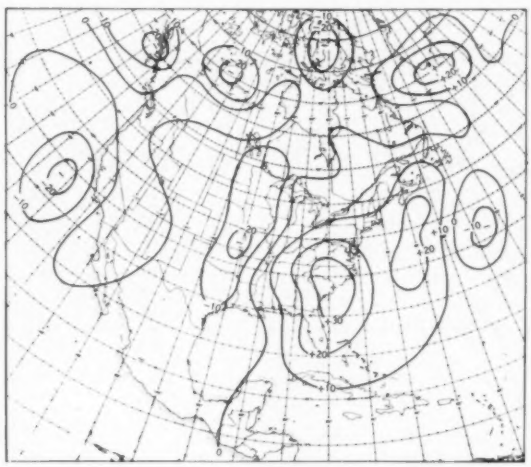

FIGURE 8.—Error in decafeet of 12-hr. barotropic forecast from 1200 GMT December 6, 1959.

According to the analysis of the ω-equation presented earlier, such cold-air outbreaks therefore ought to be characterized regularly by a very strong low-level divergence, a relatively low surface of non-divergence, and a layer of mid- and upper-tropospheric convergence. In such cases, failures of barotropic forecasts are often observed. Cyclogenesis is also frequently seen under such conditions. In support of this diagnosis we can cite the cyclogenesis study by George and collaborators [5], who found the strong low-level cold-air push to be a reliable precursor of cyclogenesis. They found the 850-mb. chart to be most useful in recognition of the low-level cold push. J. Austin* has pointed also to the occurrence of the abnormally low warm stratosphere during the initial stages of cyclogenesis.

* In lectures at two American Meteorological Society meetings at Washington, D.C. in 1954 and 1955.

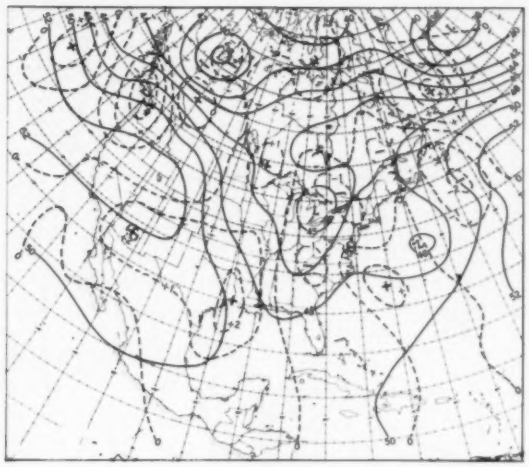

FIGURE 9.—850-mb. contours (solid lines) and 650-mb. ω (dashed lines) in units of 10^{-3} mb. sec.$^{-1}$ for 1200 GMT, December 6, 1959.

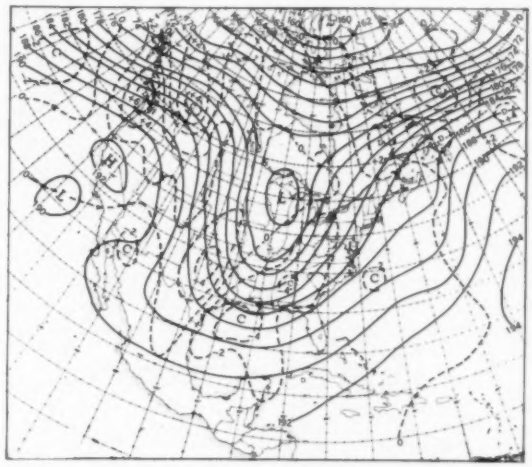

FIGURE 10.—500-mb. contours (solid lines) and divergence (dashed lines) in units of 10^{-6} sec.$^{-1}$ for 1200 GMT, December 6, 1959.

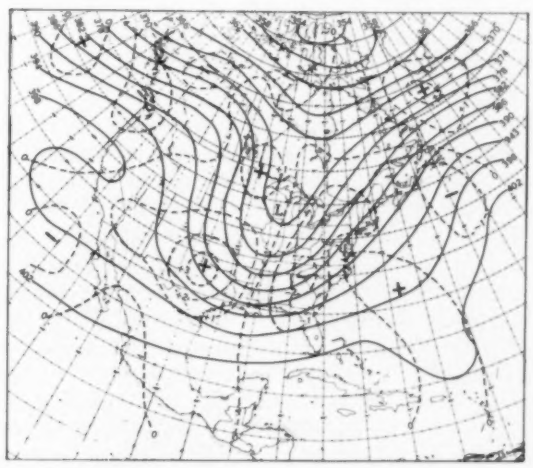

FIGURE 11.—200-mb. contours (solid lines) and 350-mb. ω (dashed lines) in units of 10^{-3} mb. sec.$^{-1}$ for 1200 GMT, December 6, 1959.

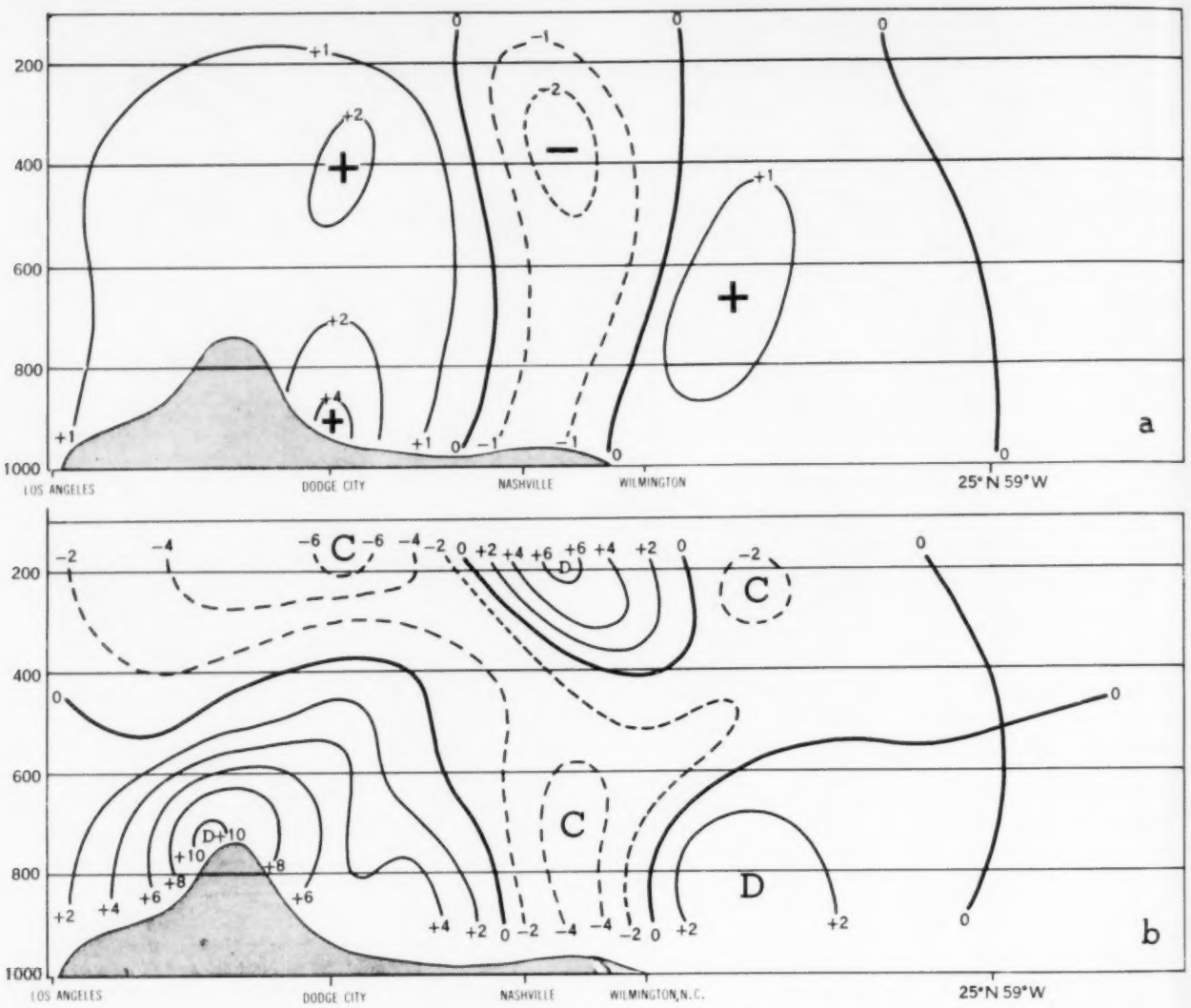

FIGURE 12.—Cross-section (a) vertical velocity (10^{-3} mb. sec.$^{-1}$) and (b) divergence (10^{-6} sec.$^{-1}$), for 1200 GMT, December 6, 1959.

Wiin-Nielsen [9] showed in his 3-level analysis of a model disturbance that an upward increase in vertical wind shear leads to a pattern of 500-mb. divergence which tends to speed up systems (convergence ahead of a trough, divergence behind), as compared with barotropic motion. Taba's [8] typical vertical profiles of the subtropical jet stream show the normal existence of such conditions. It is a common experience at the JNWP Unit that the barotropic forecasts move features too slowly in the areas occupied by a subtropical jet stream. If a subtropical jet stream is found over the forward side of a trough, as in the schematic representation of figure 13, the resulting mid-tropospheric convergence accentuates the development. Here we should point out that Riehl [7] observed this association in 1947. His paper contains special mention of the upward increase of shear under the high-level jet stream, in association with the occurrence of cyclogenesis.

5. CONCLUSIONS

The equivalent barotropic representation of the atmosphere, with a quasi-horizontal surface of non-divergence near 500 mb. separating divergence patterns of opposite sign above and below, was a realistic representation of actual conditions during a period preceding cyclogenesis. However, during two different cyclogenetic situations, the equivalent barotropic idea became invalid. During these development periods a double non-divergent surface appeared in the vicinity of the developing trough.

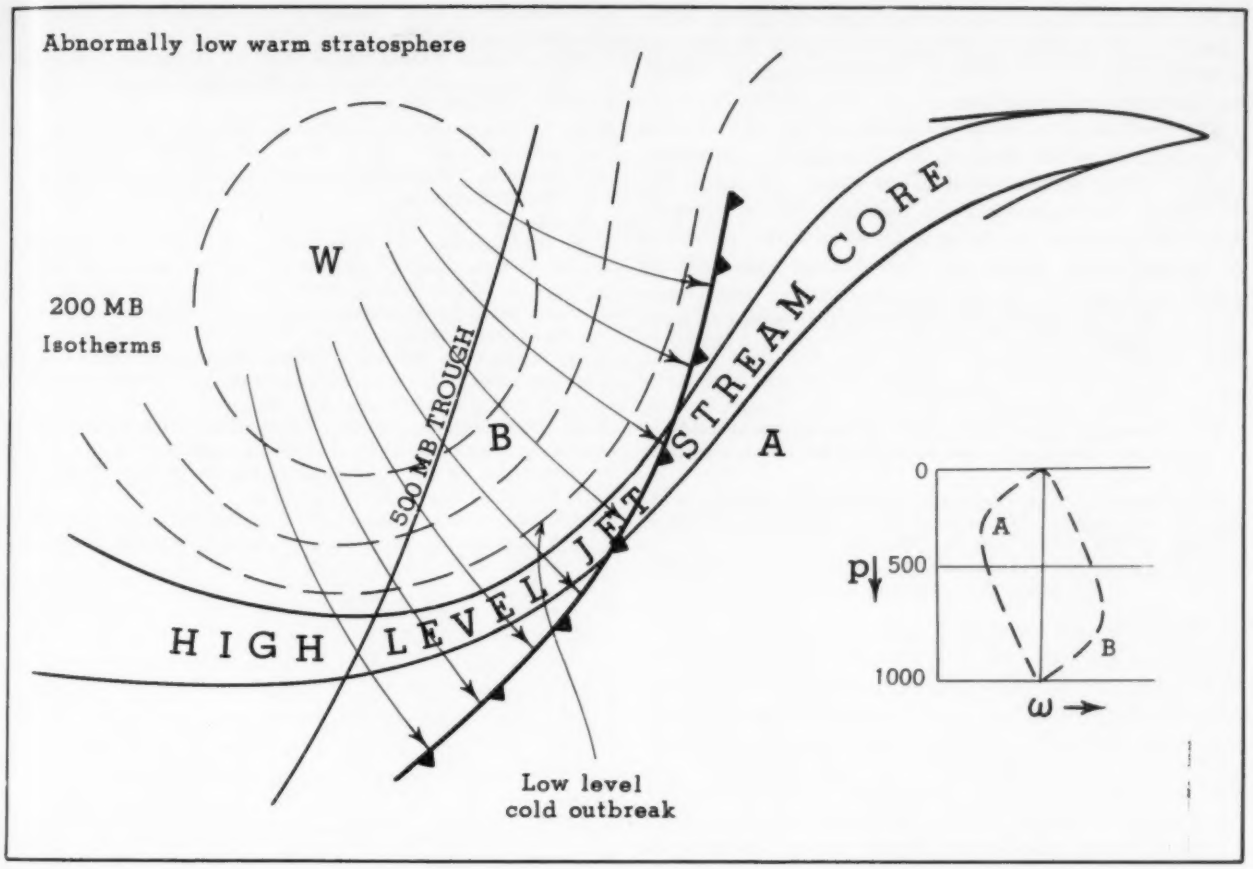

FIGURE 13.—Schematic representation of factors associated with mid-tropospheric development.

Between upper and lower divergence regions a deep mid-tropospheric convergence layer appeared. The invalidation of the equivalent barotropic representation was further demonstrated by the appearance of large errors in the barotropic forecasts.

The particular atmospheric features responsible for this mid-tropospheric convergence area near the developing trough line were the following:

(1) The low-atmospheric strong cold-air advection in and behind the low-level trough surmounted by high-level warm air advection. This led to a vertically asymmetric ω-profile, with low-level sinking and mid-tropospheric convergence.

(2) The normal phase shift with height of the system, in which the sinking cold air is brought in at lower levels under the upper cyclonic system. This accentuates the effects mentioned under (1) above.

(3) The participation of a strong high-tropospheric jet stream in the strongly curved upper flow. This accentuates the pre-trough convergence in mid-troposphere.

These features are represented in figure 13, in which the low-level cold push, the high-level jet stream, and the phase shift with height are indicated. The inset ω-profiles represent conditions at the locations A and B. One cannot expect that all of these contributing factors will be present in each case of mid-tropospheric development, but the errors of the barotropic forecasts will reach the largest values when all are present in strength.

The most serious limitations on the accuracy of the calculations presented here are the use of the geostrophic approximation, and the lack of a better vertical resolution of the atmosphere. It is just in development situations where the vertical velocities and ageostrophic motions reach their greatest magnitudes. At the same time the smaller-scale horizontal motions become of greater importance to the developmental process. It is therefore, a very large step from diagnosis to prognosis. However, in deriving an ω-equation of the general type used in this study it is necessary to state some kind of wind law. In view of the well-known sensitivity of numerical predictions

to the wind law used, it seems that a generalization of the wind law to be used in the ω-equation to that of the balance equation might be of sufficient interest to warrant recoding the machine calculations.

The problem of vertical resolution of the calculations is aggravated by the presence of a tropopause of variable height. If the vertical wind shears above and below the tropopause are each relatively invariant (but of opposite sign) serious errors can be introduced into the estimates of vertical wind derivatives from streamfunctions at widely separated levels on opposite sides of the tropopause. Further experiments to study this question seem to be in order.

REFERENCES

1. J. A. Brown and J. R. Neilon, "Case Studies of Numerical Wind Analyses," *Monthly Weather Review*, vol. 89, No. 3, Mar. 1961, pp. 83–90.
2. R. Bundgaard, "The Analysis of Horizontal Divergence in the Free Atmosphere," *Transactions American Geophysical Union*, vol. 27, No. 6, Dec. 1946, pp. 784–799.
3. J. G. Charney, "The Dynamics of Long Waves in a Baroclinic Westerly Current," *Journal of Meteorology*, vol. 4, No. 5, Oct. 1947, pp. 135–162.
4. R. G. Fleagle, "Quantitative Analysis of Factors Influencing Pressure Change," *Journal of Meteorology*, vol. 5, No. 6, Dec. 1948, pp. 281–292.
5. J. J. George and Collaborators, "Forecasting Relationships Between Upper Level Flow and Surface Meteorological Processes," *Geophysical Research Papers*, No. 23, Air Force Cambridge Research Center, Cambridge, Mass., Aug. 1953, 186 pp.
6. K. Hinkelmann, "Ein Numerisches Experiment mit den primitiven Gleichungen," pp. 486–500 of *The Atmosphere and the Sea in Motion* (Rossby Memorial Volume), Rockefeller Institute Press, in association with Oxford University Press, New York, 1959, 509 pp.
7. H. Riehl, "Jet Stream in Upper Troposphere and Cyclone Formation," *Transactions American Geophysical Union*, vol. 29, No. 2, Apr. 1948, pp. 175–186.
8. H. Taba, "The Horizontal and Vertical Wind Profiles of the Subtropical and Polar Jet for January 1–7, 1956 and the Variation of the Equivalent Barotropic Level," *Tellus*, vol. 11, No. 4, Nov. 1959, pp. 441–451.
9. A. Wiin-Nielsen, "Diagnosis of Divergence in a Three-Parameter, Numerical Prediction Model," *Monthly Weather Review*, vol. 89, No. 3, Mar. 1961, pp. 67–73.

CASE STUDIES OF NUMERICAL WIND ANALYSES

CAPT. JOHN A. BROWN, JR., USAF
and
JAMES R. NEILON, U.S. WEATHER BUREAU
Joint Numerical Weather Prediction Unit, Suitland, Md.

[Manuscript received November 9, 1960; revised January 31, 1961]

ABSTRACT

With the aid of an electronic computer, case studies of wind analyses at the 850-mb., 700-mb., 500-mb., 400-mb., 300-mb., and 200-mb. pressure levels have been made. The divergent and non-divergent wind components resulting from the u and v wind-component analyses are investigated. For the cases considered, the streamfunction fields are slightly superior to the Joint Numerical Weather Prediction operational fields, obtained initially through use of the "balance equation." The magnitude of the horizontal wind divergence values are comparable to those obtained from the winds by previous investigators employing hand-analysis techniques. However, the divergence patterns are not sufficiently accurate for the strict requirements necessary for numerical weather forecasting.

1. INTRODUCTION

Analyses of several meteorological parameters have been made during the past several years at the Joint Numerical Weather Prediction Unit (JNWP) through use of electronic computer techniques. At the present time analyses of the heights of the 850-mb. and 500-mb. pressure surfaces are made twice daily on an operational, routine basis.[1] This analysis scheme was described recently by Cressman [1].

Many attempts have been made in the past to obtain accurate representations of the flow at constant pressure surfaces, but in most cases these attempts have been made through use of hand-analysis techniques. Results of studies made in recent years such as those by Landers [4], Murakami [5], Rex [7], and Taba [11] point to the possibility of obtaining direct, accurate wind analyses over regions of dense data coverage. These authors point to considerable skill in obtaining the horizontal wind divergence at several levels in the atmosphere for their individual case studies. It is a well-known fact that even with sufficient data coverage the usefulness of divergence computed from instantaneous wind observations is dependent upon a high degree of observing accuracy. Although one can hope that observational errors are random and thereby can be reduced considerably by modern analysis procedures, it is questionable whether the reduction in error will be enough to produce sufficiently accurate divergence patterns to be useful for future forecasting purposes.

The purpose of this study was to determine whether the wind fields at constant pressure surfaces in the troposphere and lower stratosphere could be accurately analyzed over the JNWP octagonal grid in an objective sense through use of a sufficiently large electronic computer.

An attempt was also made to determine to what extent, if any, the geostrophic assumption, made in the JNWP height analysis program, is damaging to the wind forecasts from the operational divergent one-parameter forecast model.

2. ANALYSIS PROCEDURE

All computations were performed by the IBM 704 electronic computer on all or part of the regularly arranged JNWP octagonal grid which covers most of the Northern Hemisphere north of 10° latitude. The grid-point interval was 381 km. at 60° latitude on a polar stereographic projection. The analysis scheme which was employed was a modification of the JNWP operational height-analysis routine which is described in detail in [1]. Only the major features of this program will be mentioned here.

This analysis technique utilizes an initial estimate of the pattern of the field being analyzed and adjusts this guess in a prescribed manner to fit the data. Therefore, for meteorological data which are sparse in certain large regions of the grid, it is desirable to use a first guess which closely approximates the final analysis over the entire region.

Attempts were made in the early stages of this study to obtain first estimates of the wind fields at all levels under consideration, excluding 500 mb., through use of a linear regression equation employing the 500-mb. streamfunction wind, obtained from the JNWP operational "balance equation" [9], and the 500–850-mb. geostrophic thermal wind. The resulting extrapolated wind fields contained large influences of the 500-mb. cyclostrophic winds which were improperly positioned. This was particularly noticeable below the 500-mb. level where the tilt with height of the pressure patterns was more pronounced.

The non-divergent part of the geostrophic wind (for further details of this see [8]) of the operational height analyses was tested for its usefulness as a first guess. The resulting analyses were not sufficiently removed from the geostrophic influences. Therefore, because of the sensitivity of the final non-divergent and, particularly,

[1] On December 15, 1960, JNWP began analyzing on an operational routine basis the height, temperature, and wind fields for 850, 700, 500, and 300 mb.

the divergent wind components to an accurate first wind-field guess, it was decided to use the balance-equation winds for the first estimates of the final analyses at all levels.

All wind data were checked in the JNWP operational automatic data processing system.[2] Four successive passes are made through the fields, and during each of these scans the following correction C to the wind component u is made at each grid point:

$$C=-WE.$$

Here, E is the error of the linearly interpolated u-wind, obtained from the first guess (or from the values computed in the previous scan), at the observation location, and

$$W=\frac{N^2-d^2}{N^2+d^2}.$$

Here, d is the distance from the observation to the grid point being modified, and N is the radius of a circle centered at the grid point. N varies from 4.75 grid intervals during the first scan to 1.0 grid intervals during the fourth scan. W is set equal to unity during the final scan. If more than one observation falls within the circle prescribed by N, a correction C is computed for each observation and the average correction is applied at the grid point under consideration.

In addition a five-point (center and four immediate surrounding grid points) smoothing operator is applied after scans 2 and 3:

$$\bar{u}=u_0+\frac{1}{8}\bar{\nabla}^2 u. \tag{1}$$

Here, $\bar{u}$ denotes the smoothed value, u_0 is the value at the central point, and $\bar{\nabla}^2$ is the single grid-increment finite difference Laplacian operator.

After the last scan is completed a weak 9-point smoother, described by Shuman [10], is applied.

After the u wind component was analyzed by the above method, the procedure was repeated for the v wind component.

Because of the large barotropic 500-mb. height errors and the existence of dense upper-air data coverage over the region of interest, the cases for 0000 GMT, November 16, 1959 and 1200 GMT, December 6, 1959 were studied. Winds were analyzed over North America at the following pressure levels: 400, 300 and 200 mb. In addition, the 850-, 700-, and 500-mb. levels were analyzed over the entire JNWP octagonal grid. The scale factor of the map was used throughout this study. Thus velocities relative to the earth rather than to the map were obtained and examined. The effects of truncation errors were not considered in this study.

3. SYNOPTIC SITUATION

Since the results of the tests of both cases studied were similar, it was decided to direct most of the discussion to the 1200 GMT, December 6, 1959 case.

At this time the synoptic situation was as follows: a surface Low existed over Lake Huron with a cold front extending southward through western Florida and then southwestward through the Gulf of Mexico (fig. 1). A warm front extended eastward from this Low and then northeastward along the St. Lawrence Seaway. A weaker cyclonic circulation was centered about 450 miles east of Delaware. High pressure existed over the western United States with a ridge extending to a second high cell centered over southern Texas. A strong cyclonic circulation which had moved eastward through western Canada was centered near Ft. Nelson, British Columbia.

By 0000 GMT, December 7, 1959, the Low over Lake Huron had weakened into a trough which extended to a new cyclonic circulation centered over southeastern Virginia. Twelve hours later this storm was located in northeastern Pennsylvania and had intensified considerably—central pressure was slightly less than 980 mb. By this time the storm in western Canada had moved into the western edge of Hudson Bay and increased slightly in circulation. Aloft a strong ridge existed over the western United States with a sharp, intense trough over the Mississippi River valley at 1200 GMT, December 6, 1959 (fig. 2). This trough moved rapidly eastward during the following 24 hours.

4. EVALUATION OF RESULTS

According to Helmholtz's theorem the horizontal wind vector ($\mathbf{V}$) may be separated into a rotational non-divergent part and an irrotational divergent part; i.e.,

$$\mathbf{V}=\mathbf{k}\times\nabla\psi+\nabla\chi.$$

Here, $\mathbf{k}$ is the unit vector directed upward, ∇ is the horizontal gradient operator, and ψ and χ are the stream-function and velocity potential, respectively. It was decided to test each of these wind components separately.

A. THE NON-DIVERGENT WIND FIELDS

From the analyzed u and v wind components it was possible to obtain the relative vorticity (ζ) from the finite difference form of the following equation:

$$\zeta=\frac{g}{f_0}\nabla^2\hat{\psi}=\frac{\partial v}{\partial x}-\frac{\partial u}{\partial y}. \tag{2}$$

In equation (2) g is the gravitational acceleration, f_0 is the Coriolis parameter at 45° latitude, and

$$\hat{\psi}=\frac{f_0}{g}\psi.$$

Thus, $\hat{\psi}$ has dimension length. The winds were differenced over a double grid increment.

From equation (2) it was possible to obtain the field of the streamfunction, given the boundary values. These values were obtained by assigning the streamfunction of an arbitrary boundary point the value of the height of the

[2] A vertical consistency check is made on all winds greater than 15 kt. at or near the mandatory reporting levels from 1000 to 200 mb. A detailed description of this test has been given by Dent [3].

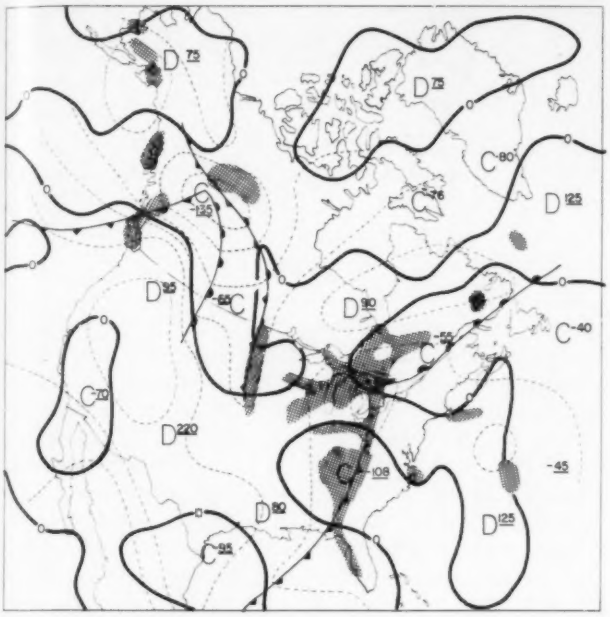

FIGURE 1.—850-mb. divergence (solid lines) and surface isobars (dashed lines) and fronts for 1200 GMT, December 6, 1959. D and C refer to divergence and convergence centers, respectively. Values are in units of 10^{-7} sec.$^{-1}$ Cross-hatching indicates precipitation areas.

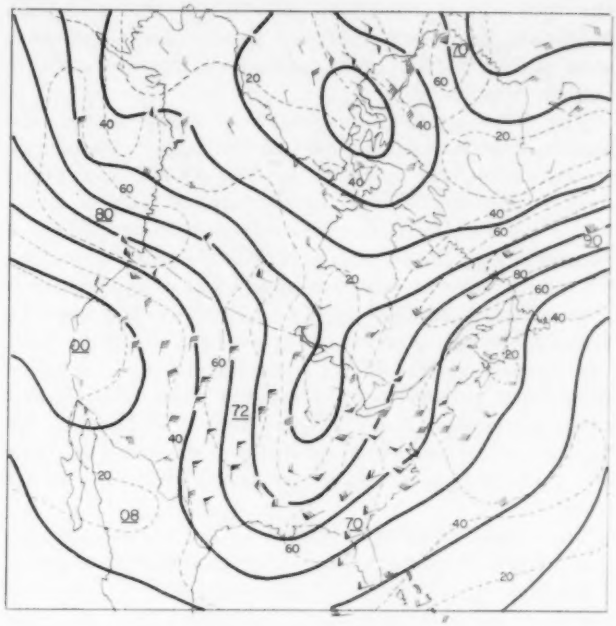

FIGURE 2.—500-mb. streamfunction lines and observed winds for 1200 GMT, December 6, 1959.

pressure surface obtained from the JNWP height analysis. From the wind components normal to the boundary it was possible to obtain a first estimate of the streamfunction at the next boundary point. Thus estimates were obtained for each boundary point. Since the integrated divergence over the region was not necessarily zero, a large discrepancy between the ψ-gradient between the first and last point and the analyzed winds at those points could result. Therefore these boundary ψ-values were adjusted, and the integrated divergence was also obtained. This was used later in obtaining the velocity potential.

The scaled streamfunction field was then obtained by the Liebmann relaxation technique using a double grid-increment finite difference Laplacian.[3] The 500-mb. result for 1200 GMT December 6, 1959 is shown in figure 2. The streamfunction isolines appear to fit the wind data quite nicely. The isotachs were computed from the analyzed winds which contained both the divergent and non-divergent components, rather than the streamfunction winds, to illustrate the accuracy of the analysis and at the same time to illustrate the effects of the analysis smoothing routines. For the 0000 GMT, November 16, 1959 case, the smoothing routines after scans 2 and 3 of the analysis procedure were omitted. Therefore, this produced analyses which were in closer agreement with the data.

The 500-mb. non-divergent wind fields obtained from this procedure were then verified over the United States and southern Canada using the reported winds. This non-divergent wind field was obtained from the streamfunction field through use of centered finite differences over a double grid-increment. The winds at the grid points were then linearly interpolated to the observation locations and compared to the observed data. The procedure was also applied to the JNWP operational streamfunction, obtained from the balance equation. The root-mean-square (RMS) and average vector errors are noted in line 2 of table 1. The same verification procedure was applied to the total analyzed wind (line 1, table 1). Here note the effects of the 2d and 3d scan smoother used in the December case.

It is not surprising that the RMS vector errors of the non-divergent wind are less than the operational errors. This is due to the fact that the operational streamfunction winds are obtained from a height analysis which utilizes

TABLE 1.—*Root-mean-square wind and height verification statistics*

500-mb. fields	0000 GMT, Nov. 16, 1959		1200 GMT Dec. 6, 1959	
	JNWP	Wind	JNWP	Wind
1. Analyzed winds (knots)	.....	5.3 (4.5)	.....	9.9 (7.8)
2. Initial non-divergent winds (knots)	15.3 *(12.2)	11.4 (9.3)	13.8 (11.3)	12.0 (9.8)
3. 12-hr. barotropic forecast winds (knots)	15.9 (13.3)	14.8 (11.8)	22.3 (18.0)	21.1 (16.3)
4. 24-hr. barotropic forecast winds (knots)	20.2 (16.9)	19.3 (16.2)	30.3 (25.3)	27.5 (22.7)
5. 36-hr. barotropic forecast winds (knots)	22.9 (19.7)	22.2 (18.8)	32.6 (27.8)	29.8 (25.4)
6. 36-hr. ψ-forecast vs. ψ-verifying winds (knots)	21.7	20.3	31.2	28.8
7. 36-hr. ψ-wind difference (knots)	43.0	.....	45.1	.....
8. Initial heights (feet)	44	81	71	105
9. 36-hr. barotropic forecast heights (feet)	348	305	423	436

*Values in parentheses are the average vector errors.

[3] A similar relaxation using a single grid-increment finite difference Laplacian produced solved streamfunction values which differed from the double grid-increment ones by as much as 50 feet at 500 mb. in the vicinity of deep Lows.

the geostrophic approximation to fit the grid-point heights to the observed winds. In addition, these winds were used for the first guess in obtaining the wind analyses made in this study.

The 500-mb. streamfunction field obtained from the analyzed winds was further tested by making a barotropic forecast from this initial field. The JNWP operational forecast program was used for this purpose. The resulting forecast streamfunction winds were compared with those obtained from the routine barotropic forecasts issued by JNWP by the same verification procedure described above. (See lines 3, 4, and 5 of table 1.) Figures in line 6 are the 36-hr. RMS vector errors computed from the 36-hr. forecast streams and the JNWP verifying streams. A 36-hr. persistence measurement computed from the JNWP streams is given in line 7. Notice that in all forecasts the barotropic forecast winds made from the wind analyses are a slight improvement over the JNWP operational results.

The height fields were obtained from the streamfunction fields in the usual manner from the balance equation. After linear interpolation of these values to the observations, the RMS height errors, computed over the same regions as were the winds, were obtained and are presented in lines 8 and 9 of table 1. The results of the larger initial height errors from the wind analyses were surprising since it was expected that the geostropic assumption made in the JNWP height analyses was damaging. If the balance equation and its method of solution were a complete representation of the atmosphere, a streamfunction which exactly represented the observed winds should produce a height field which exactly represented the observed heights. Although the balance equation produces a frictionless, non-divergent wind and the streamfunction values at the boundary points are set equal to the height values, it is difficult to explain this discrepancy quantitatively through these approximations inherent in the balance equation and its necessary boundary restrictions. Phillips [6], while studying the Appalachian storm of November 1950, noted a similar discrepancy at 400 mb. The 36-hr. forecast-minus-verifying height pattern from the JNWP forecasts for the December case is presented in figure 3. A similar pattern was obtained from the wind-analysis forecasts.

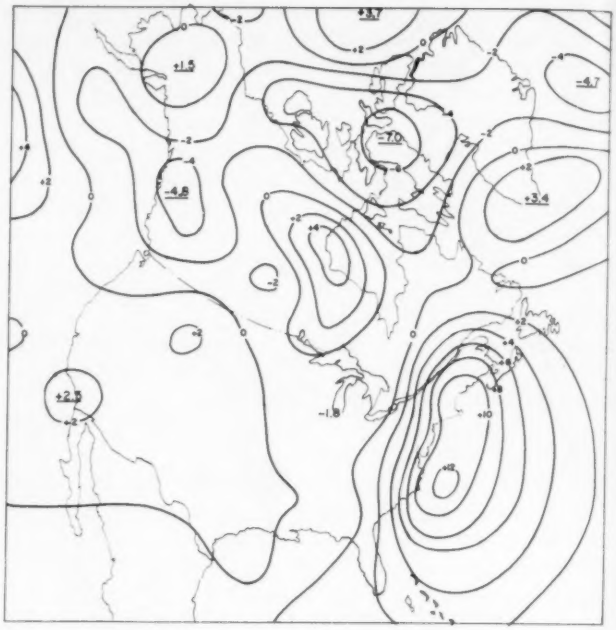

FIGURE 3.— 500-mb. JNWP operational 36-hr. forecast-minus-verifying height pattern valid at 0000 GMT, December 8, 1959. Values are in units of 10^2 ft.

B. THE DIVERGENT WIND FIELDS

The fields of horizontal wind divergence were obtained directly from the u and v wind analyses at all of the levels under consideration through use of the centered finite difference approximation. The result obtained at 850 mb. for the December case is presented in figure 1. The region of convergence found over Newfoundland and southwestward over the St. Lawrence Valley is reasonable since considerable amounts of precipitation were observed in this region. Convergence was also found over the southeastern United States where cyclonic development occurred in the succeeding hours. The results at this level over the western portion of the continent are unreliable because of the presence of the mountains. The area of convergence near the southern tip of Texas is questionable.

The velocity potential field was obtained from the divergence field in the same manner that the streamfunction field was obtained from the relative vorticity field; that is, by inverting

$$\frac{g}{f_0}\nabla^2\hat{\chi}=\frac{\partial u}{\partial x}+\frac{\partial v}{\partial y},$$

where

$$\hat{\chi}=\frac{f_0}{g}\chi$$

is the scaled velocity potential. A Liebmann relaxation was performed on the 500-mb. data again using a double grid-increment finite difference Laplacian. Rather than assign specific boundary values for $\hat{\chi}$ it was decided to use the average boundary normal gradient of $\hat{\chi}$ which was available from the procedure described in A above.

The result of this computation for the December case for 500 mb. is presented in figure 4a. The corresponding patterns of divergence are shown in figure 4b. The divergent wind is directed perpendicular to the isolines from centers of divergence (positive values) to centers of convergence (negative values). Over a large portion of the central United States this wind is less than 5 kt. Winds between 5 kt. and 10 kt. are found in the western and eastern United States and in southern parts of the grid. These latter features may be due, in part, to the effects of the first guess used in the wind analysis. Notice the extremely large divergent wind speeds which resulted over the south-central region of Canada. These result

from the large-amplitude, short wavelength, divergence pattern obtained from the wind analysis.

C. STREAMFUNCTION TENDENCY AND VERTICAL VELOCITY COMPUTATIONS

The vorticity equation can be written in the following consistent, simplified form (see Wiin-Nielsen [12]):

$$\nabla^2 \frac{\partial \hat{\psi}}{\partial t} = -J(\hat{\psi}, \eta) - \frac{f_0^2}{g} \nabla \cdot \mathbf{V}. \tag{3}$$

Here J is the Jacobian and η is absolute vorticity. The 500-mb. scaled 12-hr. streamfunction tendency field resulting from the individual terms in the right side of the above equation and their sum are presented in figure 5 together with the "observed" tendency. The latter (fig. 5d) is an approximation obtained from the balance equation streamfunction fields 12 hr. before and 12 hr. after 1200 GMT, December 6, 1959. The 12-hr. barotropic forecast made from the wind analysis study and the operational streamfunction showed positive height errors over the eastern United States. As can be seen from figure 5a, the contribution of the first term of equation (3) produced negative stream tendencies over this region which were too small in magnitude. The magnitude and pattern of the streamfunction tendency resulting from the divergence term (fig. 5b) demonstrates that if these divergence fields were to be included in a numerical forecasting model which used these fields directly to obtain initial streamfunction tendencies, the resulting initial tendencies would undoubtedly contain large errors over regions where equation (3) was valid.

At this point it should be mentioned that another modified form of the vorticity equation was used to estimate the local streamfunction tendency patterns. Wiin-Nielsen has also shown that the relative vorticity over a large region is conserved in the following equation:

$$\nabla^2 \frac{\partial \hat{\psi}}{\partial t} = -\frac{f_0}{g} \mathbf{V}_a \cdot \nabla \eta - \frac{f_0 \eta}{g} \nabla \cdot \mathbf{V}_a. \tag{4}$$

$\mathbf{V}_a$ and η refer to the total wind and absolute vorticity, respectively. The streamfunction tendency field computed from this equation was very similar to that found using equation (3). However, the contributions of the *individual* terms could not be evaluated by the relaxation procedure because of large "pillows" of opposite sign which resulted from each of the forcing functions.

This result may be more clearly understood by considering the equation

$$\int_A \nabla^2 \frac{\partial \hat{\psi}}{\partial t} \, dA = -\frac{f_0}{g} \int_A \eta \nabla \cdot \mathbf{V}_a dA,$$

where A is the area. Theoretically for a sufficiently large area the above integral approaches zero *provided the absolute vorticity and the divergence are uncorrelated*. The streamfunction tendency field which resulted from the divergence term of equation (4) contained large positive errors at 500 mb. This was evident from the discrepancy

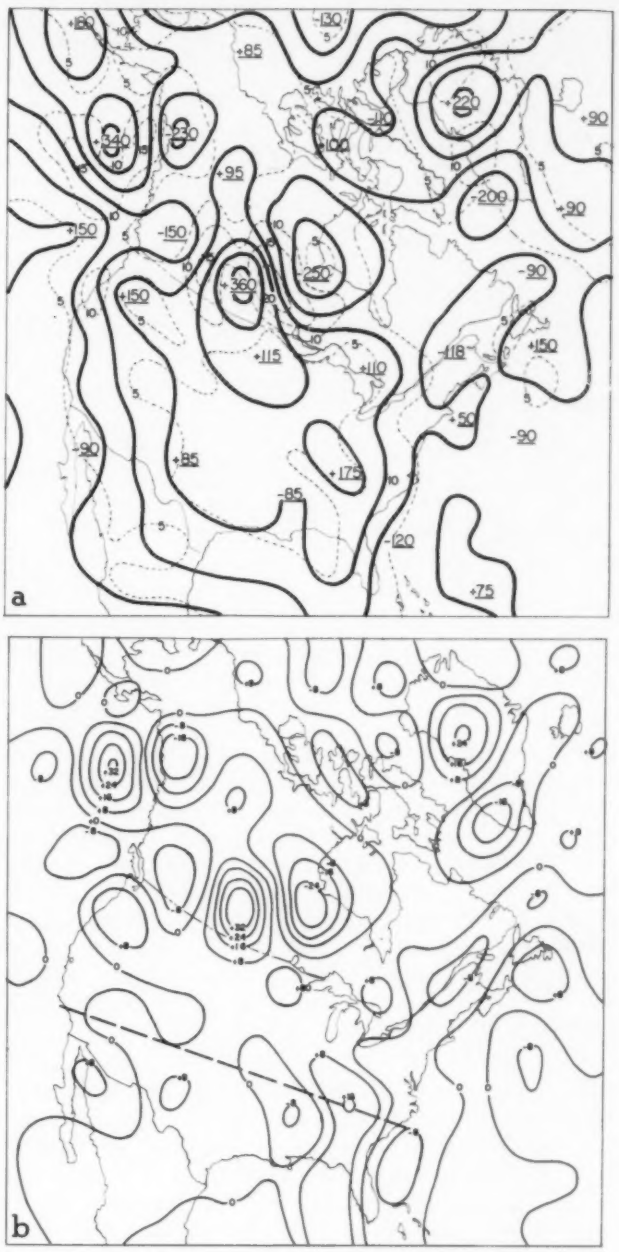

FIGURE 4.—1200 GMT, December 6, 1959. (a) 500-mb. velocity potential (solid lines) and corresponding divergent wind speed isotachs (dashed lines). Wind speeds are in knots. Plus and minus refer to centers of divergence and convergence, respectively. (b) Field of horizontal wind divergence from which (a) was obtained. Units are 10^{-7} sec.$^{-1}$ Dashed line indicates line along which vertical cross section of figure 7 was taken.

which was found in the streamfunction tendency fields resulting from the divergence terms of equations (3) and (4). Since the errors of $\frac{\partial \hat{\psi}}{\partial t}$ were positive over the central regions of the grid, the errors in $\nabla^2 \frac{\partial \hat{\psi}}{\partial t}$ were negative. Thus, according to the above equation, the vorticity and

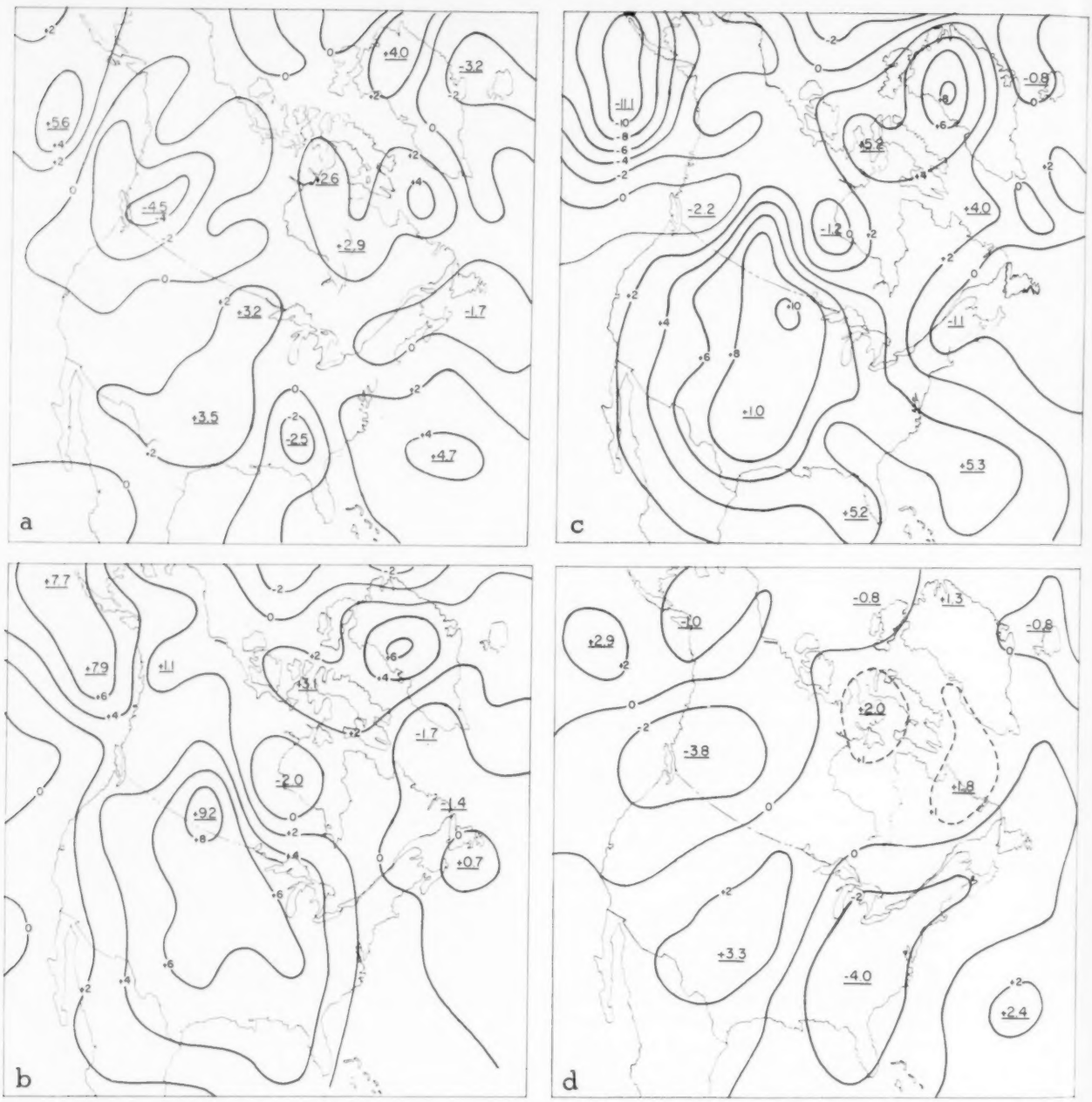

FIGURE 5.—The contribution to the 500-mb. 12-hr. scaled streamfunction tendencies for 1200 GMT, December 6, 1959, from: (a) $-J(\hat{\psi},\eta)$; (b) $-\frac{f_0^2}{g}\nabla\cdot\mathbf{V}$; and (c) $-J(\hat{\psi},\eta)-\frac{f_0^2}{g}\nabla\cdot\mathbf{V}$; (d) The streamfunction tendency obtained from operational streams 12 hr. before and 12 hr. after 1200 GMT, December 6, 1959. Units are 10^2 ft./12 hr.

divergence obtained from the wind analyses were positively correlated. In other words, at 500 mb. in regions of cyclonic vorticity horizontal divergence was prevalent, and the reverse was generally true for regions of anticyclonic vorticity.

At the 850-mb. level the individual contributions of the terms of equation (4) produced tendency pillows of the opposite sign to those found at 500 mb. Thus at these levels the vorticity and divergence were negatively correlated. Similar results were found at 700 mb.

These general results are in agreement with our present knowledge of the atmosphere. Assuming that the absolute vorticity patterns are similar throughout the lower half of the troposphere, the results imply that the level of

TABLE 2.—*Mean absolute values of divergence* (10^{-7} *sec.* $^{-1}$)

Pressure level (mb.)	Nov. 16, 1959 0000 GMT	Dec. 6, 1959 1200 GMT
850	36	43
700	35	36
500	38	47
400	46	64
300	48	63
200	43	59

least divergence over the octagonal grid exists somewhere between the 700- and 500-mb. pressure levels. This is further substantiated by the averaged divergence values computed over the United States at each of the pressure levels. (See table 2.)

A further test was applied to the divergence patterns which resulted from the wind analyses at 500 mb. If the long-wave stabilizing term and the mountain term, which exist in the JNWP operational barotropic forecast model, are neglected, the barotropic forecast equation reduces to

$$\nabla^2 \frac{\partial \hat{\psi}}{\partial t} = -J(\hat{\psi}_B, \eta_B). \tag{5}$$

The subscript B refers to the scaled barotropic streamfunction. Subtracting equation (5) from (3) produces the following approximation:

$$\nabla \cdot \mathbf{V} \approx \frac{g}{f_0^2 \Delta t} \nabla^2 \hat{\psi}_e.$$

Here $\hat{\psi}_e$ is the scaled barotropic streamfunction forecast error (forecast minus observed) and Δt is the time increment. The average wind divergence field obtained from the 24-hr. JNWP barotropic forecast from 0000 GMT, December 6, 1959 is presented in figure 6. This divergence pattern approximates the 24-hr. average pattern necessary to correct the operational JNWP barotropic forecast. The general features of this pattern may be compared with those of figure 4b, obtained directly from the wind analyses.

The approximated vertical velocity patterns were obtained from the divergence patterns (smoothed) of the analyzed winds through the use of the continuity equation:

$$\frac{\partial \omega}{\partial p} = -\nabla \cdot \mathbf{V}.$$

Here p refers to pressure and $\omega = dp/dt$. Assuming that ω is negligible at 1000 mb. and that the divergences vary linearly between the levels at which they were measured, it is possible to compute ω at all of the data levels. A cross-section of these patterns for the December case is presented in figure 7a. Figure 7b is the corresponding cross-section of the divergence fields. These cross-sections were made along a line extending from Norfolk to Los Angeles (dashed line in fig. 4b). These patterns are similar to those of the classical picture; i.e., convergence at lower levels and divergence at the upper levels appear in regions ahead of the trough and the reverse in regions to the rear of the trough. The vertical velocity errors introduced by the neglect of mountain effects are undoubtedly significant. Cross-sections of vertical velocity

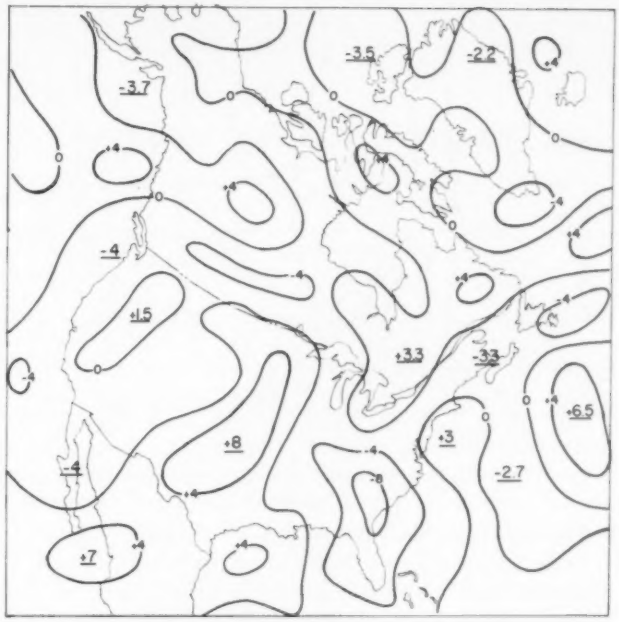

FIGURE 6.—500-mb. estimate of the horizontal wind divergence for 1200 GMT, December 6, 1959, obtained from the error field of the JNWP 24-hr. operational streamfunction forecast from 0000 GMT, December 6, 1959. Units are 10^{-6} sec.$^{-1}$

and divergence fields from Cressman's [2] three-parameter quasi-geostrophic model for this time and over the same region may be used for comparison. (See fig. 12 of Cressman's paper.) The large discrepancy found in the vertical velocities near the Continental Divide is undoubtedly due to the lower boundary restriction used in the present study. However, the large-scale features of both sets of cross-sections are in agreement in the main. The magnitudes of the divergence values are generally larger in the wind analysis study.

5. SUMMARY AND CONCLUSIONS

Although the u and v wind fields were analyzed independently, the wind fields produced by the analysis scheme "fitted" the wind observations more accurately than did the original wind fields that were used as first estimates of the final analysis. Since it was desirable to have a good first estimate of the final analysis, the JNWP operational streamfunction, obtained from the balance equation, was used for this purpose.

The streamfunction winds obtained from the wind analyses also fitted the data more accurately than did the JNWP streamfunction winds, and in both cases the former produced slightly improved barotropic wind forecasts. However, the initial height field produced from the wind-adjusted streamfunction field, which in turn was obtained through use of the balance equation program, was inferior to the operational JNWP height analysis.

The employment of the newer streamfunction in preference to the present JNWP operational one is not

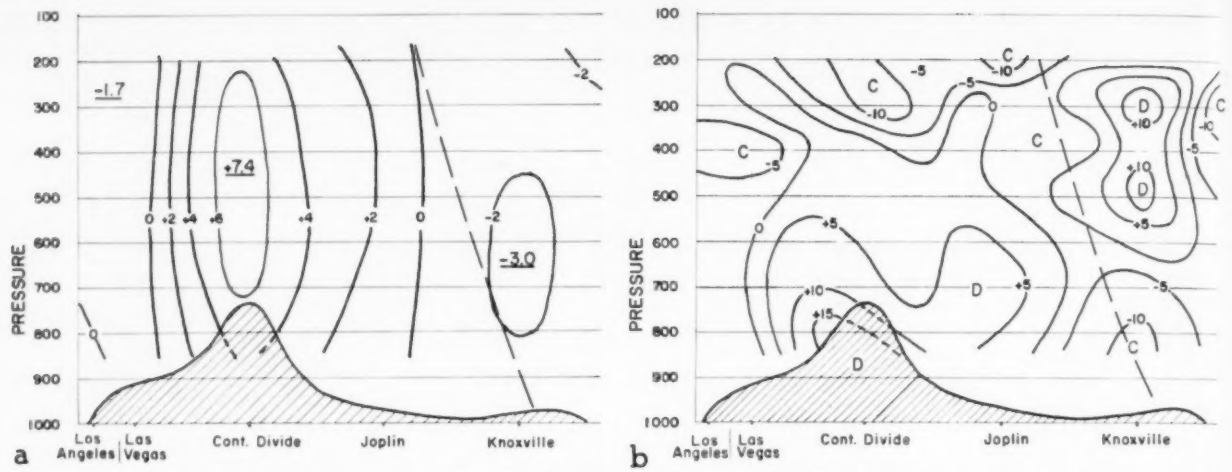

FIGURE 7.—(a) Cross-section obtained from the observed winds of 1200 GMT, December 6, 1959. Units are 10^{-3} mb. sec.$^{-1}$ (b) Corresponding horizontal wind divergence cross-section. Values are in units of 10^{-6} sec.$^{-1}$

economically feasible with the present JNWP numerical forecasting models. Preliminary tests indicate that a streamfunction of about the same quality as obtained in this study may be produced from the balance equation streamfunction by a more economical procedure.

Briefly, this entails a slight modification of the present machine analysis program to enable it to produce streamfunction analyses, using wind data only, through use of the following equations (rather than the geostrophic assumption):

$$u=-\frac{\partial \psi}{\partial y}, \qquad v=\frac{\partial \psi}{\partial x}.$$

This improved streamfunction and the one found in the present study may also prove to be more desirable, particularly in the upper troposphere and lower stratosphere, since the ellipticity criterion ($\zeta_g > -\frac{f}{2}$, where ζ_g is the geostrophic relative vorticity), which must be satisfied in solving the balance equation, may be violated in regions of dense data coverage.

The average magnitudes of the horizontal divergences resulting from the u and v wind analyses are comparable to those found by Landers and others using hand-analysis techniques. The magnitudes obtained by direct measurements appear to be larger than those obtained by most implicit calculations. As a first approximation, if we assume that the 500-mb. barotropic forecast errors are due largely to the horizontal wind divergence contribution, it would appear that the amplitudes of the divergence fields obtained in this study are of the correct order of magnitude. Although difficult to evaluate, the divergence patterns over flat terrain appear to be more accurately represented at the lower levels of the troposphere where observational density and accuracy are greater.

However, the divergence patterns obtained in this study could not be utilized by a numerical forecasting model which included the cyclogenetic mechanism and required accurate initial horizontal wind divergence measurements.

ACKNOWLEDGMENTS

The authors wish to express their thanks to Dr. G. P. Cressman, Dr. A. Wiin-Nielsen, and Dr. F. G. Shuman of the JNWP Unit for their suggestions and interest in this investigation. An expression of thanks is also extended to Mr. Arthur Kneer for programming assistance rendered.

REFERENCES

1. G. P. Cressman, "An Operational Objective Analysis System," *Monthly Weather Review*, vol. 87, no. 10, Oct. 1959, pp. 367–374.
2. G. P. Cressman, "A Diagnostic Study of Mid-Tropospheric Development," *Monthly Weather Review*, vol. 89, No. 3, Mar. 1961, pp. 74–82.
3. G. R. Dent, "Hydrostatic and Wind Check in the ADP Program," *Office Note* no. 16, Joint Numerical Weather Prediction Unit, April 1960, 4 pp.
4. H. Landers, "A Three-Dimensional Study of the Horizontal Velocity Divergence," *Journal of Meteorology*, vol. 12, no. 5, Oct. 1955, pp. 415–427.
5. T. Murakami, "Numerical Analysis of Wind and Its Application to the Numerical Weather Forecasting," *Journal of Meteorological Society of Japan*, Series II, vol. 36, no. 1, Feb. 1958, pp. 11–22.
6. N. A. Phillips, "Geostrophic Errors in Predicting the Appalachian Storm of November 1950," *Geophysica*, vol. 6, no. 3–4, 1958, pp. 389–405.
7. D. F. Rex "Vertical Atmospheric Motions in the Equatorial Central Pacific," *Geophysica*, vol. 6, no. 3–4, 1958, pp. 479–501.
8. F. G. Shuman, "Predictive Consequences of Certain Physical Inconsistencies in the Geostrophic Barotropic Model," *Monthly Weather Review*, vol. 85, no. 7, July 1957, pp. 229–234.
9. F. G. Shuman, "Numerical Methods in Weather Prediction: I. The Balance Equation," *Monthly Weather Review*, vol. 85, no. 10, Oct. 1957, pp. 329–332.
10. F. G. Shuman, "Numerical Methods in Weather Prediction: II. Smoothing and Filtering," *Monthly Weather Review*, vol. 85, no. 11, Nov. 1957, pp. 357–361.
11. H. Taba, "A Comparative Study of the Field of Divergence and Vertical Motion by Means of the Continuity and Vorticity Equation," Report, Contract AF 61(514)–963, International Meteorological Institute, University of Stockholm, 1960, 15 pp.
12. A. Wiin-Nielsen, "On Certain Integral Constraints for the Time-Integration of Baroclinic Models," *Tellus*, vol. 11, no. 1, Feb. 1959, pp. 45–59.

A NOTE ON CLEAR AIR TURBULENCE DURING APRIL AND MAY 1960

FRANK J. SMIGIELSKI

District Meteorological Office, U.S. Weather Bureau, Washington, D.C.

[Manuscript received July 6, 1960; revised Dec. 21, 1960]

1. INTRODUCTION

During the months of April and May 1960 a number of teletypewriter transmissions of pilot reports of clear air turbulence in the United States were gathered for a study of this phenomenon. The study was undertaken to see if any clues to forecasting clear air turbulence in the levels between 500 and 300 mb. could be found. These levels were chosen because of the larger number of flights that are made at levels between 18,000 and 30,000 ft. both by jet and turbo-prop aircraft. The approach of this study was to outline areas where clear air turbulence was encountered by pilots and to examine these locations in relation to upper-air flow patterns, horizontal and vertical wind shears, and 500-mb. height changes.

2. CLEAR AIR TURBULENCE IN RELATION TO UPPER-AIR FEATURES

Clear air turbulence was most often reported when the 500-mb. flow showed a closed Low or a well defined trough as its primary circulation. In this type of circulation, the turbulence was quite often reported to the east and southeast of the trough line or low center and immediately to the west of the area of maximum winds and was associated with strong horizontal shear. Figure 1 shows a typical 500-mb. pattern when clear air turbulence was reported. In this case clear air turbulence was reported at levels between 17,000 and 21,000 ft.; all reports indicated moderate to severe turbulence. Strong horizontal and vertical shear was present, as is shown in figure 2, a cross section from Peoria, Ill. to New York City based upon upper-air observations 2 or 3 hours before the time of the turbulence reports.

Figure 3 shows a case of closed circulation at 300 mb. that was associated with reports of clear air turbulence. Turbulence was reported at 29,000 ft. in the vicinity of Morgantown, W. Va. about 2 hours before the time of the upper air observations. Earlier in the day, severe clear air turbulence was reported at 31,000 ft. between Cleveland and Chicago. Figure 4 shows another type of upper-air pattern that gave rise to clear air turbulence.

Balzer and Harrison [1] noted a lack of cases of clear air turbulence over the Rockies and northern Plains. A possible explanation of this could be the mean positions of troughs and ridges aloft over the United States: a mean ridge lies over the Rockies, and a mean trough farther east over the Central States [2]. This would give a greater amount of clear air turbulence over the area from the eastern Plains eastward to the east coast. Along the Pacific coast, it is not uncommon in certain portions of the year to have a cut-off Low over the southwestern United States, and along the California coastline, with a trough northward along the coast. In these cases, a greater amount of clear air turbulence cases would occur in the western United States. Clem [3] showed a clearcut maximum level of clear air turbulence over the southwestern and northwestern United States between 27,000 and 40,000 ft. in winter, and this would fit the pressure patterns for clear air turbulence.

In the study of horizontal wind shear in relation to

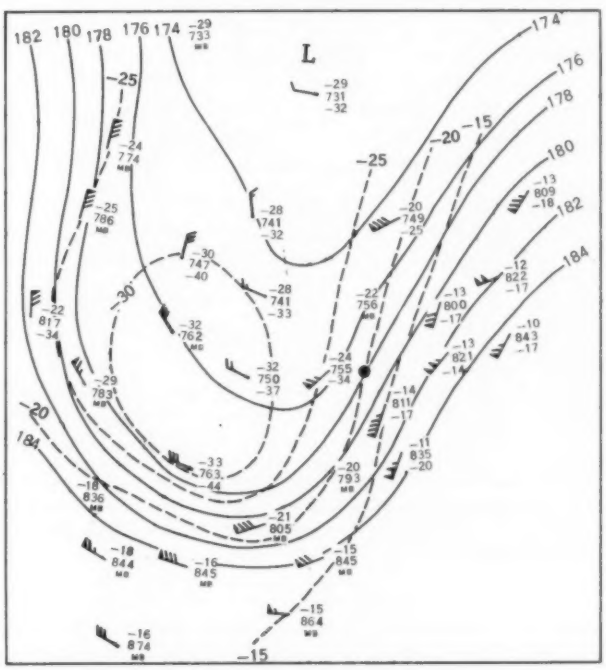

FIGURE 1.—500-mb. chart, 1200 GMT, April 5, 1960. Solid lines are contours; dashed lines are isotherms; solid circle indicates report of clear air turbulence.

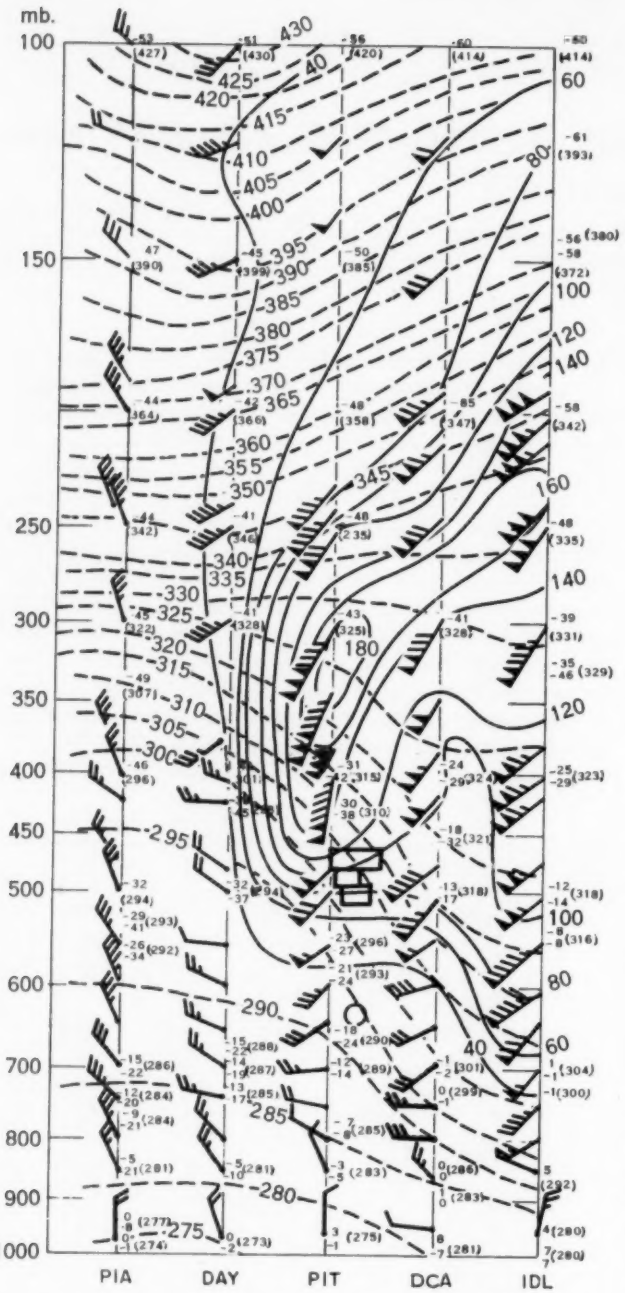

FIGURE 2.—Vertical section from Peoria, Ill. to New York City, 1200 GMT, April 5, 1960. Solid lines are isotachs; dashed lines are isentropes; blocks indicate reports of turbulence; circle indicates report of smooth air.

clear air turbulence, it would seem that the direction of travel of the aircraft would be a factor in the effect of the turbulence on the aircraft. In those reports of turbulence for which the direction of aircraft travel could be determined it was found that the direction was most

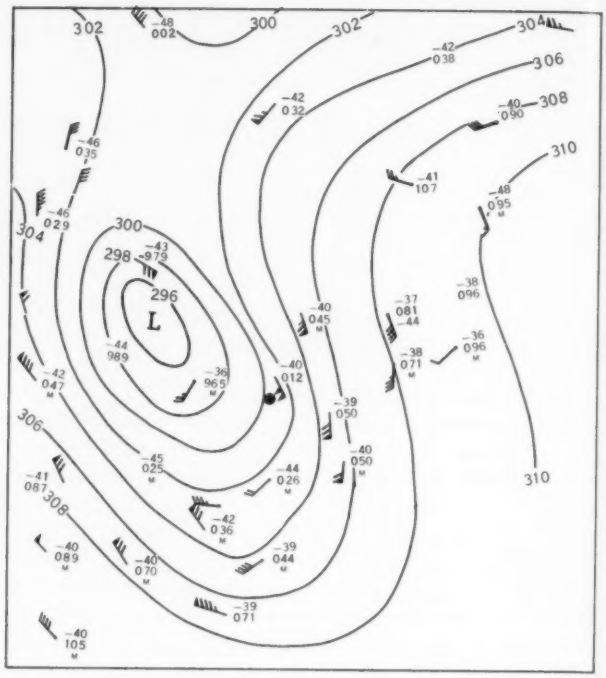

FIGURE 3.—300-mb. chart, 0000 GMT, May 9, 1960. Solid lines are contours; solid circle indicates report of clear air turbulence.

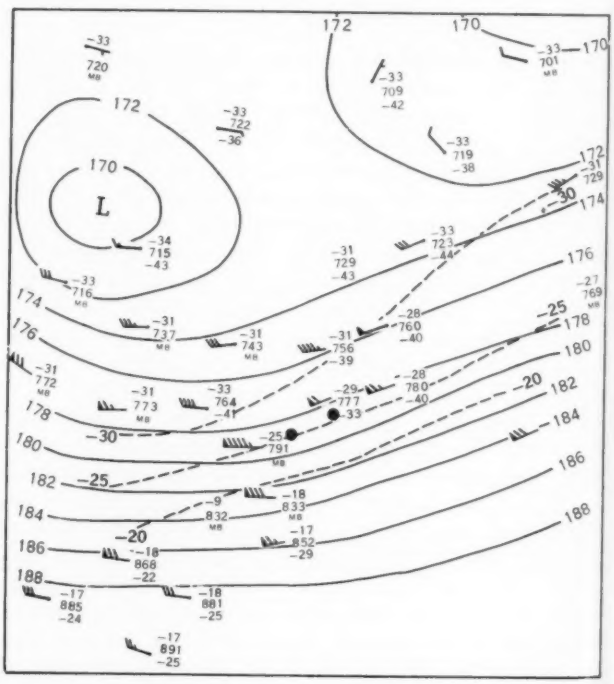

FIGURE 4.—500-mb. chart, 1200 GMT, April 8, 1960. Solid lines are contours; dashed lines are isotherms; solid circle indicates report of turbulence.

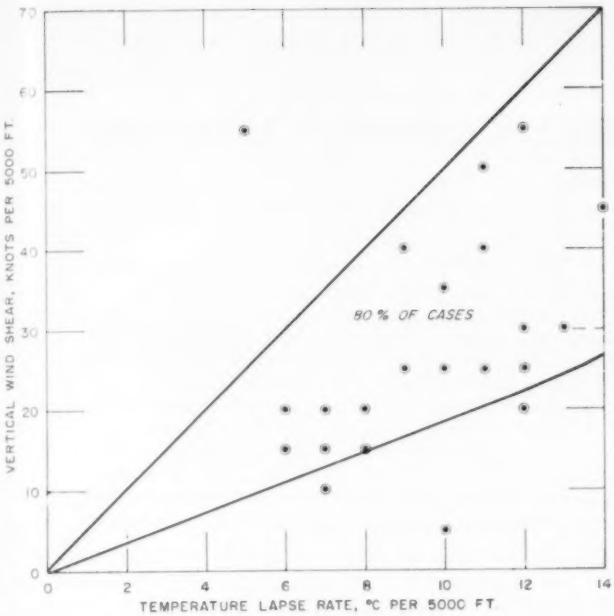

FIGURE 5.—Clear air turbulence reports during April and May 1960, plotted as a function of vertical wind shear and temperature lapse rate.

often from the low pressure to the high pressure side of the upper-level flow and most often was nearly perpendicular to the streamlines. An added effect in cases where a well-developed trough existed, especially at 500 mb., was upslope motion, as suggested in figures 1 and 4 by the isotherms.

Arakawa [4] derived an equation that yields a critical value of horizontal shear of 15 knots per degree of latitude. Any value above this limit would yield heavy turbulence. Harrison and staff [5] give a critical shear value of 50 knots per 150 nautical miles. It is thought, however, that because clear air turbulence is generally reported in a narrower horizontal band than 150 miles, the practical calculation of shear from the wind difference over a finite normal distance should perhaps use an interval of about 50 nautical miles. This would yield more representative values of the shear necessary to produce clear air turbulence. It is unfortunate that the wide spacing of upper-air reporting stations makes use of this smaller interval extremely difficult.

In an attempt to correlate vertical wind shear and vertical temperature gradient over a 5,000-ft. interval in the turbulence cases, a great variation in the paired values was found. Figure 5 shows pilot reports of clear air turbulence plotted with ordinate of vertical wind shear over a 5,000-ft. interval regardless of sign and abscissa of change in temperature in degrees Celsius over the same vertical interval. The cases studied make up only a small sample, but they do indicate that clear air turbulence can exist with a vertical wind shear of less than 10 knots per 5,000 ft., and with temperature lapse rates of 5° C. per 5,000 ft. or greater. The graph shows that a vertical wind shear of 15 knots per 5,000 ft. is enough to produce clear air turbulence if the lapse rate is more than 5° C. per 5,000 ft. The strong vertical wind shear of 55 knots per 5,000 ft. that is plotted on the graph (fig. 5) is for the same date and time as figures 1 and 2.

Clear air turbulence was reported in areas of 24-hour height falls at 500 mb. The correlation here was only a little over 0.5, but suggests a relation of kinetic height changes to clear air turbulence. Taking the changes over a 24-hour period tends to mask such a relation; it is believed that if changes over a smaller interval of time, say 6 hours, could be computed, a better relation between clear air turbulence and height changes at 500 mb. might be found.

3. SUMMARY

Clear air turbulence was most often reported at levels above 15,000 ft. whenever the 500-mb. chart showed a closed Low or a well defined trough. The turbulence was then found in the southwesterly flow ahead of the trough line, on the low pressure side of the maximum wind field.

The reports received indicated the existence of clear air turbulence in the vicinity of the jet core, on the poleward or low pressure side of the jet; this is in close agreement with the findings of Bannon [6] and Jones [7] in investigations of clear air turbulence in the British Isles. But clear air turbulence is not a phenomenon of the jet stream alone, for it was reported as far as 20,000 ft. below the level of maximum winds.

There was evidence that a strong horizontal shear across a trough line adds to the intensity of clear air turbulence. Some evidence pointed to the existence of clear air turbulence in the right quadrant of negative height falls at 500 mb., but the correlation was not very strong.

REFERENCES

1. M. E. Balzer, and H. T. Harrison, "The Nature of High Level Clear Air Turbulence," United Air Lines, *UAL Meteorology Circular*, No. 48, Denver, Colo., July 1, 1959.
2. U.S. Weather Bureau, "Normal Weather Charts for the Northern Hemisphere," *Technical Paper* No. 21, October 1952, 74 pp.
3. L. H. Clem, "Clear Air Turbulence over the United States," *Aeronautical Engineering Review*, vol. 16, No. 11, Nov. 1957, pp. 63–68.
4. H. Arakawa, "Possible Heavy Turbulent Exchange Between the Extratropical Air and the Polar Stratospheric Air," *Tellus*, vol. 3, No. 3, Aug. 1951, pp. 208–211.
5. H. T. Harrison and Staff, "The Use of Horizontal Wind Shear in Forecasting High Level Clear Air Turbulence," United Air Lines, *UAL Meteorology Circular*, No. 49, Denver, Colo., July 15, 1959.
6. J. K. Bannon, "Severe Turbulence Encountered Near the Jet Stream," *Meteorological Magazine*, vol. 80, No. 951, September 1951, pp. 265–269.
7. D. C. E. Jones, "Investigation of High Altitude Clear Air Turbulence Near Jet Streams: Special Flights by R.A.F. and R.A.E. Aircraft," Meteorological Research Committee (London) *MRP* 827, July 24, 1953.

ANALYSIS OF CLEAR AIR TURBULENCE DURING APRIL 1960

DEVER COLSON

U.S. Weather Bureau, Washington, D.C.

[Manuscript received November 17, 1960; revised January 4, 1961]

ABSTRACT

Clear air turbulence (C-A-T) occurrences over the United States reported by pilots in April 1960 are analyzed with reference to weather conditions, wind speed, horizontal and vertical wind shear, thermal stability, and jet stream location and curvature. The day-by-day plot of the occurrences shows that the peak of the C-A-T activity was associated with sharp and well developed troughs which extended far to the south. In the analysis of the data, it is found useful to separate the cases east and west of 103° W. longitude. The cases west of 103° W. indicate greater importance of higher stability and less importance of large horizontal wind shear. The cases east of 103° W., away from the influence of the western mountains, indicate greater importance of decreased stability when combined with either large horizontal or vertical wind shear. Well developed jet streams were apparent with the occurrences in both areas. However, the western cases show a preponderance of cyclonic curvature while the eastern cases show nearly equal division between cyclonic and anticyclonic curvature.

1. INTRODUCTION

The purpose of this study was to make a preliminary analysis of the Clear Air Turbulence (C-A-T) occurrences for April 1960 with reference to the meteorological conditions in order to determine the problems involved in obtaining all the necessary data, in analyzing the data, and in interpreting the results. This study provides some groundwork and guidelines for a broader investigation of C-A-T in addition to furnishing some tentative conclusions regarding the meteorological conditions associated with C-A-T.

Pilot reports for this period collected from the Washington National Airport, United Airlines, and American Airlines, were scanned for clear air turbulence (C-A-T) occurrences. Table 1 is a tabulation of all cases of turbulence over 10,000 feet, except those which definitely were described as in or near thunderstorms, squall lines, or with icing in clouds.

2. METHOD OF ANALYSIS

Since light turbulence is not a major concern to aircraft operations, only the moderate and severe turbulence occurrences were used in the analysis. The following parameters were examined in connection with each occurrence:

a. Surface weather—thunderstorms, squall lines, fronts, showers, clouds.
b. Wind Speed.
c. Horizontal wind shear (in knots per 100 miles).
d. Vertical wind shear (in knots per 1000 feet).
e. Thermal stability (potential temperature lapse rate, ° C. per 1000 feet).
f. Location, intensity, and curvature of the jet stream.

TABLE 1.—*Clear air turbulence occurrences over the United States for April 1960.*

Light	195
Moderate	223
Severe	66
Unknown intensity	6

In this analysis, the parameters were evaluated as near as possible at the actual location and level of the reported turbulence even though greater values of these parameters might be found at some nearby location or level. The actual evaluations were based on the upper-level charts as analyzed at the National Weather Analysis Center (NAWAC) and on all the appropriate rawinsonde, radiosonde, and pilot balloon reports. In most cases, this analysis called for considerable interpolation between observation sites and times. As far as possible, a spacing of 100 miles centered at the site of actual occurrence was used in the evaluation of the horizontal wind shear and a 2000-ft. layer centered at the level of the actual turbulence was used for the evaluation of the vertical wind shear and the stability.

Many of the reports were not specific as to whether the turbulence occurred in clear air or in clouds. The presence of thunderstorms, squall lines, widespread showers and cloud cover as determined by surface maps and other weather data reduced the number of C-A-T cases to approximately 170.

3. SYNOPTIC PATTERNS

The locations of the C-A-T occurrences were plotted on both the maximum wind and 300-mb. charts for the chart time nearest the time of the turbulence. Forty percent of the C-A-T occurrences were between 0600 and 1800 GMT and 60 percent between 1800 and 0600 GMT.

The larger number of occurrences in the latter period is likely due to a greater number of flights during these afternoon and evening hours.

Figure 1 shows the day-by-day occurrences of C-A-T during this period. The four major peaks in the C-A-T activity corresponded to the presence of large-amplitude major troughs aloft in the C-A-T areas during these periods. This is in agreement with the findings of Harrison [1].

This is illustrated in the sequence of 300-mb. charts as analyzed by NAWAC for the April 12–14 period (fig. 2). As the trough deepened and moved eastward, the C-A-T occurrences moved with the trough until it began to dissipate. Similar sequences were apparent during the other peak periods but are not shown in this paper.

4. LOCAL PARAMETERS

The first examination showed a wide scatter in the values of the various local meteorological parameters in connection with the observed C-A-T occurrences. It was not until the occurrences over the coastal ranges and the Rocky Mountains were separated from the occurrences to the east of the Rockies that some patterns and conclusions could be drawn.

Table 2 shows the range in the values of the wind speed, horizontal and vertical wind shear, stability, and the presence and curvature of the jet stream associated with the C-A-T occurrences. A line at approximately 103° W. was used to separate the cases over the western mountains and those to the east of the mountains.

The scatter in the values of the wind speed and the vertical wind shear is about equally great in the eastern and the western occurrences. Over 70 percent of the occurrences had wind speeds of 50 knots or more and about 45 percent of the occurrences were associated with vertical wind shear of 4 knots per 1000 feet or more. A great

TABLE 2.—*Number of cases of occurrence of values of meteorological parameters associated with the C-A-T occurrences.*

	Wind speed (knots)				Horizontal wind shear (knots per 100 miles)			
	0–49	50–74	75–99	≥100	0–14	15–24	25–34	≥35
East of 103° W.	18	28	19	8	18	24	20	12
West of 103° W.	27	33	17	11	36	34	15	5
	Vertical wind shear (knots per 1000 feet)				Lapse rate (potential temperature) (°C. per 1000 feet)				
	0–1.0	1.1–2.4	2.5–3.9	4.0–6.9	≥7.0	0–1.0	1.1–2.4	2.5–3.9	4.0–5.9	≥6.0
East of 103° W.	13	6	13	13	20	26	12	18	11	3
West of 103° W.	21	10	9	21	15	20	11	15	18	12
	Jet stream present		Jet stream curvature		Cold Low present					
	Yes		No		Cyclonic		Anticyclonic			
East of 103° W.	63		10		34		29		3	
West of 103° W.	76		14		56		20		6	

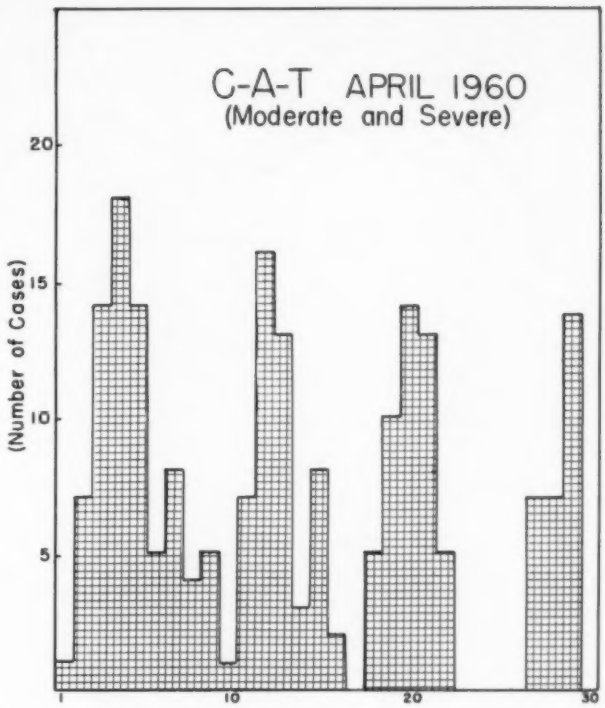

FIGURE 1.—Day-by-day occurrences of clear air turbulence (C-A-T) during April 1960.

preponderance of the occurrences were associated with a pronounced jet stream. However, the western cases show a preponderance of cyclonic curvature while the eastern cases show nearly equal division between cyclonic and anticyclonic curvature of the jet stream.

There appears to be a difference between the western and eastern occurrences with regard to the horizontal wind shear and the stability. Over 77 percent of the western occurrences were associated with a horizontal wind shear of less than 25 knots per 100 miles while only 57 percent of the eastern occurrences were associated with horizontal wind shears of less than 25 knots per 100 miles. Over 46 percent of the western cases had lapse rates of potential temperature ($\Delta\theta/\Delta z$) greater than 4° C. per 1,000 feet as compared to only 20 percent of the eastern occurrences.

Figures 3 and 4 relate the horizontal and vertical wind shear for the C-A-T occurrences in these two areas. The relationship with stability is also indicated through the symbol used for the plotted occurrences. Lines indicating the criteria of 25 knots per 100 miles for horizontal shear and 5 knots per 1,000 feet for vertical shear are drawn on the charts. These criteria are close to the 50 knots per 150 miles given by Harrison [1] and the 6 knots per 1,000 feet given by George [2].

It is important to note that only 16 percent of the eastern C-A-T occurrences (fig. 3), had both the horizontal and vertical shear in excess of the above two criteria and

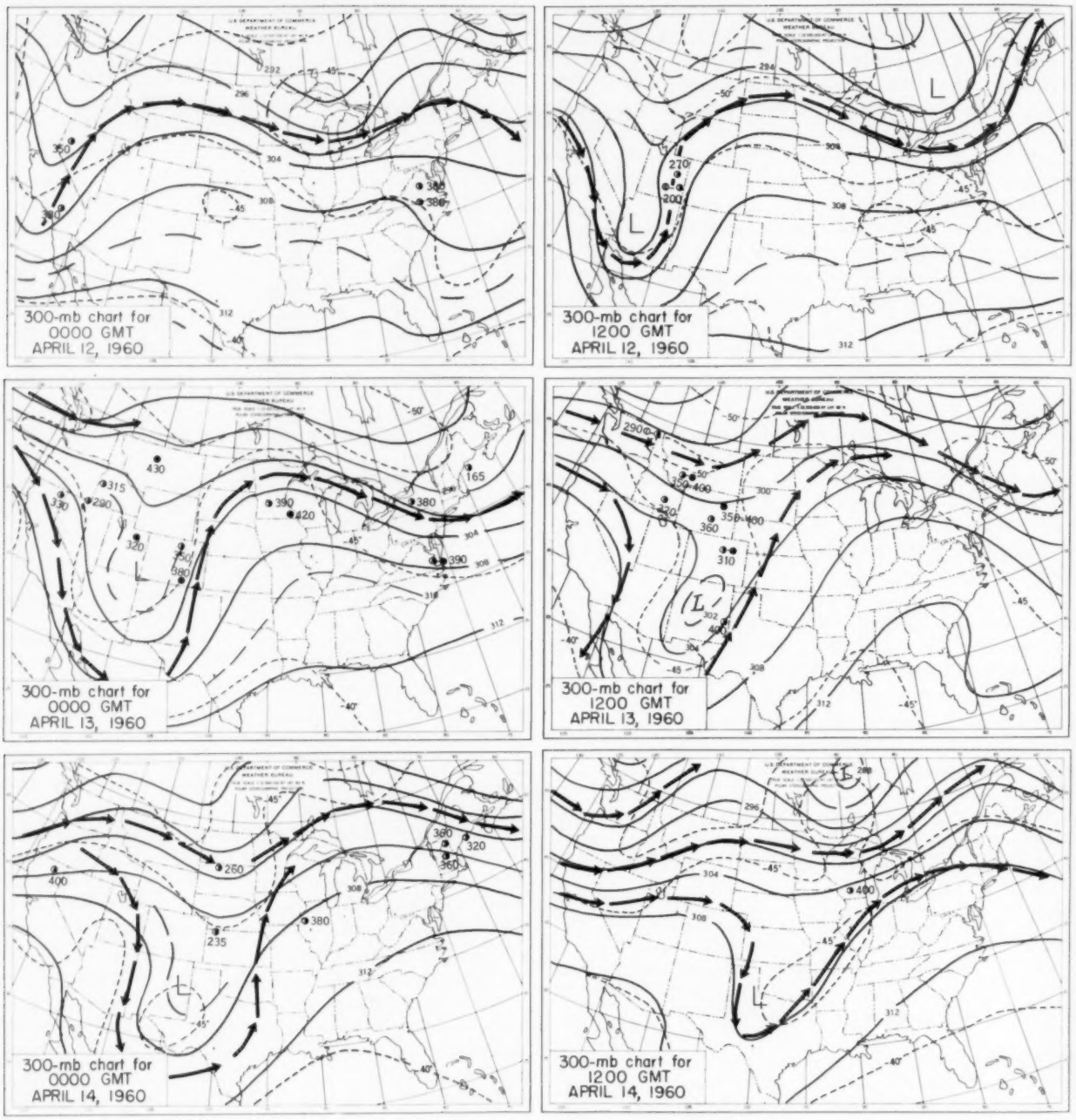

FIGURE 2.—Sequence of 300-mb. charts for the April 12–14, 1960 period of pronounced C-A-T activity. Contours (labeled in hundreds of feet) are given by solid lines, isotherms (°C.) by dashed lines. Jet axis is shown by arrows. Reports of turbulence are plotted as circles (◌ light intensity, ◑ moderate, and ● severe) with height of report in hundreds of feet.

that 33 percent of the cases had both the horizontal and vertical shear below these criteria. However, in 67 percent of the cases, either the horizontal or the vertical wind shear did exceed these criteria. This suggests that it is not necessary to have both a large horizontal wind shear and a large vertical wind shear.

It is interesting to note that where the vertical wind shear was less than 5 knots per 1,000 feet, 53 percent of the eastern C-A-T occurrences had $\Delta\theta/\Delta z$ equal to or less than 1.5° C. per 1,000 feet and only 17 percent had $\Delta\theta/\Delta z$ equal to or greater than 4.5° C. per 1,000 feet. Where the vertical shear was more than 5 knots per 1,000 feet, only

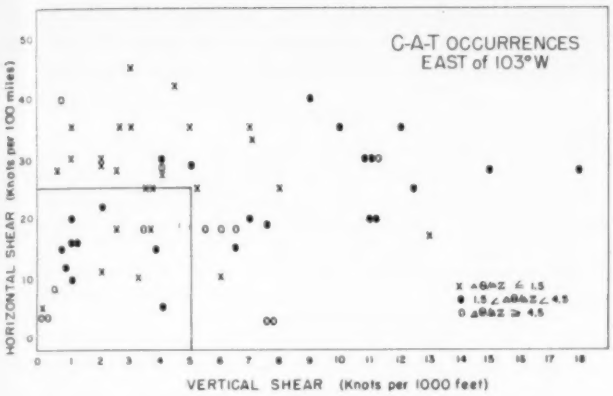

FIGURE 3.—Horizontal and vertical shear for the C-A-T occurrences east of 103° W.

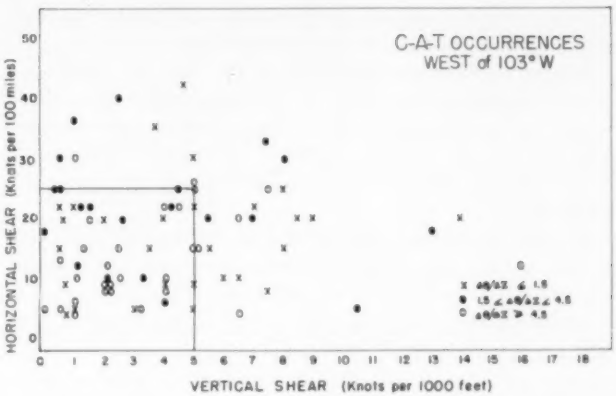

FIGURE 4.—Horizontal and vertical shear for the C-A-T occurrences west of 103° W.

20 percent of the occurrences were associated with the less stable situations. This suggests that lower stability is necessary in the cases where large vertical shear is missing.

Where the horizontal wind shear was equal to or greater than 25 knots per 100 miles, over 58 percent of the eastern C-A-T occurrences were associated with low stability ($\Delta\theta/\Delta z$ equal to or less than 1.5° C. per 1,000 feet) and only 7 percent were associated with high stability ($\Delta\theta/\Delta z$ equal to or greater than 4.5° C. per 1,000 feet). Where the horizontal wind shear was less than 25 knots per 100 miles, the occurrences were associated with a more even distribution of the stability values. Apparently, low stability is more important in the situations with large horizontal wind shear.

Over 62 percent of the western C-A-T occurrences (fig. 4) had both the horizontal wind shear less than 25 knots per 100 miles and the vertical shear less than 5 knots per 1,000 feet. This is in decided contrast to the 33 percent of the eastern cases in this category. This would indicate that strong horizontal and vertical shear are not as important over the mountains as over the eastern area.

Over 33 percent of the western cases were associated with low stability ($\Delta\theta/\Delta z$ equal to or less than 1.5° C. per 1000 feet) and 37 percent with high stability ($\Delta\theta/\Delta z$ equal to or greater than 4.5° C. per 1000 feet). This is in contrast to the 48 percent with low stability and 13 percent with high stability in the eastern C-A-T occurrences.

This indication of the greater importance of high stability over the mountains is in agreement with past work on mountain waves [3] which called for a fairly stable layer with little evidence of any pronounced horizontal wind shear.

In the April data, there were nine cases which seemed to be associated with upper level cold Lows. Six of these nine cases were along the west coast. Other C-A-T cases seemed to be related to very cold tropopause situations. These relationships will require further study.

5. CONCLUSIONS

Because of the indefiniteness of many of the original pilot reports and the possibilities of incorrect evaluation of the meteorological parameters at the scene of the turbulence, conclusions cannot be drawn with too much certainty from the analysis of data in this study. However, it is felt that the general indications as stated are valid.

One important fact which must be recognized in such studies is that the distance between the present upper-air stations is much larger than the scale of the observed turbulence. It is unlikely that there will ever be a network of upper-air stations sufficiently dense and with sufficient frequency of observations to insure the determination of the exact value of the parameters in the actual area and at the time of turbulence occurrence.

This leads to the suggestion that large-scale patterns associated with the development of clear air turbulence should be stressed. These patterns can be detected and measured on the standard synoptic weather charts. Considerable attention must then be given to the various possible atmospheric processes which will lead to the development of these local turbulence situations [4, 5].

Over the western mountains, apparently both the low stability situations which favor mixing and turbulent motions and also the more stable wave situations are important. East of the mountains, low stability is an important factor along with either a strong horizontal or a strong vertical wind shear.

Recent work by Clodman, Morgan, and Ball [6] stressed the importance of gravity waves over continental areas. They pointed out that the combined gravity wave-vertical wind shear mechanism is predominant over land areas. The conclusions in this study seem to be in fair agreement with their ideas. In spite of the much larger area east of 103° W., there were 90 C-A-T cases to the west and 74 cases to the east of the dividing line. The larger

number of occurrences over the mountains supports their stress on the influence of the underlying terrain.

Again, there is the handicap of the lack of knowledge about what is taking place in the areas other than those reporting turbulence. A more intensive observation program is needed in which reports of all the non-occurrences of C-A-T as well as the occurrences are available for analysis.

In the meantime, the Weather Bureau is collecting weekly a summary of pilot reports covering C-A-T occurrences from all of the Airway Forecast Centers as well as various airlines. Further papers covering these studies will be forthcoming.

ACKNOWLEDGMENTS

The writer wishes to acknowledge the encouragement and suggestions given by Dr. Harry Wexler and Mr. Newton Lieurance in this clear air turbulence research program. Special thanks must be given to Miss Sarah Kroll for her valuable assistance in the data compilation and analysis and in the preparation of the manuscript.

REFERENCES

1. H. T. Harrison, "The Use of Horizontal Wind Shear in Forecasting High Level Clear Air Turbulence," United Air Lines, Inc., *Meteorology Circular* No. 49, Denver, July 15, 1959.
2. J. J. George, *A Method for the Prediction of Clear Air Turbulence*, Eastern Air Lines, August 1960.
3. DeVer Colson, "Meteorological Problems in Forecasting Mountain Waves," *Bulletin of the American Meteorological Society*, vol. 35, No. 8, Oct. 1954, pp. 363–371.
4. M. E. Balzer and H. T. Harrison, "The Nature of High Level Clear Air Turbulence," United Air Lines, Inc. *Meteorology Circular* No. 48, Denver, July 1, 1959.
5. E. L. Keitz, "Differential Advection as a Factor in Clear-Air Turbulence," *Journal of Meteorology*, vol. 16, No. 1, Feb. 1959, pp. 57–62.
6. J. Clodman, G. M. Morgan Jr., J. T. Ball, *High Level Turbulence*, Research Division, College of Engineering, New York University, Contract No. AF 19(604)–5208, September 1960.

Recent Articles in Other Weather Bureau Periodicals

Mariners Weather Log, vol. 5
No. 1, January 1961
"North Atlantic Tropical Cyclones, 1960," by G. W. Cry, pp. 1–7.
"Commission on Maritime Meteorology," by W. W. Shinners, pp. 7–9.
Weekly Weather and Crop Bulletin, National Summary, vol. XLVII
No. 46, November 4, 1960
"Mean Percentage of Possible Sunshine, November" (Map for United States) p. 8.
No. 48, November 28, 1960
"Mean Percentage of Possible Sunshine, December," p. 8.
No.52, December 26, 1960
"Index of Special Articles in Weekly Weather and Crop Bulletin 1960", p. 8.
Vol. XLVIII
No. 2, January 9, 1961
"Climatological Probabilities of the Weather of Inauguration Day," by M. L. Waggoner, p. 8.
No. 4, January 23, 1961
"Disaster Designations and Emergency Production Loans," January 1–December 31, 1960 (Map for contiguous United States plus descriptions for Alaska, Hawaii, Puerto Rico, and Virgin Islands) (Data from Federal Register.)

THE HURRICANE SEASON OF 1960

GORDON E. DUNN

Weather Bureau Office, Miami, Fla.

1. GENERAL SUMMARY

The hurricane season of 1960 was subnormal from the standpoints of both frequency and intensity. Seven tropical cyclones developed in the Atlantic and four reached hurricane intensity (fig. 1). However, only one hurricane—Donna—was of major intensity, although Ethel may have been so for a few hours. Donna was the most destructive hurricane ever to strike Florida and one of the most damaging ever to affect the United States. It is also believed to have caused hurricane winds over a greater proportion of the United States coastline than any other known hurricane. Tropical cyclones were well distributed throughout the season except in October which was remarkably free from even the weak disturbed conditions normally observed in the Tropics. Tracks of the tropical cyclones are shown in figure 1.

The mean 700-mb. circulation for June [1] was attended by above normal heights in the Atlantic over most areas north of 30° N. and below normal over most of the Tropics and subtropics. This circulation type is usually associated with at least normal tropical cyclone activity. The June cyclone (unnamed) formed in a manner described by Riehl [2] in which a westerly trough of large amplitude extending well into the Tropics fractures and the southern portion retrogrades followed by the development of a tropical cyclone.

The maximum positive 700-mb. height anomaly in the Atlantic for July was about 150 feet in the middle Atlantic between 40° and 50° N. with a United States east coast trough of considerable amplitude [3]. Normal tropical cyclone frequency in the Atlantic area during July is only one storm every two years [4]; thus the two tropical cyclones represent considerably above normal activity. Abby developed in very low latitudes and did not come under the influence of the east coast trough. Indeed, much of Abby's track (fig. 1) was along the lowest latitude of record for July.

The formation of Brenda was rather similar to that of the unnamed June storm.

Stark [5] noted a major reversal in the large-scale 700-mb. mean circulation over North America and adjacent ocean areas between the first and last halves of August. The belt of positive height anomalies shifted northward from 30°–40° N. during the first half to 40°–50° N. during the latter half of the month. Although heights remained near or above normal through most of the Tropics and subtropics—a condition not very favorable for tropical cyclone formation—the circulation during the latter half of the month more nearly conformed to the favorable type described by Ballenzweig [6] and Cleo formed on the 18th.

In contrast to the subnormal activity in the Atlantic, tropical cyclone frequency in the western Pacific in August was unprecedented [5]. Eleven storms were reported, nine reaching typhoon intensity. A positive 700-mb. height anomaly was located some 1000 miles east of Japan with a negative anomaly over Formosa (possibly in part due to some six tropical cyclones tracked over or near the area) resulting in unusually deep easterlies in the formation area.

Tropical cyclone activity was normal during September with two hurricanes, one tropical storm, and several tropical disturbances which moved along paths rather similar to those of Donna and Florence (fig. 1) but never reached storm intensity. The 700-mb. anomaly pattern in the Atlantic agreed rather well with the composite chart described by Ballenzweig [7] as favorable for tropical cyclone development. The mean circulation for September was predominantly one of high index and the axis of mean 700-mb. zonal wind speed maximum was displaced a substantial distance north of normal over North America [8].

Tropical cyclone activity in the Atlantic was nonexistent during October. The mean circulation for the month in the Atlantic area was most unusual [9]. Due to blocking, the subtropical ridge and maximum westerly winds were displaced to the south of their normal positions.

All but two of the 1960 North Atlantic tropical cyclones developed in or reached the Gulf of Mexico and all recurvatures in the Tropics and subtropics were west of longitude 70° (fig. 1) indicating an Azores-Bermuda anticyclone of considerable constancy and strength June through September.

Damage and fatality statistics are shown in table 1. Estimates are necessarily approximate. In Donna's damage total for Florida, citrus damage has not been included although 30 percent of the grapefruit and 10 percent of the oranges were lost. The subsequent increase in citrus prices is thought to have compensated for the crop damage. Insurance companies paid off about $90,000,000 in property losses in Florida and it is esti-

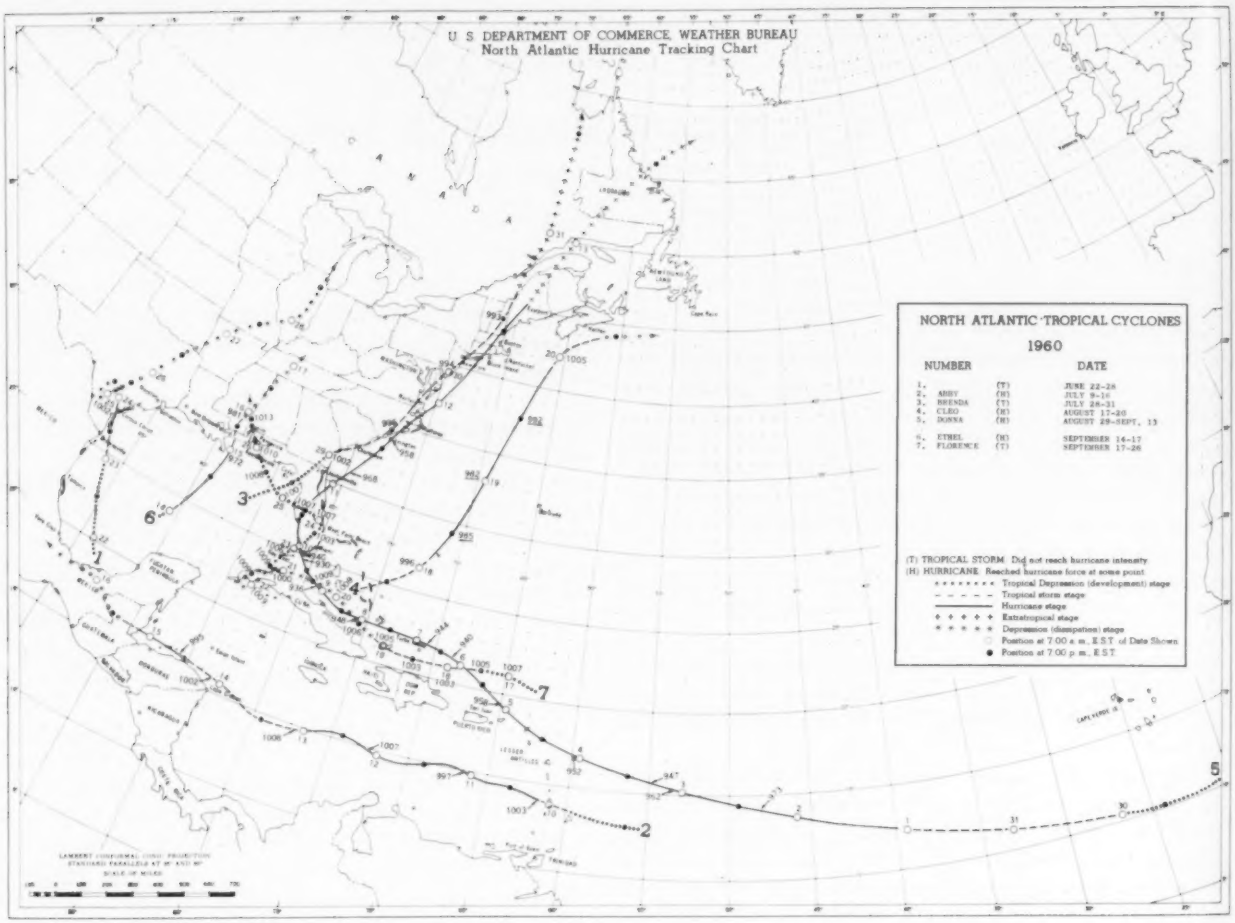

FIGURE 1.—Tracks of North Atlantic tropical cyclones, 1960, with minimum pressures. Underlined pressures in Cleo are estimated as function of observed winds.

mated about one-third of the property damaged was insured.

2. INDIVIDUAL TROPICAL CYCLONES

Tropical Storm (unnamed), June 22–28.—A routine reconnaissance flight into the extreme southwestern Gulf of Mexico on June 22 found a large mass of weather including heavy thunderstorms and squally winds up to 35 kt. The lowest observed pressure along the reconnaissance track was 1008 mb. with no circulation reported, although the Mexican coastal stations did indicate a slight circulation.

On the morning of June 23 the 200-mb. level had become more favorable for intensification and the barometer had fallen significantly along the Mexican coast from Tampico to Brownsville indicating a northerly drift of the disturbed condition. A Navy reconnaissance plane was dispatched to the area and found maximum winds of only 15 kt. but sea level pressure of 1006 mb. However, it is believed the plane did not fly under the most severe weather.

During the night of June 23–24 the tropical storm moved

TABLE 1.—*Fatality and damage statistics, North Atlantic tropical cyclones of 1960*

Storm	Intensity	Date	Damage	Deaths	Principal areas affected
Unnamed	Storm	June 23–26	$3,600,000	15	Texas.
Abby	Hurricane	July 10	600,000	6	St. Lucia, Martinique.
		July 15	slight	0	Honduras, Br. Honduras.
Brenda	Storm	July 28–29	5,000,000	0	Florida.
Cleo	Hurricane	Aug. 17–20	slight	0	Off-shore Atlantic.
Donna	Hurricane	Sept. 9–12	300,000,000	13	Florida.
			56,500,000	8	North Carolina.
			30,000,000	29	Elsewhere U.S.
			13,000,000	114	Antilles and Bahamas.
			400,000,000	164	All areas.
Ethel	Hurricane	Sept. 14–15	1,000,000	0	Central Gulf Coast.
Florence	Storm	Sept. 22–26	slight	0	Florida.
Total within United States			$396,160,000+	65	
" outside United States			13,600,000+	120	

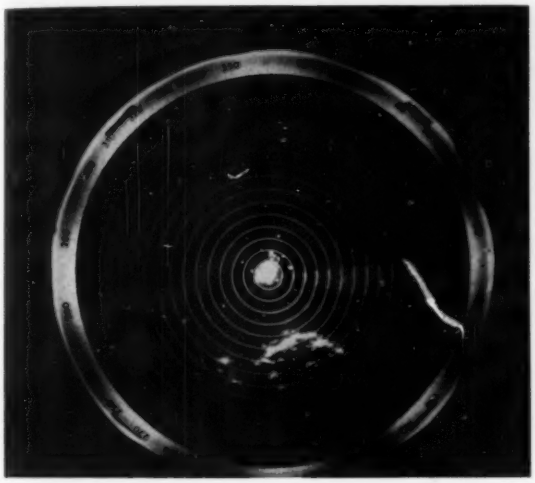

FIGURE 2.—First rain band of tropical storm of June 23, 1960, showing characteristic curvature. Taken at Freeport, Tex. Range markers at 20 statute miles. Photo courtesy Dow Chemical Co.

inland, south and about 30 miles west of Corpus Christi, Tex. Rockport reported sustained winds of 40 m.p.h. with gusts to 60 and Padre Island Park 50 m.p.h. with gusts to 60. The lowest reported pressure was 1002.4 mb. at Alice at 0300 CST on the 24th. Corpus Christi reported a tide of 3.5 ft. above mean low water. It appears that there was no wall cloud. There was some mild curvature on the rain bands seen on airborne radar on the 23d and the Dow Chemical Co. radar at Freeport near noon on the 23d reported a characteristically curved rain band (fig. 2). Apparent cloud centers were reported by radars at Victoria and Kelly Air Force Base on several occasions. Three fishing piers were wrecked on Copano Bay; one shrimp boat sank with three lives lost, and another was beached. The storm moved very slowly on June 24–25 attended by heavy rains of 5 to 15 inches or more from Corpus Christi to San Antonio and northeastward with considerable flooding. Port Lavaca reported 29.76 inches of rain for the period June 23–26. Tornadoes were reported on the 26th as the dying storm moved north-northeastward. Unusually heavy rains extended into Arkansas and southern Illinois.

Fifteen persons apparently were drowned either in the high seas or subsequent floods. Damage, mostly from the floods, is estimated at $3,600,000.

Hurricane Abby, July 9–16.—The first indication of the disturbance which finally grew into hurricane Abby was received from a ship about 3.5° east of the island of Barbados, at 0500 EST on July 9. Showery weather was reported with east-southeast winds of near 40 kt. Some shower activity had been occurring in the Lesser Antilles, and 24-hour pressure changes were small but negative. At 0100 EST on the 10th, a report received from the SS *Del Oro*, located at 13.8° N., 59.7° W., with sea level pressure of 1007.6 mb. and wind ENE 45 kt., indicated a strong easterly wave or a small vortex. A small center passed just to the north of Barbados during the next few hours.

At 0800 EST July 10, an advisory was issued on tropical storm Abby, based on reports from the Leeward Islands and a few ships. The storm was moving toward the west-northwest and was forecast to reach hurricane intensity during the day. Reconnaissance aircraft were dispatched to the area and confirmed the existence of hurricane Abby by 1100 EST. Highest winds were estimated at 90–100 m.p.h. over a small area near the center. Gale warnings and a hurricane watch were ordered for the Virgin Islands and Puerto Rico and for the island of Hispaniola as the hurricane moved westward.

On July 11 and 12, the hurricane continued on a westerly course, with doubt concerning its intensity. From reconnaissance aircraft and surface ship reports, it appeared to be rather poorly organized and much of the time was barely discernible on aircraft radar. By the morning of the 13th, the hurricane had diminished in intensity, with maximum winds estimated at 60 m.p.h. in a few squalls near the center in the northern semicircle. By early morning of the 14th, the storm had reintensified to hurricane strength with highest winds of 80 m.p.h. estimated by reconnaissance aircraft. The hurricane retained this strength but remained quite small in size as it skirted along the northern cost of Honduras, passing inland in extreme southern British Honduras early on the morning of the 15th. Advisories were discontinued after the cyclone moved inland.

Considerable rain occurred in Central America from Honduras north-northwestward into most of southern Mexico and the Gulf of Campeche as the remnants of Abby continued west-northwestward over the land area. Reconnaissance aircraft in the southwestern Gulf of Mexico on the 16th confirmed that the radar center of circulation did not emerge over the Gulf of Campeche but remained over the rugged terrain of the Isthmus of Tehuantepec.

An airborne radar picture of Abby (fig. 3), as the storm just about attained hurricane intensity off the northwestern tip of St. Lucia, shows the characteristic figure-nine and the asymmetrical cloud and precipitation pattern in the early formative stage at low latitudes. Only in a few squalls in the main rain band on the north and east sides were hurricane winds occurring. The radar picture in figure 4 on the morning of July 15 as the hurricane was approaching the coast of British Honduras shows a hurricane with a perfectly round eye and complete wall cloud. The eye was apparently not observed by the Swan Island radar as it passed within approximately 70 n. mi. of the station the day before.

At 500 mb. on July 8 and 9, the subtropical ridge was centered over Florida at about latitude 27° N. and extended eastward into the Atlantic north of the Antilles

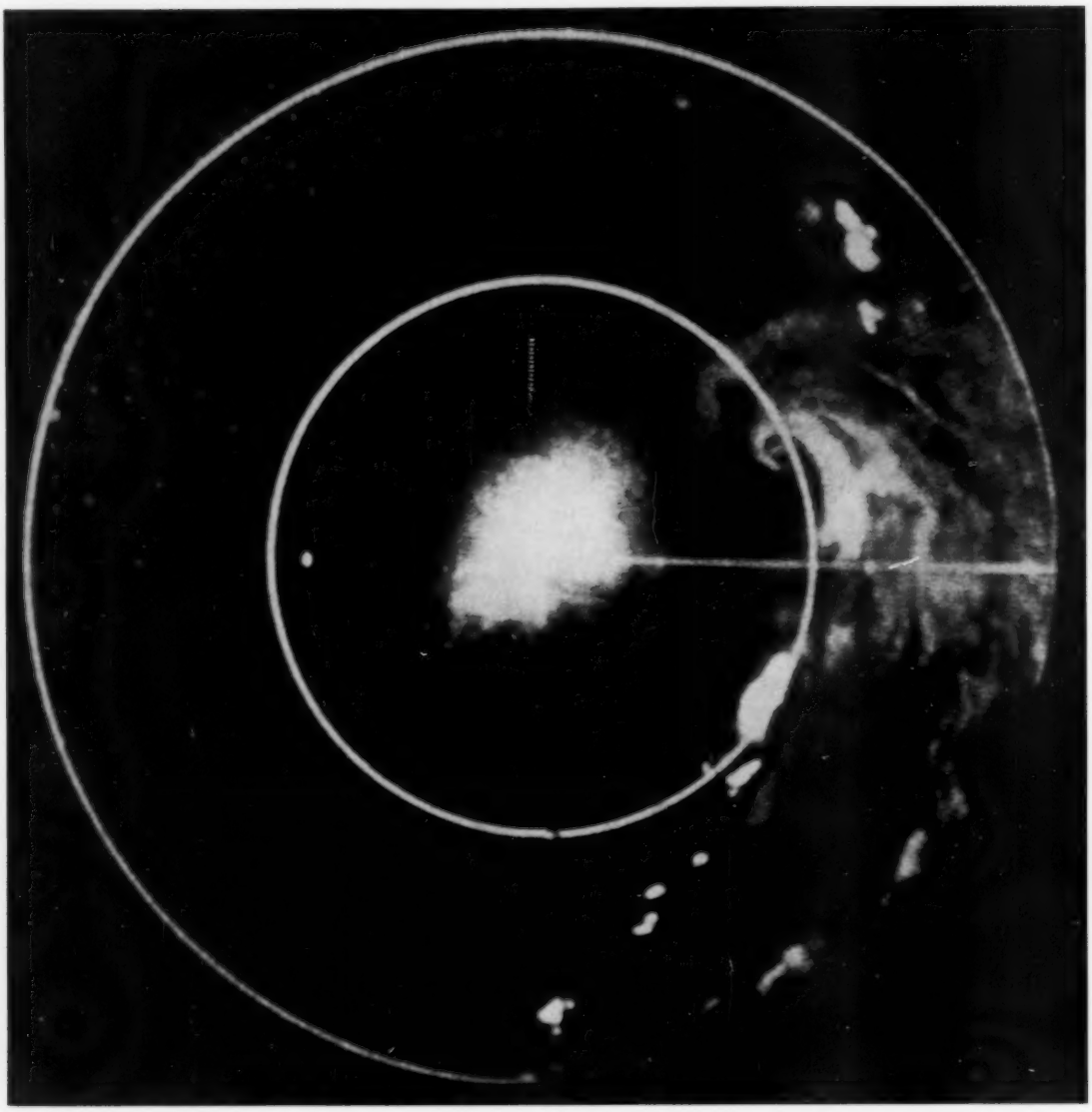

FIGURE 3.—Airborne radar picture of hurricane Abby in formative stages off St. Lucia. Note the characteristic figure-9 echo of a developing storm. Official U. S. Navy photo.

at about the same latitude. Easterly winds 10 to 20 kt. prevailed at Trinidad and northward across the Leeward and Windward Islands. By 1900 EST of the 9th, the winds had become light easterly at Trinidad and backed to northeasterly and increased substantially in the Windward Islands. The winds remained easterly and of moderate speeds in the Antilles until Abby passed inland over the Yucatan Peninsula.

Only minor fluctuations were noted in winds at 500 mb. at Curaçao and San Andres, the direction remaining easterly and the speeds dropping off slightly on the south side of the storm. The subtropical ridge persisted over the Gulf of Mexico as Abby continued westward into Mexico.

At 200 mb., beginning on the 9th, moderate to strong easterly to southerly flow developed over the eastern Caribbean, with the appearance of a vigorous anticyclone off and to the east of the Windward Islands. This indicated strong outflow, and favored intensification of Abby, according to Riehl. On the 12th and 13th, this circulation had about disappeared, although a weak anticyclone persisted over Abby. By the morning of the 14th, the anticyclone at 200 mb. had again become more vigorous and, at the same time, Abby reintensified to full hurricane strength.

Abby appeared to be fairly well organized when it first formed and moved into the extreme eastern Caribbean. Reconnaissance and surface reports, particularly

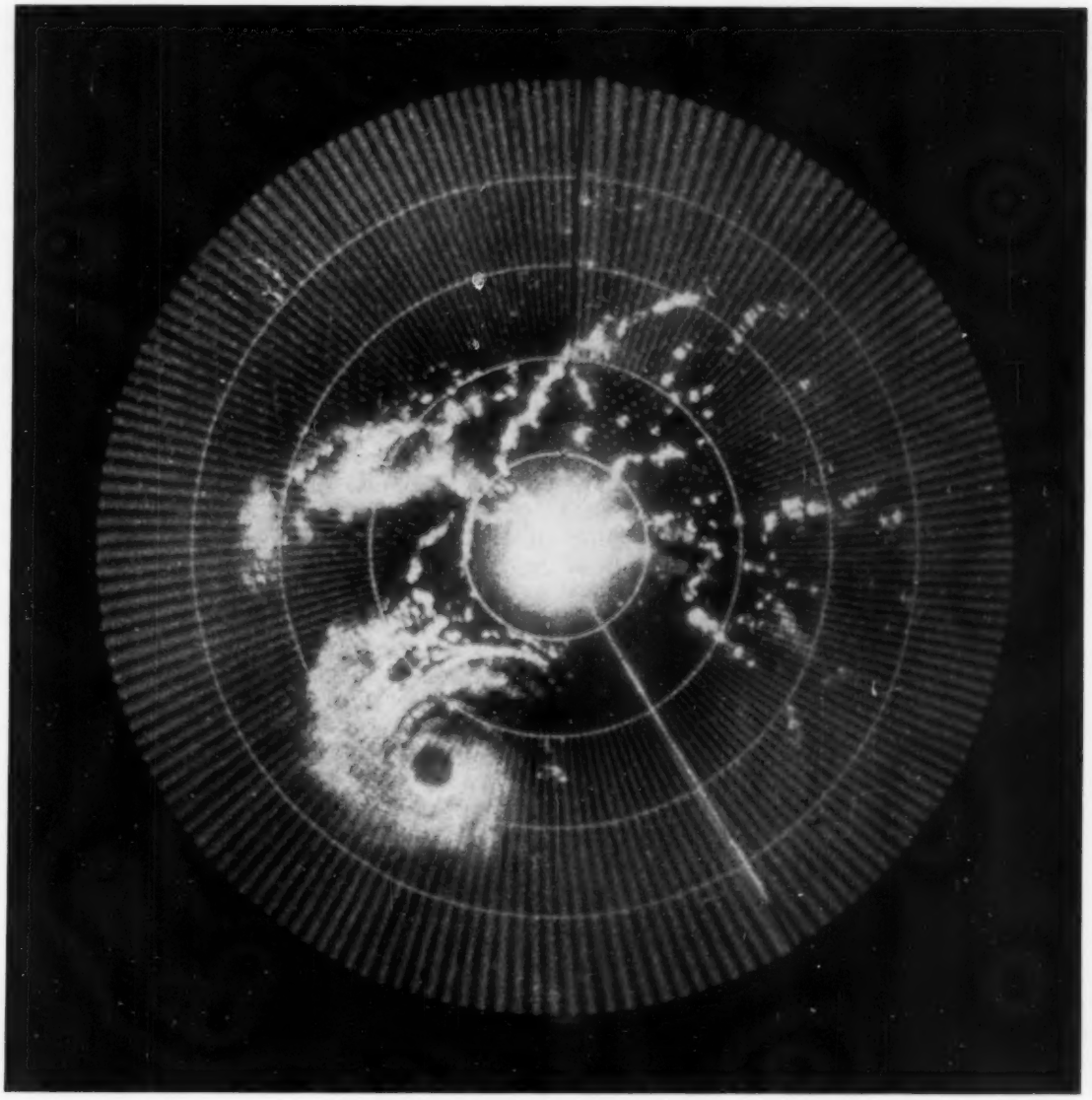

FIGURE 4.—Hurricane Abby on the morning of July 15 as it was approaching the coast of British Honduras. Note the complete wall cloud. Official U. S. Navy Photo.

on the 11th, 12th, and 13th, indicated a very small circulation, and a minimum of convective activity. This is possibly one reason for the loss of intensity. The area was covered with considerable stratified cloudiness, and radar coverage was difficult.

Peak wind gusts of 55 kt. were observed at St. Lucia when Abby passed about over the island, and the lowest pressure was 29.80 inches (1009.1 mb.). Rainfall was 6.80 inches in 24 hours. Martinique reported gusts of 66 kt.

Six lives were lost on St. Lucia when the roof of a house collapsed. Damage was estimated at $435,000 to property and banana and coconut plantations on St. Lucia. No estimate has been received from Martinique, however 33 percent of the banana and cane crop was lost, and considerable damage resulted to roads and bridges. Only slight damage occurred elsewhere in the Lesser Antilles. No loss of life has been reported from Central America. Property damage in British Honduras was light but damage to crops quite heavy.

Some remnants of Abby apparently continued across southern Mexico and developed into hurricane Celeste off the west coast [3].

Tropical Storm Brenda, July 28–31.—A weak cyclonic circulation that can be traced back to a position just off the southwestern Florida coast on July 27 began to deepen some 150 miles west of the Tampa Bay area the next day. By the night of July 28, pressure had dropped to near 1000

mb. as the Low began accelerating and moving northeastward onto the Florida coast southwest of Cross City. Thereafter the storm continued with gradually accelerating speed along the Carolina coasts on July 29, through the mid-Atlantic States on the 30th, finally passing through the New England States on the 31st and dissipating over southeastern Canada.

The storm was not officially named until the 29th when reconnaissance aircraft indicated tropical storm structure. Earlier aircraft and surface reports indicated rather light winds over an area within 50 to 100 miles of the lowest pressure. A tropical storm is usually associated with a zone of concentrated winds near the center, but not until the Low began accelerating northeastward and had reached the coastal area of the Carolinas was this type of pattern apparent.

Wind gusts in squalls to 60 m.p.h. were reported from many locations along the Atlantic coast and the central portion of the Florida Gulf coast. A gust of 65 m.p.h. was recorded at Cape Cod Canal, however, the highest sustained wind at an official Weather Bureau station was 58 m.p.h. at Cape Hatteras. The storm had no opportunity to reach hurricane force as the track was mostly over land after making landfall on the Florida coast.

Rainfall was heavy along the entire coast from Florida to Maine ranging from over 13 inches around Tampa to 4 to 6 inches in most other areas. There was considerable flooding in the west-central portion of the Florida peninsula. Elsewhere the rainfall was beneficial especially in the mid-Atlantic States.

Tides were not excessive due to the rather rapid movement of the storm and the fact that the center remained over or near land. While the storm was developing in the eastern Gulf, tides of 3 to 5 feet were reported along the Florida west coast in the Tampa Bay area and southwesterly winds in combination with high tides produced waves in excess of 10 feet with considerable erosion along the beaches.

Some traffic deaths have been associated with the heavy rains, however no deaths can be directly attributed to the storm. Total property damage was estimated near $5,000,000.

Hurricane Cleo, August 17–20.—Hurricane Cleo formed in a broad area of squally weather some 350 miles northeast of Nassau, Bahamas, on August 18. From surface considerations, the formation was unique in that a marked trough with at least one circulation center was present to the north of the area of formation. Thus, Cleo's development did not conform to the normal increasing easterlies and cyclonic vorticity in the north portion of the trough which usually accompany tropical cyclone development.

Hurricane Cleo remained small and moved about parallel to the Atlantic coast at an initial forward speed of 12 kt., later accelerating to 20 to 30 kt. It appears to have attained its greatest intensity as it approached southeastern New England when winds near the center were estimated at 80 kt.

Except during the early and late stages of the storm, there was never a good correlation between reported winds and central pressures. Wind reports from aircraft were consistently high compared with winds calculated from sea level pressures obtained by aircraft penetrations. Some compromise has been made and this accounts for the estimated sea level pressure noted on the storm track (fig. 1).

There was no known loss of life and very little, if any, damage directly attributed to this hurricane.

Hurricane Donna, August 29–September 13.—Donna, the one major hurricane of the season and the most destructive ever to strike Florida, was detected by aerial reconnaissance on the afternoon of September 2 near 14° N., 49° W. Maximum observed surface winds at that time were 120 kt. and there was a well-developed eye with a central pressure of 973 mb. The existence of a tropical storm or hurricane had been indicated earlier in the day by surface ships, apparently on the fringes of the circulation, which reported shifting winds up to 45 kt., and pressures as low as 1004 mb. Although lack of data makes it impossible to ascertain the exact time or place of increase to hurricane intensity, it seems likely that this occurred near 40° W. on September 1 and that the early stages of Donna were linked to disturbed weather near the African West Coast in late August. The passage of an active easterly wave through the area was suggested by unusually heavy rain at Dakar, with which the crash of an airliner there on August 29 was associated, and by heavy rain in the Cape Verde Islands on the 30th. An aircraft also reported indications of a tropical disturbance near 10° N., 24° W. on that date. Although no additional evidence of storm development was received until September 2, extrapolation of Donna's track back to the African coast gives reasonable continuity with these disturbed conditions. A study by Dunn [10] shows that tropical cyclones of the "Cape Verde" type typically behave in this manner, passing through the islands as unstable waves and attaining hurricane strength some 10° to 15° to the west.

On August 29 and 30 a ridge of anomalously-high surface pressure extended from near the Azores northeastward, a pattern long recognized [11] as associated with tropical cyclogenesis in the eastern Atlantic. The subtropical ridge at the 500-mb. level also was unusually strong during this period. However, it extended from northwestern Africa to the Azores; a northeastward protrusion toward western Europe was not so much in evidence as in some other cases of storm formation in this area. At the time Donna was discovered, a minor tropical depression was centered some 500 miles east of Bermuda, moving northward into a frontal trough. Thereafter, surface pressures began to rise to the north and northeast of the hurricane and for the next two or three days a ridge of above-normal pressure, surface and aloft, extended westward from just south of the Azores, preventing any marked meridional component of motion. Consequently, Donna continued toward the west-northwest on approximately the climatological track, but at a slightly faster-than-average rate

of about 17 kt. This course took the hurricane through the northern Leeward Islands during the evening of September 4 with the eye passing over Barbuda, St. Barthelemy, Sint Maarten, Anguila, and about 10 miles to the south of Anegada.

A slight decrease in intensity apparently occurred as the hurricane approached the Leeward Islands. The maximum sustained wind observed at Sint Maarten was 110 kt. and the lowest barometer reading 952 mb., compared to earlier reports from reconnaissance of 140-kt. winds and dropsonde measurements of 947 mb. Observers on the reconnaissance aircraft also had the impression that a slight weakening occurred September 5. However, no major changes took place during the first few days Donna was under observation and the radar presentation was characterized as that of an intense, "idealized" hurricane.

Only minor damage was reported at St. Thomas, Virgin Islands, with the wind reaching a gust speed of 52 kt. as the storm center passed about 35 miles to the northeast on September 5. Movement continued toward the west-northwest on the 5th and highest sustained winds were only 33 kt. at San Juan, P.R., as the hurricane passed some 85 miles to the north. However, high tides of 4 to 6 feet and heavy surf resulted on the northern and eastern coasts of Puerto Rico and serious floods developed over the northern and eastern portions of the island on the morning of September 6. Flood warnings had been issued following the detection by the San Juan radar of heavy rain moving in on the southern and eastern coastal sections on the evening of the 5th. However, despite the warnings, 107 persons were drowned. The greatest loss of life was at Humacao where 84 deaths occurred. The people in this area had returned to their homes, many of which were built on the river bed, after the hurricane center had passed to the north. According to reports, they failed to heed the subsequent flood warnings. The rain totaled 10 inches or more over a considerable area and measured over 15 inches on some of the mountain slopes.

The track of Donna from September 5 to 7 was affected by a short-wave trough passing to the north. There were temporary indications of recurvature at this time but the southern portion of the trough weakened, perhaps partially as a result of anticyclogenesis associated with the hurricane. Pressures north of the center continued to rise as the trough continued eastward and, as a result, the hurricane's course changed from west-northwest to west. In the meantime, Donna had more than regained any previous loss of intensity. The central pressure given by dropsonde was 940 mb. on the 6th and 944 mb. on the 7th.

Turks Island, in the southeastern Bahamas, escaped the full fury of the hurricane as it passed to the north, and highest winds were only 45–50 kt. However, rainfall was extremely heavy and amounted to over 20 inches, much of which fell in a 12-hour period. Several other islands in the southeastern Bahamas were less fortunate. The eye passed over or very near Mayaguana, Acklins Island, Fortune Island, and Ragged Island. No deaths were reported but only a few of the more substantial buildings were left standing in many of the island villages. At Mayaguana, which was battered by hurricane-force winds for 13 hours, many of the residents took shelter in buildings of the missile-tracking base. The maximum winds in Donna at this time are not known with certainty. At Ragged Island the anemometer failed at 130 kt. The observer estimated the maximum at Fortune Island at 150 kt. after the anemometer and supporting tower blew away. Most of the islands in the western Bahamas were somewhat north of the storm track and no extensive damage resulted although Andros Island experienced hurricane winds for several hours.

On September 9, Donna skirted the northeastern coast of Cuba, bringing gales and heavy rains to much of the island, then took a west-northwest course, toward the Florida Keys. The center crossed over the middle Keys just northeast of Marathon between 0200 and 0300 EST on September 10. It is estimated that sustained winds near the center reached 120 kt. and momentary gusts were at least 155 kt. The central pressure had continued to drop as the hurricane moved across the warm waters of the Florida Straits and was approximately 930 mb. when the center reached the Keys. Miller [12] has made computations relating the probable minimum pressure to temperatures of the underlying water surface. His calculations indicate that a temperature of 86° F. would be required to produce a central pressure of 930 mb. It is of interest to note that there are only a few areas in the hurricane belt, mostly in the Gulf of Mexico and near the Florida Keys, where such high sea-surface temperatures are likely, and that the lowest pressure ever recorded in the Western Hemisphere (892 mb.) occurred in the Keys Hurricane of 1935.

Shortly after it passed the longitude of Puerto Rico, Donna slowed considerably in forward speed and moved at 6 to 10 kt. until it reached the Florida Keys on the 10th. There were many light and variable winds in the middle and upper troposphere and the steering pattern during this period was never clearly defined. At 0700 EST on September 8, when the hurricane was located only 380 miles southeast of Miami and moving westward at about 10 kt. *the Miami wind at 500 mb. was still blowing from the west.* It seems evident that there was a contribution from the storm itself to its movement.

On September 10 a low pressure system was moving across southeastern Canada with a cold front extending through New England thence southwestward, becoming stationary from Tennessee to Texas. No marked surface-pressure trough accompanied the front south of about 40° N. However, at about this time, the ridge of high pressure which had persisted to the north of the storm began to decay. This occurred in response to an upstream increase in amplitude in the westerlies and the establishment of a long-wave trough in the east-central United States. As a result, Donna began recurvature at this point and moved northwestward along the southwestern coast

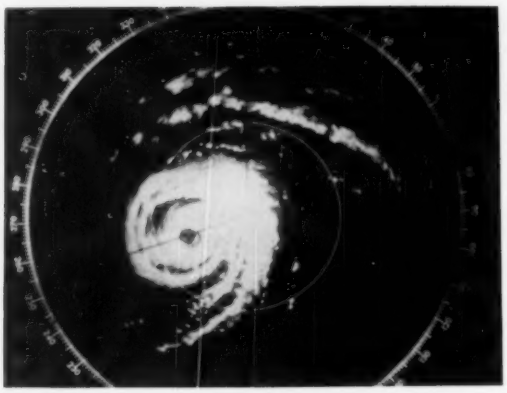

FIGURE 5.—Radar picture of Donna at its closest position to Miami, illustrating all the features of the classical hurricane. 0730 EST September 10, 1960; strobe 100 n. mi.

of the Florida peninsula. The eye passed over Naples and Fort Myers as the hurricane turned northward, moved inland, and then continued northeastward to re-enter the Atlantic just north of Daytona Beach about 0400 EST, September 11. Sustained winds of over 90 kt. with gusts of 100 to 130 kt. probably occurred on the lower west coast from Everglades City to Naples and there were sustained winds of near hurricane force with higher gusts near the center as it moved across the peninsula. Despite the trajectory over land and a filling of central pressure from 950 mb. at Fort Myers to 970 mb. on the east coast, the storm was still intense and well organized when it moved into the Atlantic again.

The storm surge on the Florida Keys reached as much as 13 feet above normal levels and was generally 8 to 12 feet some 40 miles to the northeast of the track and 20 miles to the southwest. Destruction from the combination of wind and water in this area ranged from major to almost complete. Tide departures tapered off to the north to 3 to 4 feet above normal in the Miami-Palm Beach area. On the southwestern Florida coast, the storm surge was locally up to 11 feet above normal. The surge reached as far north as Naples, and Fort Myers reported levels 4 to 7 feet above normal. On the Gulf coast north of Bradenton and the Atlantic coast north of Palm Beach, tides were mostly 1 to 3 feet above normal. Maps showing the high water marks recovered in the Florida Keys and along the west coast of Florida will be presented in a forthcoming article, by D. L. Harris, in the *Review*.

The effect of the hurricane on the flora and fauna of the Everglades National Park is being studied by specialists in these subjects. The largest stand of big mangrove trees in the world is located here and was about 50 percent or more killed, with a complete kill in some areas for reasons which are not yet wholly understood. Almost all large mangrove trees which survived the 1935 hurricane were killed by Donna. This is true to a somewhat lesser extent of the mahogany trees. It is interesting to note that new mangrove trees growing after the 1935 hurricane were not as large as those standing in 1935 indicating a longer period free from major hurricane occurrence prior to 1935 in this area. The great white heron, only found in the United States in extreme southern Florida and once in danger of extinction, suffered about a 35 to 40 percent loss but about 600 birds remain. One of the two or three largest nesting concentrations of the American bald eagle in the United States, exclusive of Alaska, is also in the Park. All eagle nests were destroyed but four months later some twelve had been rebuilt.

Figure 5 shows a radar picture at the time Donna was closest to Miami. Present are the features of the classical hurricane. The round eye about 21 miles in diameter and the thick wall cloud some 17 to 20 miles in diameter are observable. At the time, the heavy rain band visible over the Miami station was producing rain at the rate of about one inch per hour.

Donna began a gradual acceleration as it moved through northeastern Florida and was advancing at about 12 kt. when it passed into the Atlantic. Rapid re-intensification occurred over the ocean and when the center was about 80 miles southeast of Charleston, S.C., on the afternoon of September 11, the SS *Mae* reported winds of 105 kt. and 20- to 30-foot seas. Several small brief tornadic storms were reported in coastal South Carolina with about ten people hospitalized and considerable property damage in the Charleston area. Winds along the beaches near Charleston reached about 60 kt. in gusts. However, the coastal section near the North Carolina ine received sustained hurricane-force winds.

A short-wave trough was moving through the Great Lakes region on September 11 and, under the influence of an increased southerly flow, Donna accelerated to a speed of about 30 kt. toward the northeast, reaching the North Carolina coast just northeast of Wilmington during the evening of the 11th, then passing into the Atlantic again near the Virginia line about 0500 EST of the next morning. During its passage over North Carolina, Donna's eye was unusually large with the area of calm or light variable winds ranging from 50 to 80 miles in diameter. Some small-scale irregularities in speed and direction of motion during this period may be partially attributable to differential friction between land and water. Such an effect was suggested as the cause of erratic behavior of some of the 1955 hurricanes in this area [13]. Minimum pressures reported along this section of the track ranged from 958 to 967 mb. and highest winds were in the 70-90-kt. bracket with some estimates of 100-kt. gusts. Tides reached 4 to 8 feet above normal at various places along the North Carolina coast and waves were reported from 15 to 20 feet. Several small tornadoes or locally destructive storms occurred in the forward portions of the hurricane and at least eight persons required hospitalization. Five other tropical storms have taken rather similar tracks across North Carolina in the past decade and Hardy [14] reported that residents in a few areas felt that Donna was the most destructive. He points out, however, that this is probably true only in limited sections in the northeastern portion of the State.

When Donna again reached the ocean, it resumed its rapid movement with a forward speed of 30 to 35 kt., moving northeastward a short distance off the coast and crossing Long Island shortly after noon on September 12. Winds of about hurricane force, but with gusts locally to about 90 kt., brushed the Maryland, Delaware, and southern New Jersey coasts. Residents at Ocean City, Md., described the storm as the worst in the city's history. Damage to property in other areas along the immediate shore was heavy and considerable agricultural losses were suffered inland.

Sustained winds reached about 90 kt. at several points on Long Island and 50 to 60 kt. on western Long Island and in New York City. Gusts of 100 kt. or higher were reported at Montauk, L.I., and Block Island, R.I., and peak gusts reached or exceeded hurricane force east of the center through southern New England and northward to the New Hampshire coast area. Winds to the west of the track were somewhat less and there were no sustained hurricane-force winds reported on the mainland in New England except for isolated cases where local topographic effects were responsible. One such exception was a sustained 80-kt. wind, with gusts of over 120 kt., at Blue Hill Observatory at Milton, Mass. The minimum central pressure recorded at Brookhaven, L.I., was 961 mb., approximately the same as the minimum along the track through North Carolina. Gradual filling and weakening occurred farther north as the center continued rapidly northeastward, moving through Maine just west of Caribou and into Canada late on September 13. Winds of hurricane force still persisted in squalls near the center until about the time it reached the Canadian border. The storm then moved northeastward through Labrador and into the Atlantic as a weakening frontal disturbance. Complete meteorological data for individual stations in the hurricane's path can be found in *Climatological Data, National Summary* for September 1960.

There was evidence that Donna was beginning to assume extratropical characteristics as early as September 12. Many of the maximum winds reported in the Middle Atlantic States were from the northwest, indicating that cooler, dryer air was beginning to invade the circulation. Another feature contributing to peculiar distributions of wind and pressure extremes was the unusually large eye of Donna. During the period the hurricane was moving from North Carolina to southern New England this was as much as 50 to over 100 miles in diameter, an extreme and probably unprecedented size for a hurricane eye.

Tides were well above normal along the entire Middle Atlantic coastline and ranged about 6 feet above normal near Atlantic City, N.J., and in the New York City-Long Island area. Departures of 5 to 10 feet above normal occurred along the southern New England coast but fortunately the damage potential was lessened by the arrival of the storm surge at the time of normal low tide. Even so, considerable damage to coastal properties was reported all along the Middle Atlantic and New England coast as a result of combined effects of winds and tides and there were extensive damages from flooding farther inland, particularly from the Catskills to Long Island. A map showing the peak tide and peak surges in New York and southern New England will be given in a forthcoming article, by D. L. Harris, in the *Review*.

Donna was unique in that it gave hurricane force winds to Florida, the Middle Atlantic States, and New England. However, although it was one of the most destructive hurricanes of all time, loss of life was remarkably low. This can be attributed to three factors—timely and accurate warnings, effective dissemination by news media and other agencies, and the taking of proper precautions by the public. The accuracy of the warnings is in large part a reflection of the continuous tracking by aircraft reconnaissance and land-based radar, which was probably the most complete of any hurricane in history.

Results of the various objective forecast techniques ranged from poor to excellent with median 24-hour errors for the individual methods ranging from 68 to 132 n. mi. The results of the various systems cannot be compared since the number of forecasts and the times of the forecasts with each were not the same, being dependent on the available data. Each method, including the one with the lowest median error, showed serious errors during at least one of the three critical periods—the abortive recurvature off Puerto Rico, the recurvature over Florida, or the acceleration off the Atlantic coast.

Hurricane Ethel, September 14–17.—Hurricane Ethel developed rapidly in the central Gulf of Mexico early on September 14. Its position and intensity were established by the 0930 CST report from MAMOS (Marine Automatic Meteorological Observing Station) in the central Gulf of Mexico. The hurricane moved northward and continued to intensify rapidly during the day with a central pressure of 972 mb. and winds of 140 kt. reported by reconnaissance aircraft that afternoon. During the night of September 14–15, cool dry air entered the circulation and the hurricane's intensity diminished quickly. The hurricane center reached the coast near Biloxi, Miss., with the lowest pressure 981.4 mb. during the afternoon of September 15 at Keesler Air Force Base. It continued to weaken as it moved northward through eastern Mississippi that night. The remnants of the storm were located in central Tennessee on the morning of September 17.

The highest sustained wind reported by a land station was 78 kt. with gusts to 90 at Venice, La., at 0415 CST, September 15. Burrwood, La., reported winds of 45 kt. with gusts to 60. The highest tide reported was 7 feet above mean sea level on Quarantine Bay on the east side of the Mississippi River about 0400 CST on the 15th. Tides of 2 to 5 feet above mean sea level occurred from the mouth of the Mississippi River eastward to St. Marks, Fla. Local rains of 5 to 6 inches or more were reported through southeastern Mississippi, southwestern Alabama, and extreme northwestern Florida but no significant flooding occurred.

The total storm damage probably did not much exceed one million dollars and there was no loss of life.

Tropical Storm Florence, September 17–26.—An extensive shower area was noted well to the northeast of the Leeward Islands September 16 although there were no indications of a definite circulation. By the morning of the 17th, pressures through the eastern Antilles had fallen 3 to 5 mb. with light south and southwest winds indicating the possibility that a circulation had developed. On the evening of the 17th, reports from shipping to the north of Puerto Rico placed a closed circulation near 21° N., 66° W. with winds up to 35 m.p.h. The Low continued westward about 10 m.p.h. and reconnaissance aircraft located a broad, ill-defined center with maximum winds around 40 m.p.h. on the morning of the 18th near 21° N., 69° W.

Tropical Storm Florence moved on a west to west-northwest track near 12 m.p.h., gradually weakening until the 20th when reconnaissance aircraft found only a weak Low south of Andros Island in the Bahamas with no significant weather or strong winds. The remains of Florence moved into the western end of Cuba and became nearly stationary until the evening of the 22d when conditions became more favorable for redevelopment. The Low began moving northeastward and was located just off the southwestern Florida coast by the morning of the 23d with winds up to 30 m.p.h. and widespread rain over southeastern Florida. It then became blocked by a large high pressure system along the mid-Atlantic coast after reaching the vicinity of Lake Okeechobee the evening of the 23d and changed to a west-northwest track, drifting into the eastern Gulf of Mexico near Tampa early on the 25th. The Low continued quite weak over the Gulf and moved into the Pensacola area on the morning of the 26th with winds less than 25 m.p.h. but with a rather large rain area that covered the southern portions of Alabama and Georgia and northwestern Florida.

Florence was never a well-defined tropical storm and maximum winds were just barely of tropical storm intensity (for only a short period) although gusts to 52 m.p.h. were reported in the Vero Beach area in a squall when the Low was nearest that station. The only significant damage in this storm was from local flooding in Florida. Rainfall totals of 3 to 6 inches or more were reported during passage of the Low on ground that was already saturated from the previous heavy rains of Donna. Monthly totals for September were well over 20 inches at many spots in southeastern Florida with a few totals in excess of 30 inches. No damage of consequence was reported over the eastern Gulf States with rainfall probably beneficial to crops. No known fatalities or injuries have been reported.

REFERENCES

1. C. M. Woffinden, "The Weather and Circulation of June 1960," *Monthly Weather Review*, vol. 88, No. 6, June 1960, pp. 229–234.
2. H. Riehl, *Tropical Meteorology*, McGraw-Hill Book Co., Inc., New York, 1954, 392 pp. (pp. 226–227).
3. R. A. Green, "The Weather and Circulation of July 1960," *Monthly Weather Review*, vol. 88, No. 7, July 1960, pp. 257–262.
4. G. E. Dunn and B. I. Miller, *Atlantic Hurricanes*, Louisiana State University Press, Baton Rouge, La., 326 pp. (p. 35).
5. L. P. Stark, "The Weather and Circulation of August 1960," *Monthly Weather Review*, vol. 88, No. 8, Aug. 1960, pp. 286–293.
6. E. M. Ballenzweig, "Seasonal Variations in the Frequency of North Atlantic Tropical Cyclones Related to the General Circulation," *National Hurricane Research Project Report* No. 9, Washington, D.C. July 1957.
7. E. M. Ballenzweig, "Relation of Long-Period Circulation Anomalies to Tropical Storm Formation and Motion," *Journal of Meteorology*, vol. 16, No. 2, Apr. 1959, pp. 121–139.
8. C. F. Tisdale, "The Weather and Circulation of September 1960," *Monthly Weather Review*, vol. 88, Nos. 9–12, Sept.-Dec. 1960, pp. 353–361.
9. J. F. Andrews, "The Weather and Circulation of October 1960," *Monthly Weather Review*, vol. 89, No. 1, Jan. 1961, pp. 24–30.
10. G. E. Dunn, "Areas of Hurricane Development," *Monthly Weather Review*, vol. 84, No. 2, Feb. 1956, pp. 47–51.
11. E. B. Garriott, "The West Indian Hurricanes of September 1906," *Monthly Weather Review*, vol. 34, No. 9, Sept. 1906, pp. 416–423.
12. B. I. Miller, "On the Maximum Intensity of Hurricanes," *Journal of Meteorology*, vol. 15, No. 2, Apr. 1958, pp. 184–195.
13. G. E. Dunn, W. R. Davis, and P. L. Moore, "Hurricanes of 1955," *Monthly Weather Review*, vol. 83, No. 12, Dec. 1955, pp. 315–326.
14. A. V. Hardy, "Hurricane Donna in North Carolina," *Weatherwise*, vol. 13, No. 5, Oct. 1960, pp. 213–214.

THE WEATHER AND CIRCULATION OF DECEMBER 1960[1]

An Unusually Cold Month in the United States

ROBERT H. GELHARD

Extended Forecast Section, U.S. Weather Bureau, Washington, D.C.

1. HIGHLIGHTS

Average temperatures throughout most of the contiguous United States during December 1960 underwent a marked reversal from the warm regime which had dominated the fall season [1, 2]. Subzero temperatures were frequent in the northern half of the country east of the Rocky Mountains, and freezing temperatures threatened winter vegetable and citrus crops from southern California eastward through the Rio Grande Valley to central Florida.

Snow cover, which had been restricted to the eastern slopes of the Rockies and extreme northern Plains, spread throughout the northern half of the country early in December and for the most part remained throughout the month. In the southern Plains, precipitation in excess of normal resulted in some flooding around mid-month, while drought conditions in the Great Basin which had been alleviated somewhat in November resumed during December.

2. THE GENERAL CIRCULATION

The general circulation at 700 mb. for December 1960 (fig. 1) represented a distinct change from the predominantly zonal or high-index state of the preceding month [1], particularly in the western portion of the Northern Hemisphere from western Europe to the central Pacific Ocean. A comparison of figure 1 with the mean 700-mb. height pattern for the preceding month shows that the diffuse planetary wave system of November became resolved into a series of well-defined troughs and ridges located in climatologically preferred areas [3].

The field of anomalous 700-mb. height changes (changes after the normal change has been removed) from November to December (fig. 2) helps delineate the areas of greatest amplification. The greatest change, +680 feet, took place in the central Atlantic with the development of the Azores High at a higher than normal latitude. This was associated with a northward shift of the mean westerlies and subsequent deepening of the downstream trough in the eastern Mediterranean where anomalous heights fell by 310 feet (fig. 2). The 5-day mean charts (not shown) show that amplification of the wave pattern of the general circulation apparently began with the rather sudden development of the Azores High late in November. Subsequently this amplification seems to have spread upstream, first to western North America and then to northeastern Asia.

Relatively little change occurred in the eastern part of the hemisphere except in northeastern Asia. Nearly all of Asia was dominated by a vast Siberian High at sea level, extending from the Black Sea to Japan (fig. 3). Generally stormy conditions existed in Europe and the Mediterranean area, but the modifying effects of maritime air did not penetrate beyond European Russia.

3. THE INDEX CYCLE

The change in the westerly circulation from November to December was a classic example of an index cycle as described by Namias [4, 5]. Figure 4 shows the march of indices of temperate (35°–55° N.) and subtropical (20°–35° N.) westerlies at 700 mb., as defined by overlapping 5-day mean maps computed three times per week. The index referred to here is for the western half of the Northern Hemisphere from 0° to 180° W. The temperate westerlies reached a peak near the end of the third week in November and then began a four-week decline before making a rapid recovery late in December. The dotted line, giving the daily components of the mean index, is included to show the very sharp drop in the index which is damped somewhat by the averaging process and coincided with the first of several severe storms in the Southwest. The decline in the temperate latitude index was accompanied by southward displacement of the westerlies except in the North Atlantic, so that the subtropical index rose as rapidly as the zonal index fell, reaching a peak December 21, a day after the minimum in the temperate index.

Although there seems to be a strong preference for index cycles to occur in late winter, they are not uniquely fixed with respect to month. One necessary condition for the onset of an index cycle seems to be an abundant supply of cold air in polar regions. Figure 5A shows that the 1000–700-mb. thickness for November averaged 130 feet below normal in northwestern North America, thereby satisfying this condition. However, in order to maintain the atmospheric heat balance, the containment of polar

[1] Articles describing the weather of January, February, and March 1961 will appear in the April, May, and June 1961 issues, respectively, of the *Monthly Weather Review*.

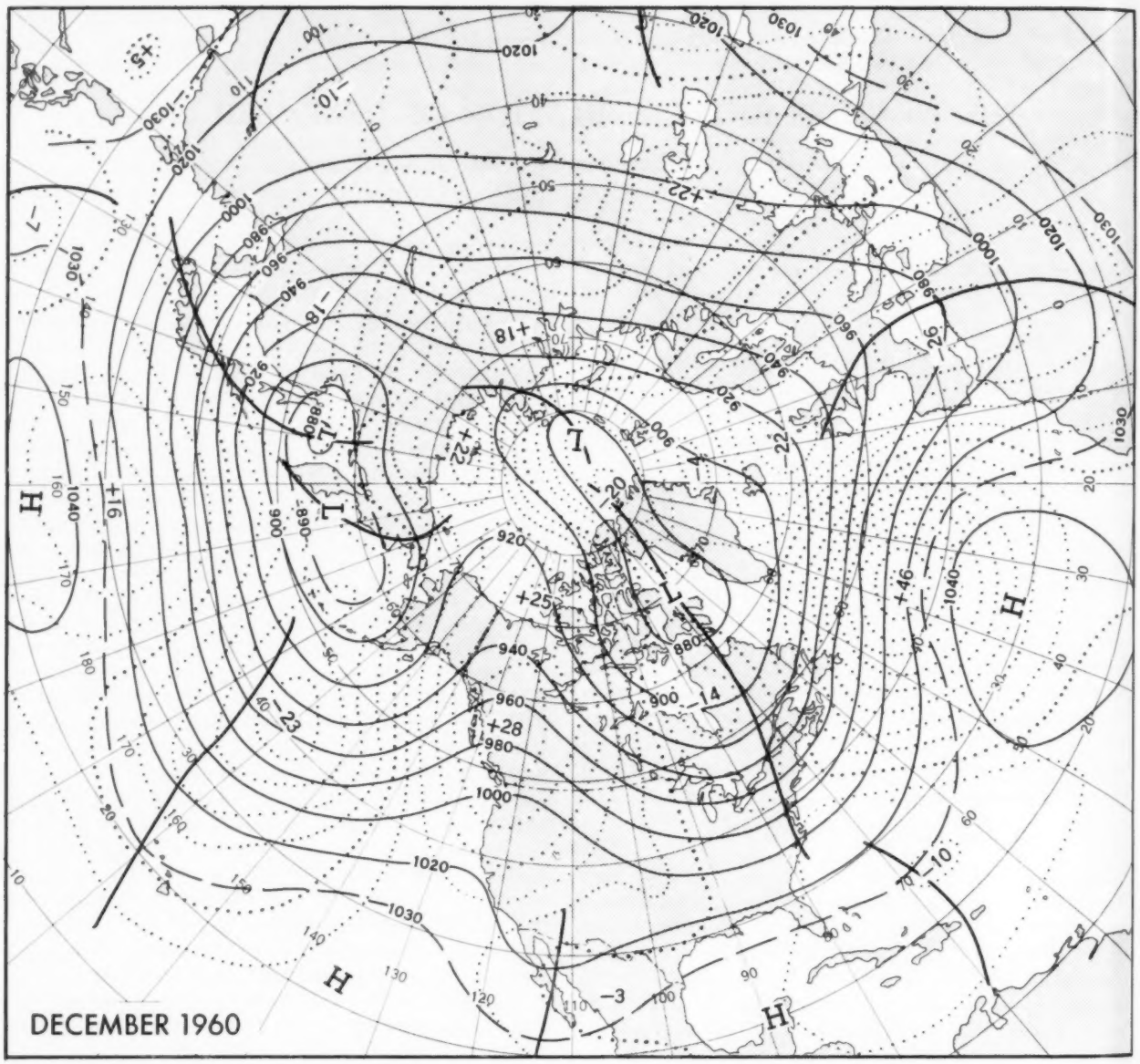

FIGURE 1.—Mean 700-mb. height contours (solid) and departures from normal (dotted), both in tens of feet, for December 1960. Stronger than normal northwesterly flow between the intense ridge in western North America and the deep trough along the east coast produced very cold weather in most of the contiguous United States.

air brought about by fast westerlies must end at some point. This point was reached in December, resulting in completion of the index cycle and redistribution of cold and warm air masses, as strikingly illustrated by the 1000–700-mb. thickness anomaly patterns for December and November, figures 5A and 5B, showing a complete reversal in sign of the thickness anomalies. The effects of this exchange on the surface weather will be discussed in more detail below.

4. TEMPERATURE

The decline of the zonal index and amplification of the circulation pattern through the first three weeks of December had a marked influence on the weather of the United States. Persistent northerly anomalous flow east of the Continental Divide (fig. 1), closely paralleling the sea level isobars (fig. 3), brought colder weather to most of the contiguous United States. Of a hundred stations

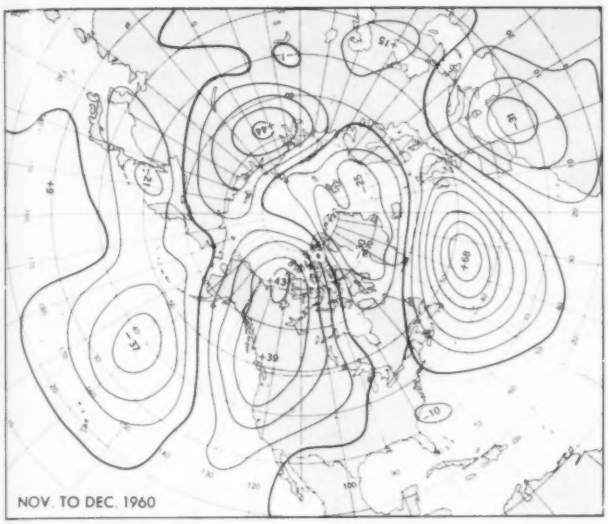

FIGURE 2.—Difference between monthly mean 700-mb. height anomalies for November and December 1960 (December minus November) in tens of feet. Anomalous rises in western North America and falls in the east were associated with amplification of the long-wave pattern.

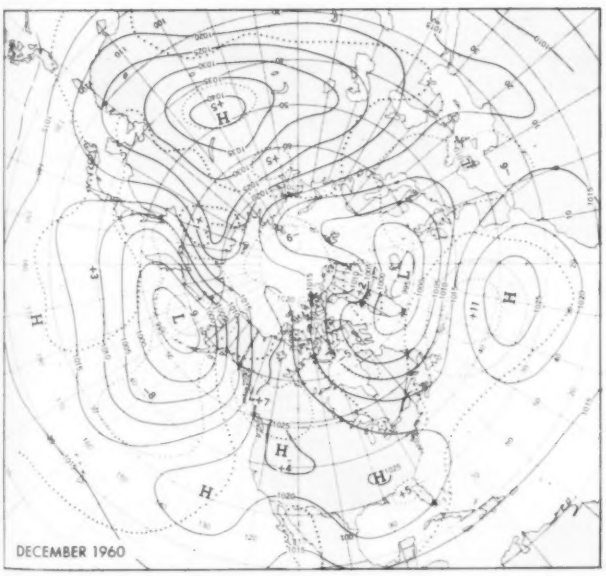

FIGURE 3.—Average sea level pressure (solid lines) and its departure from normal (dotted lines) in millibars for December 1960. High pressure was accompanied by cold weather in the contiguous United States.

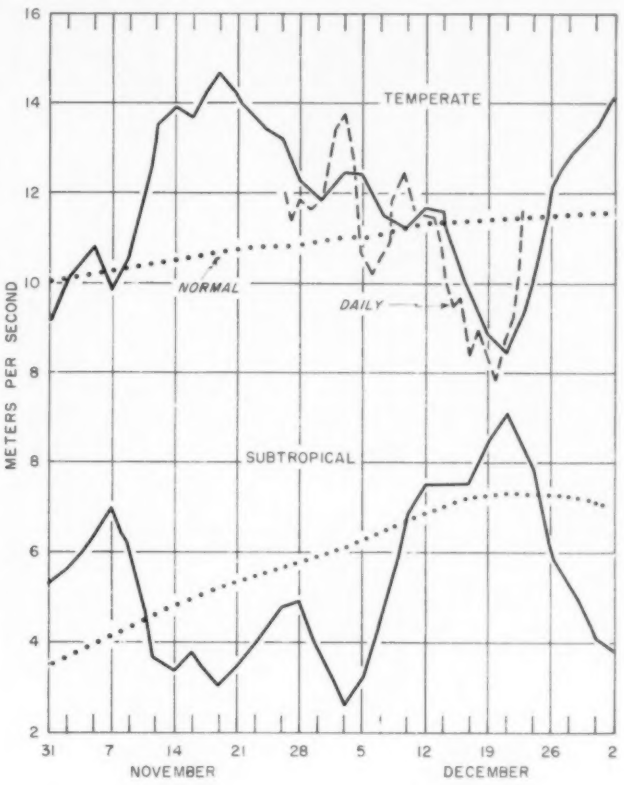

FIGURE 4.—Time variation of 5-day mean 700-mb. indices in meters per second for the western zone of the Northern Hemisphere from 0° to 180° W. Temperate index applies between 35° and 55° N., and subtropical index between 20° and 35° N. Values are for 5-day periods ending on dates indicated. The dashed line represents a daily index, and the dotted lines are the normals based on the data of Weather Bureau *Technical Paper No. 21*.

distributed uniformly across the nation, 78 percent decreased in average temperature by at least one temperature class (out of five classes) from November to December (fig. 6A). Of the remaining 22 percent, only 3 percent increased. Even in the area of no change or increase, only in the extreme northern Plains were temperatures above normal for December.

The Great Basin area and California remained cool under the influence of large stagnant anticyclones. In spite of abundant sunshine, record daily minimum temperatures in the cool dry air mass kept mean temperatures below normal. An interesting effect of these persistent Basin Highs was reported from Boise, Idaho, where the average wind speed was only 4.6 m.p.h., the lightest in 21 years.

The most unseasonably cold part of the country was the East and South as far west as Arizona (fig. 7). Figure 8A shows the trajectory of migratory anticyclones carrying cold air masses from Canada just west of the Great Lakes and through the Ohio Valley. Throughout the area from the Mississippi Valley eastward some record daily minimum temperatures were established along with record low temperatures for the month, such as −9° F. at three

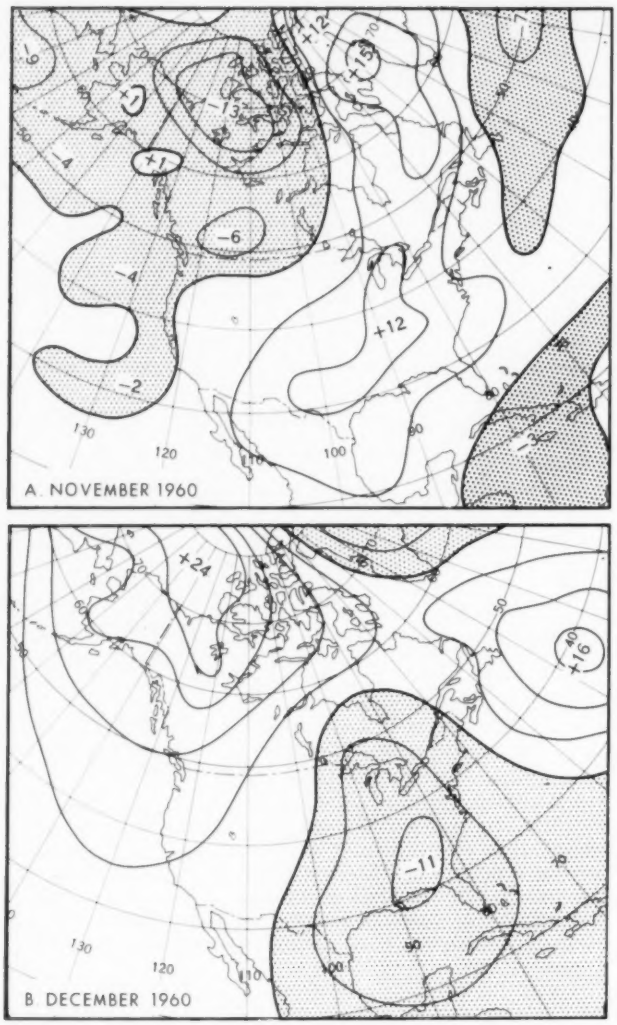

FIGURE 5.—Mean departures from normal of 1000–700-mb. thickness for (A) November 1960 and (B) December 1960, both in tens of feet. Note the complete reversal in phase as the index cycle progressed.

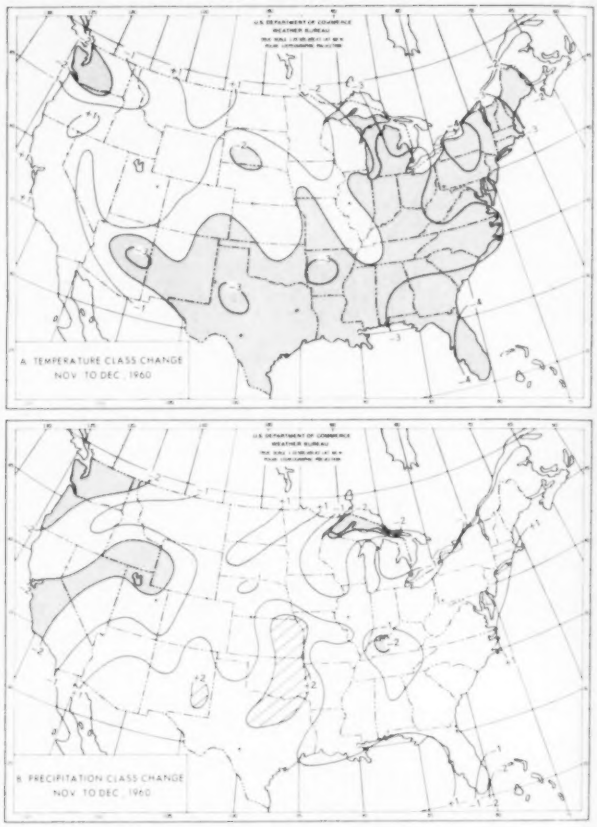

FIGURE 6.—(A) The number of classes the anomaly of monthly mean temperature changed from November to December 1960, and (B) the number of classes the total precipitation category changed from November to December 1960. Areas of positive change greater than two classes are hatched, and areas of negative change greater than two classes are stippled.

stations in Kentucky and −7.5° F. at Evansville, Ind. For most stations, average December temperatures were the lowest in from 10 to 25 years and close to record intensity. In Florida, freezing temperatures threatened citrus and vegetable crops as far south as Tampa on five occasions. Richmond, Va. reported December 1960 as the only month on record with every daily minimum temperature below 32° F.

In the lower Mississippi Valley and Southern Plains anticyclonic conditions prevailed at sea level (fig. 3), chiefly emanating from Great Basin Highs. However, there was also some contribution from polar air masses, as evidenced by subfreezing temperatures in the Rio Grande Valley and resultant crop damage.

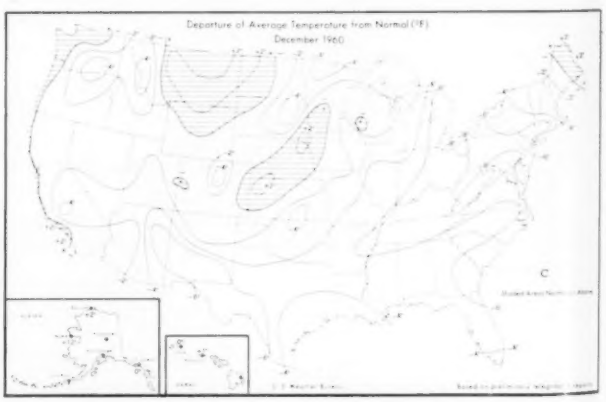

FIGURE 7.—Temperature departure from normal (°F.) for December 1960 (from [6]). Widespread cold was associated with circulation shown in figures 1 and 3.

Below normal temperatures in Arizona and New Mexico were maintained by persistent cloudiness due to cyclonic conditions aloft (fig. 1) which were quite pronounced during the first three weeks of the period. In addition, heavy snows early in the period probably contributed to lower than normal temperatures. Late in the month a warming trend began in the Southwest, coincident with the rising zonal index.

While new records for daily minimum temperature were common throughout most of the country, warm air in advance of a severe storm in the central Great Plains produced record high maximum temperatures in the Northeast near the end of the first week in December.

The amplification of the trough-ridge system in the eastern Pacific and western North America, which provided the mechanism for bringing cold air into the contiguous United States, was also responsible for the warmest December on record for most of Alaska. A strong anomalous southerly component of the average flow, shown by the height anomaly pattern in figure 1 (coincident with the sea level isobars, fig. 3), produced an influx of warm maritime air throughout most of the month. The extent of the exchange of air masses is well illustrated by the change in the 1000–700-mb. thickness charts for November and December (fig. 5).

5. PRECIPITATION

In general, excessive precipitation in the contiguous United States was restricted to the central third of the country and to the North Atlantic coast (fig. 9). An unusual feature of December's precipitation regime was the large amount of snowfall occurring so early in the season. In the Southwest and the Northeast many new monthly snowfall records were established, such as 10 inches at El Paso, Tex., and Winslow, Ariz., 17 inches at Dayton, Ohio, and 21 inches at Worcester, Mass. Moderate amounts were reported elsewhere except for the Great Lakes and most of the Great Basin where representative stations such as Lansing, Mich., and Salt Lake City, Utah, reported their driest Decembers on record. In contrast, Waco and Dallas, Tex., reported the wettest December on record.

It is interesting to compare the precipitation patterns for November [1] and December in terms of high and low index circulations. November's pattern was wet in the west and relatively dry east of the Rocky Mountains—a pattern often associated with fast westerly flow. However, in December amplification of the ridge in western North America and deepening of the upstream trough produced a strongly meridional steering current aloft, and the westerlies were weaker than normal throughout the West (fig. 10). The intensity of the western ridge was great enough to block effectively the passage of migratory cyclones from the west (fig. 8B), so that the Pacific Northwest during this low-index regime received from 25 to 50 percent less precipitation than normal, and the Great Basin received less than half of normal. On the other

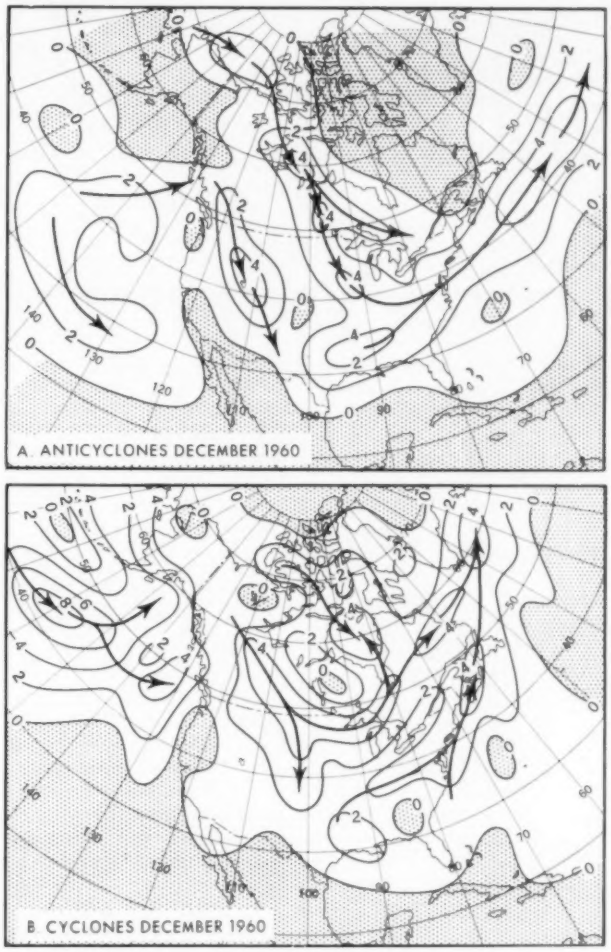

FIGURE 8.—Number of (A) anticyclone passages and (B) cyclone passages (within equal-area quadrilaterals of 66,000 n. mi.²) during December 1960. Primary tracks of migratory sea level systems are indicated by solid arrows. Areas of zero frequency are stippled.

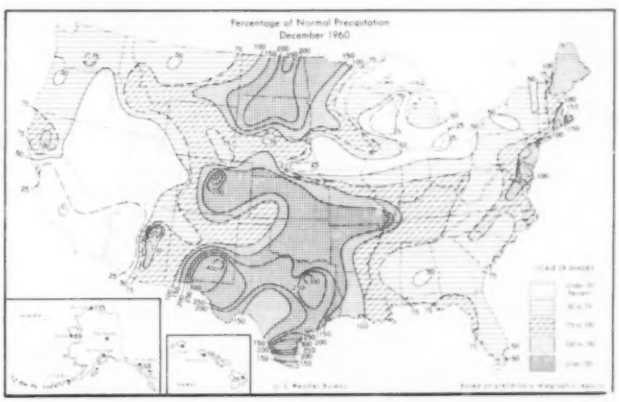

FIGURE 9.—Percentage of normal precipitation for December 1960 (from [6]). Amounts were generally in excess of normal between the Mississippi River and the Continental Divide but deficient elsewhere.

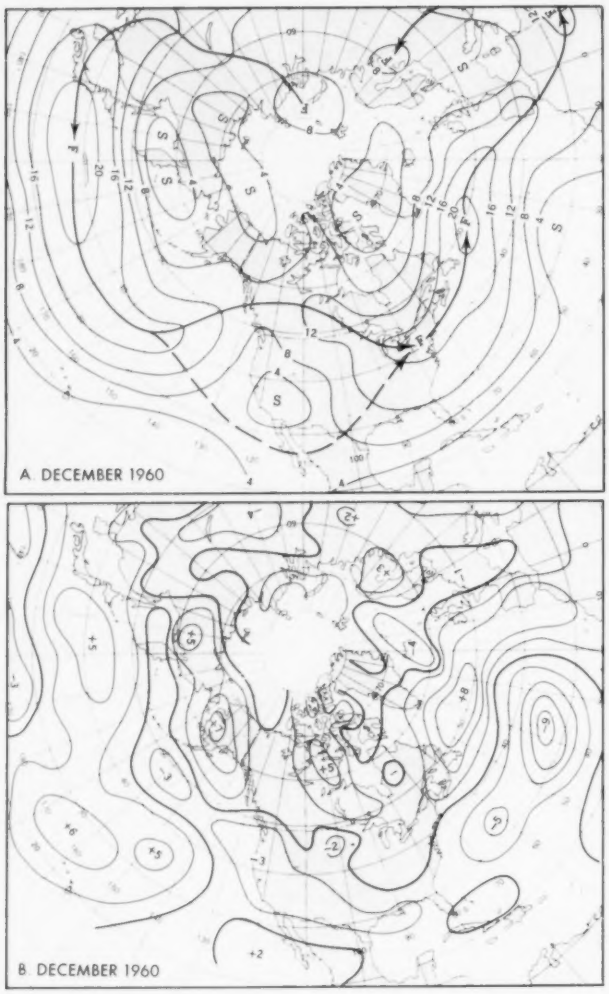

FIGURE 10.—(A) Mean 700-mb. isotachs in meters per second for December 1960. Solid arrows indicate primary axes and dashed arrows secondary axes of maximum wind speed. (B) Departure from normal of mean wind speeds for December 1960 (in meters per second). Weaker than normal westerlies were associated with wet weather in the Great Plains and dry weather west of the Continental Divide.

hand, the weakness of the westerlies diminished foehn drying and favored upslope precipitation in the Plains region between the Mississippi River and the Continental Divide (fig. 10B).

Another common feature of low-index circulations is the presence of areas of mid-tropospheric confluent flow at fairly low latitudes such as that found in the Texas area (fig. 1). While this was not an unusually strong confluent zone, there was sufficient contrast between cold and warm air masses to lead to three major storms in the southern Plains and up to 400 percent of normal precipitation with some flooding in eastern Texas and southern Arkansas. These same storms produced heavy snows as they moved through the Ohio Valley, roughly along the track shown in figure 8B. They were responsible for record December snowfalls from northern Virginia through New England as they deepened in the area east of the mean trough near the Middle Atlantic coast (fig. 1).

Figure 6B illustrates well the general change from the precipitation regime of November to that of December; that is, from wet to dry in the West, a general increase in the Plains States, and little change elsewhere. While it has been mentioned that November had a typical high-index precipitation pattern, December's pattern was not necessarily typical of low index since distribution of precipitation is dependent on the precise geographical location of the quasi-stationary trough and ridge systems, which can exhibit considerable variation during periods of low index.

REFERENCES

1. J. F. O'Connor, "The Weather and Circulation of November 1960," *Monthly Weather Review*, vol. 89, No. 2, Feb. 1961, pp. 55–38.
2. W. H. Klein, "The Circulation and Weather of 1960," *Weatherwise*, vol. 14, No. 1, Feb. 1961.
3. W. H. Klein and J. S. Winston, "Geographical Frequency of Troughs and Ridges on Mean 700-mb. Charts," *Monthly Weather Review*, vol. 86, No. 9, Sept. 1958, pp. 344–358.
4. J. Namias, "The Index Cycle and Its Role in the General Circulation," *Journal of Meteorology*, vol. 7, No. 2, Apr. 1950, pp. 130–139.
5. J. Namias, "Thirty-Day Forecasting: A Review of a Ten-Year Experiment," *Meteorological Monographs*, vol. 2, No. 6, American Meteorological Society, Boston, July 1953, 83 pp. (See pp. 35–40, and 63–66.)
6. U.S. Weather Bureau, *Weekly Weather and Crop Bulletin, National Summary*, vol. XLVIII, Nos. 1 and 2, Jan. 2 and 9, 1961.

U.S. GOVERNMENT PRINTING OFFICE: 1961